Aus dem Veterinärwissenschaftlichen Department der Tierärztlichen
Fakultät der Ludwig-Maximilians-Universität München

Arbeit angefertigt unter der Leitung von
Prof. Dr. Dr. Dr. habil. Fred Sinowatz

angefertigt an der
Klinik für Urologie
Universitätsklinikum Tübingen
(Prof. Dr. Karl-Dietrich Sievert)

A collagen cell carrier seeded with autologous urothelial cells for reconstructive surgery of the urethra

Inaugural-Dissertation
zur Erlangung der tiermedizinischen Doktorwürde
der Tierärztlichen Fakultät der Ludwig-Maximilians-Universität München

von
Lisa Carmen Angelika Daum
aus Nürnberg

München, 2013

Gedruckt mit Genehmigung der Tierärztlichen Fakultät
der Ludwig-Maximilians-Universität München

Dekan: Univ.-Prof. Dr. Joachim Braun

Berichterstatter: Univ.-Prof. Dr. Dr. Dr. habil. Fred Sinowatz

Korreferent: Priv.-Doz. Dr. Valeri Zakhartchenko

Tag der Promotion: 20. Juli 2013

Meiner Familie

<u>Parts of this work were presented at the following congresses</u>:

Lisa Daum, Sabine Maurer, Arnulf Stenzl, Martin Vaegler, Karl-Dietrich Sievert (2011): A new biodegradable collagen cell carrier for tissue engineering of matrix-stabilized urothelium. World Conference on Regenerative Medicine 2011, Leipzig

Lisa Daum, Martin Vaegler, Sabine Maurer, Arnulf Stenzl, Karl-Dietrich Sievert (2012): Stabiles bioartifizielles Urothel auf Kollagenmatrix - Konstruktion und Applikation. 53. Jahrestagung der Südwestdeutschen Gesellschaft für Urologie 2012, Wiesbaden

Lisa Daum, Martin Vaegler, Sabine Maurer, Arnulf Stenzl, Karl-Dietrich Sievert (2012): Biodegradable collagen cell carriers stabilize tissue-engineered urothelium for pre-clinical application. 3rd International Conference "Strategies in Tissue Engineering" 2012, Würzburg

Martin Vaegler, Lisa Daum, Sabine Maurer, Arnulf Stenzl, Karl-Dietrich Sievert (2012): Matrix-stabilization of tissue-engineered urothelium: construction and pre-clinical application. 64. Jahrestagung der Deutschen Gesellschaft für Urologie 2012, Leipzig

Index

Abbreviations

Aa.	arteriae
ACSM	acellular corpus spongiosum matrix
app.	approximately
BAMG	bladder acellular matrix graft
BPE	bovine pituitary extract
BrdU	bromodeoxyuridine (5-bromo-2'-deoxyuridine)
°C	degree Celsius
$CaCl_2$	calcium chloride
CCC	collagen cell carrier
CH	charrière
CK	cytokeratin
cKSFM	complete keratinocyte serum-free medium
cm	centimetre
CO_2	carbon dioxide
Cy	cyanine
DAB	3,3'-diaminobenzidine
DAPI	4',6-diamidino-2-phenylindole
DMSO	dimethylsulphoxide
DNA	deoxyribonucleic acid
DPBS	Dulbecco's phosphate buffered saline
e.g.	“exempli gratia” = for example
EDTA	ethylenediaminetetraacetic acid
EGF	epidermal growth factor
ELISA	enzyme linked immunosorbent assay
etc.	et cetera
EUS	external urethral sphincter
FCS	fetal calf serum
Fig.	figure
FITC	fluorescein isothiocyanate
FLUTD/FLUTI	feline lower urinary tract disease/ inflammation
G	gauge
g	grams OR gravitational force
GMP	good manufacturing practice

h	hours
HBSS	Hank's balanced salt solution
HE	haematoxylin-eosin
HEPES	2-(4-(2-hydroxyethyl)piperazine-1-yl)ethanesulfonic acid
HL	human ureter
HRP	horseradish peroxidase
HUC	human urothelial cells
i.e.	"id est" = that is
IgG	immunoglobulin G
i.m.	intramuscular
IUS	internal urethral sphincter
i.v.	intravenous
IVC	individually ventilated cage
KC	keratinocyte
KCl	potassium chloride
kg	kilograms
kIU	kilo international units
KSFM	keratinocyte serum-free medium
l	litre
M	mole
mg	milligrams
min	minutes
ml	millilitre
mm	millimetre
mM	millimole
MSBL	minipig bladder
MSC	mesenchymal stem cells
MSHL	minipig ureter
MTS	3-(4,5-dimethyl-thiazol-2-yl)-5-(3-carboxymethoxyphenyl)-2-(4-sulfophenyl)-2H-tetrazolium
MTT	3-(4,5-dimethyl-thiazoyl-2-yl)2,5 diphenyl-tetrazolium bromide
n.a.	not available
ng	nanograms
nm	nanometre

OD	optical density
p	passage
PBS	phosphate-buffered saline
PFA	paraformaldehyde
PGA	polyglycolic acid
PKH	Paul Karl Horan
PLGA	poly (lactic-co-glycolic acid)
Prol	proliferation
PUC	porcine urothelial cells
RT	room temperature
s	seconds
SIS	small intestinal submucosa
Strat	stratification
Tab.	table
TE	tissue engineering
UC	urothelial cells
UK	United Kingdom
US	United States
V.	vena
VEGF	vascular endothelial growth factor
Vol	volume
vs.	versus
Vv.	venae
v/v	volume to volume
w	with
w/o	without
WST	water-soluble tetrazolium salt
XTT	2,3-bis(2-methoxy-4-nitro-5-sulfophenyl)-5-[(phenylamino)carbonyl]-2H-tetrazolium hydroxide)
ZO	zonula occludens
µg	micrograms
µl	microlitre
µm	micrometre
Ω	ohm

1 Summary

Tissue engineering (TE) is a new therapeutic approach to cope with the lack of donor organs or tissues. It aims to create organ substitutes to improve the function of the recipient's organ or to replace it. The three basic principles of TE comprise the use of: 1) isolated cells or cell substitutes, 2) signal molecules that promote cell proliferation such as growth factors and 3) matrices i.e. natural or synthetic scaffolds. Using biomaterials as scaffolds, autologous cell-based transplants can be stabilised and consequently, a solid artificial organ can be constructed in vitro.
This investigation was supposed to verify the suitability of a cell seeded collagen based scaffold (collagen cell carrier - CCC) to repair urethral lesions especially urethral strictures as an innovative therapeutic concept. Therefore, viability and proliferation of human and porcine urothelial cells as well as their adherence on the new cell carrier were examined. In vivo biocompatibility was tested by ectopic transplantation in nude rats and finally, cell seeded collagen matrices were applied in minipigs' urethras after induction of a urethral stricture.
In vitro as well as in vivo investigations proved the excellent suitability of CCC as a cell carrier to create artificial autologous urothelial transplants. Metabolic activity and proliferation of urothelial cells as well as their adherence on CCC were comparable to plastic seeding when high numbers of cells were used. The nude rat model and the minipig model proved the biocompatibility, integration, and degradation of the cell-matrix constructs in vivo.
Hence the results of this study are of greatest value for future therapeutic options for urethral strictures and lay the foundations for potential clinical application.

1 Zusammenfassung

Tissue Engineering (TE) ist ein neuer therapeutischer Ansatz, um dem Mangel an Spenderorganen oder -geweben gerecht zu werden. Er zielt darauf ab, Ersatzorgane herzustellen, um die Organfunktion des Empfängers zu verbessern oder zu ersetzen. Die drei Grundprinzipien des TE beinhalten die Nutzung von: 1) isolierten Zellen oder Zellersatz, 2) Signalmolekülen wie Wachstumsfaktoren, die die Zellproliferation fördern und 3) Matrices, das heißt natürlichen oder synthetischen Trägermaterialien. Durch die Nutzung von Biomaterialien als Trägermaterial können autologe zellbasierte Transplantate stabilisiert werden und damit ein strapazierfähiges künstliches Organ in vitro hergestellt werden.

Mit dieser Untersuchung sollte die Tauglichkeit eines zellbesiedelten kollagenbasierten Gerüsts (collagen cell carrier - CCC) geprüft werden, Harnröhrenläsionen insbesondere Harnröhrenstrikturen als innovatives Therapiekonzept zu beheben. Dazu wurde die Viabilität und Proliferation humaner und porciner Urothelzellen ebenso wie deren Adhärenz auf dem neuen Zellträger untersucht. In vivo wurde die Biokompatibilität durch ektopische Transplantation im Nacktrattenmodell getestet und abschließend wurden zellbesiedelte Kollagenmatrices nach Induktion einer Harnröhrenstriktur in die Harnröhre von Minipigs eingesetzt.

Sowohl die in vitro als auch die in vivo Daten belegten die exzellente Tauglichkeit von CCC als Trägermatrix zur Konstruktion artifizieller autologer Urotheltransplantate. Wurde eine große Anzahl an Zellen verwendet, so waren die metabolische Aktivität und Proliferation als auch die Adhärenz auf CCC vergleichbar mit der bei Aussaat auf Plastik. Das Nacktrattenmodell und das Minipigmodell wiesen die Biokompatibilität, die Integration und die Degradation der Zell-Matrix-Konstrukte in vivo nach.

Damit sind die Ergebnisse dieser Studie von größter Bedeutung für die zukünftigen Therapiemöglichkeiten von Harnröhrenstrikturen und legen den Grundstein für die potentielle klinische Anwendung.

2 Introduction

2.1 New concepts in regenerative medicine

The need for new alternative therapy approaches in regenerative medicine is enormous: Organ donation cannot meet the requirements for transplants and current therapies often do not provide satisfying solutions with regard to the long-term outcome (LANGER & VACANTI, 1993). Compromises have to be made to arrange for an adequate individual therapy that can never achieve a total remission leading back to the original physiological state. Furthermore, organ donation does not provide a therapeutic opportunity for certain indications e.g. urethral damage. Therefore, new therapies are under investigation aiming to restore tissue that anatomically and functionally corresponds to the original.

Tissue engineering (TE) is an interdisciplinary approach that combines life sciences with engineering and the ultimate goal is to design new organs or tissues that can restore, maintain or improve physiological function (FUCHS et al., 2001). The restoration and therewith the functional recovery of the relevant organ or tissue shall lead to an enhanced surgery outcome as well as improved patient satisfaction. Therefore, it is a promising technique for reconstructive surgery in the 21st century. Although TE has been rapidly evolving throughout the last years and numerous experimental trials have been conducted, the transfer into the clinical routine has not yet been realised.

Concerning the basic methodical approaches of TE, some research groups favour synthetic or natural scaffolds while others work on cell-based therapies or the combination of both (cell seeding of materials). Biomaterials or artificial scaffolds used for reconstruction primarily have to feature the following properties: biocompatibility, no immunogenicity, sufficient mechanical stability, support of cell growth and angiogenesis, and preferably biodegradability (FUCHS et al., 2001;WÜNSCH et al., 2005). Tissue-engineered transplants have to guarantee integration into the host and sufficient functional substitution of the original tissue without evoking distinct inflammatory reactions. Furthermore, they should be producible off-the-shelf and economically efficient. Besides biocompatibility and immunogenicity issues, the lack of neovascularisation and nerve ingrowth often limits sustained success (FEIL et al., 2011). For autologous approaches donor site morbidity can impair integration and incorporation into the host.

In contrast to numerous visions being pursued for the introduction of TE techniques in routine clinical use in human medicine, TE is still in its infancy in veterinary medicine. In fact, stem cells are currently the most important research field. Anyhow, it is gaining more importance on the one hand in terms of animal models for human medicine and on the other hand for the treatment of musculoskeletal disorders in horses and dogs (KOCH et al., 2009; RIBITSCH et al., 2010; FORTIER & TRAVIS, 2011).

2.2 <u>The urethra</u>

2.2.1 Anatomy and physiology of the human urethra

The urethra is part of the lower urinary tract and develops from the middle and lower section of the urogenital sinus, that also generates the bladder and genital glands (SÖKELAND et al., 2008). The blood supply and drainage come from branches of the Aa. and Vv. pudendae.

There are three **tissue layers** to be distinguished within the urethra: the mucosa, the muscular layer, and the adventitia. The innermost coating consists of the epithelium with subepithelial blood vessels, glands, and connective tissue underneath (lamina propria). The proximal urethra is coated with urothelium which passes into a multilayer isoprismatic (pseudostratified) and then into a squamous epithelium at the distal end of the urethra. The subsequent muscular tissue is built of smooth muscle forming the internal urethral sphincter (IUS) muscle and partially striated muscle (external urethral sphincter, EUS). Another layer of connective tissue forms the outside of the urethra (HAUTMANN, 2010).

In males the urethra can be divided into three parts, the prostatic (Pars prostatica), membranous (Pars membranacea), and the penile, bulbar, or spongy urethra (Pars spongiosa/cavernosa) and reaches about 22 cm of length (KOHLER et al., 2008). Others distinguish a fourth, the preprostatic part (PETERSEN, 1992) or even six different sections: bladder neck, prostatic, membranous, bulbar, penile, and fossa navicularis (YIEE & BASKIN, 2010). The intersection of the bladder and the urethra forms the IUS, a circular smooth muscle portion playing an important role in the continence mechanism. The spermatic duct and the prostatic ducts enter the urethra in the prostatic part. The EUS muscle is a striated muscle formed by the membranous section of the urethra. It covers the ventral side of the prostate and displays an omega-shaped structure around the urethra with the opening on the dorsal side. Anyhow, the muscle fibres meet at the dorsal side of the urethra, partly forming a circular muscular coating (WALLNER et al., 2009). Being mobile and surrounded by the corpus spongiosum and the corpora cavernosa the penile section is also called Pars pendulans or Pars liber (SÖKELAND et al., 2008). The ducts of the urethral or periurethral glands (also Littré glands) and the bulbourethral gland (also Cowper's glands) enter in the spongy urethra. Persisting inflammations alongside these ducts can cause urethral strictures (RÖDDER et al., 2006). While passing the prostate the urethra curves 35-40° ventrally and almost 90° during its passage through the pelvis. This constitutes the narrowest point of the male urethra and can evoke problems in catheterisation and endoscopy of the bladder (PRADIDARCHEEP et al., 2011).

In females the urethra is much shorter achieving an average length of 3.8 ±0.3 cm (MACURA et al., 2004). Here, the IUS and EUS are integrated into the pelvic floor muscles. The EUS consists of a superior omega-shaped part adjacent to the bladder with the opening on the dorsal side and an inferior part without contact to the bladder. The superior part covers the ventral and lateral side of the urethra while the inferior part covers the ventral and lateral side of the urethra and the lateral aspect of the vagina. This latter part is also known as the urethrovaginal sphincter. The EUS has no bony contacts but is attached to the levator ani muscle by a tendinous connection. The IUS forms a circular coating analogous to the male urethra in the superior part (WALLNER et al., 2009).

2.2.2 The urothelium

Urothelium covers the renal pelvis, ureter, bladder, and proximal parts of the urethra. In contrast to the renal pelvis/ureteral urothelium, which is mesoderm-derived, the bladder/urethral urothelium is of endodermal origin (WU et al., 2009). Urothelium is known as a typical transitional epithelium meaning that all cells are in contact with the basal membrane. However, electronic microscopy and immunohistological studies have revealed that this is not the case. In fact, it consists of a basal layer, intermediate cell layers, and a superficial cell layer (PRADIDARCHEEP et al., 2011). The topmost layer is constituted by the so-called “umbrella cells”, which are known as highly differentiated cells that do not extend to the basal membrane and generate a permeability barrier between the blood and urine preventing toxic substances and electrolytes from exchange. The two potential pathways, movement through tight junctions or transcellular movement via apical membrane have to be impeded to guarantee impermeability, meaning that molecular exchange can only occur through active transport. With the transepithelial electric resistance in rabbit bladders reaching up to 75 000 Ω/cm^2 it is one of the most effective biological barriers, if not the most effective one (LEWIS, 2000). Yet, infection, radiation, or toxic chemicals leading to inflammation can significantly reduce the barrier function. With a turnover rate of app. 200 days bladder urothelium is revolving quite slowly, however, progenitor cells can be found throughout it (WU et al., 2009). Due to urothelial plaques the inner surface of the urethra and bladder is quite flexible and therewith able to adapt to changes in tension and filling level. These plaques are concave biomembrane structures on the luminal surface as well as in the cytoplasm of the superficial umbrella cells and are made of uroplakin, 2D protein crystals (WU et al., 2009). The travelling of plaques in vesicles from the surface into the cytoplasm of the umbrella cells and back is thought to account for the excellent adaptive ability of the urothelium. The luminal urothelial surface is covered with glycosaminoglycans likewise contributing to the impermeability of the urothelial barrier (LEWIS, 2000).

2.3 Urethral stricture in veterinary practice

In veterinary medicine alike in humans a urethral stricture appears first of all in male individuals, but it is still a rather uncommon event. Hence publications concerning this subject are rare. It occurs in male cats and dogs primarily as a sequela after catheterisation or surgery or in consequence of uroliths or trauma and is accompanied by stranguria, dysuria, pollakisuria, prolonged urination, and overflow incontinence. Diagnostic gold standards are retrograde urethrography and urodynamics, which is only feasible in specialist veterinary clinics (RAND, 2009). The treatment of transection injury, which can result from trauma, requires accurate and sophisticated surgery to prevent stricture formation (BOOTHE, 2000). The bypassing of the injured urethral segment can be essential for the healing process.
Urethral strictures occur **in goats and sheep** as a sequela after perineal urethrostomy. Therefore, Stone et al. tested prepubic urethrostomy in a sheep and a goat with failed perineal urethrostomy attempt (STONE et al., 1997). The goat showed stricture recurrence after two months and was euthanised. Despite survival of the sheep for three years it showed periodical urinary tract infections and finally died from renal failure due to pyelonephritis. As both animals died due to sequelae of

this procedure it cannot be recommended as a primary option. Anyhow, in cases where other techniques are not successful, an improved prepubic urethrostomy procedure could possibly lead to a relief. Based on a case report of buccal mucosa graft urethroplasty for reversal of perineal urethrostomy in a goat the authors estimated this method to be a beneficial alternative for urethral reconstruction (GILL & SOD, 2004). In small ruminants urolithiasis is a quite prevalent affliction, which can result in urethral strictures as a critical complication. In a case report of Cruz-Arambulo et al. urethral calculi were diagnosed in a male crossbreed goat-sheep that showed signs of stranguria and dysuria. Most likely these evoked chronic inflammation that led to secondary stricture formation. Positive contrast cystography, normograde urethrography, and retrograde urethrography were performed and revealed a urethral stricture in addition to other lower urinary tract defects (CRUZ-ARAMBULO et al., 2003).

In cats the urethral stricture can be assigned to the feline lower urinary tract disease/ inflammation (FLUTD/FLUTI) or feline urologic symptoms (FUS) complex, involving a symptom composite of stranguria, dysuria, pollakisuria or haematuria and mostly being idiopathic or attributed to obstructive diseases (NELSON & COUTO, 2003). Some authors include urolithiasis to the FLUTD complex, others presume idiopathic aetiology as a requirement. Cats with recurrent FLUTD episodes, in which a causal therapy is not possible, are usually ultimately treated by perineal urethrostomy to guarantee an unhindered urinary outflow. Although overall surgery outcome is favourable, stricture formation constitutes the most frequent short term complication after perineal urethrostomy (BASS et al., 2005). However, Corgozinho et al. did not observe any strictures after perineal urethrostomy in 15 cats (CORGOZINHO et al., 2007).

In case reports of Bennett et al. and Wood et al. a urethral stricture in a male and female **dog** was treated successfully with balloon dilatation (BENNETT et al., 2005; WOOD et al., 2007). Though, analogous to human medicine, urethrostomy or surgical interventions like anastomosis or grafting are more frequent. When porcine small intestinal submucosa (SIS) was used as an onlay graft for complex urethral augmentation in a dog, the stricture recurred after six months. After triple treatment by balloon dilatation the stricture was under control, but the dog remained to display mild to moderate incontinence. As the stricture was very close to the bladder outlet, this was most certainly due to damage of the sphincter structures (POWERS et al., 2010).

As urethral strictures play a much more important role in human medicine, animals are used to serve as a model organism to develop new therapeutic options. Different grafts were therefore tested in dogs for experimental purposes: When the urethral mucosa of ten female dogs was completely removed and replaced by colonic mucosa a normal voiding stream and urethra morphology was assessed in nine animals after surgery (XU et al., 2003). The histological analysis of the grafted urethras revealed that after 12 weeks the plicated surface and unilaminar cylindric epithelium of colonic mucosa had been substituted by metaplastic transitional epithelium. Grafting by dint of autologous fascia lata isolated from the thigh showed a similar outcome. Good graft survival and incorporation was assessed in all 14 dogs involved in this study (ATALAN et al., 2005).

2.4 Urethral stricture in humans

2.4.1 Epidemiology and Pathogenesis

„A urethral stricture is a scar of the subepithelial tissue of the corpus spongiosum that constricts the urethral lumen“ (MUNDY & ANDRICH, 2011). Urethral strictures have always been a common complaint but are decreasing in the last decades despite the ageing of the population. Unfortunately scientific prevalence data for urethral strictures in Germany is missing. Yet app. 2% of men who undergo intermittent self-catheterisation over two years develop urethral strictures requiring therapeutic intervention (MADERSBACHER, 2001). Estimated prevalences in the UK rise from app. 1/10 000 men under 34 years of age to over 1/1000 above 65 years (MCMILLAN et al., 1994). The US even report a rate of 0.6% for males over 65 years suffering from a urethral stricture (SANTUCCI et al., 2007).
Most strictures in the developed world are iatrogenic resulting of repeated catheterisation, transurethral surgery, cystoscopy, prostatectomy surgery, or hypospadias repair (FENTON et al., 2005; KASHEFI et al., 2008; TANG et al., 2008). Patients with strictures due to hypospadias surgery are at a higher risk to develop further complications like meatal dystopia, residual curvature, meatal stenosis or fistula formation (FISCH, 2001). Other aetiologies for urethral stricture are urethral inflammation or trauma. Strictures are also found related to lichen sclerosus disease (STACK & SCHLOSSBERG, 1998). Altogether, chemical, physical, or biological noxes can provoke a urethral stricture. Congenital strictures are rare and often accompanied by other urologic disorders like hypospadias (RÖDDER et al., 2006).

Nevertheless, the aetiology remains unknown in 30% of the patients suffering from urethral strictures (KLEVECKA et al., 2010).

Although objective data is lacking cicatricial urethral strictures in women are much less common than in men. This is probably due to the reduced length and the greater diameter of the female urethra. Anyhow, strictures appear due to radiation therapy for gynaecologic malignancies, genital trauma, previous manipulations or incontinence surgery, or urethritis (TRITSCHLER et al., 2011).

Concerning pathogenesis it was shown that in the course of a metaplasia the columnar epithelium converts into a squamous one. This epithelium featuring a reduced flexibility tends to split and crack resulting in subsequent extravasation of urine and subepithelial fibrosis (spongiofibrosis). Remaining untreated the stricture can lead to inflammatory reactions such as cystitis, prostatitis, epididymo-orchitis, or urolithiasis and recurrent infections (CHAMBERS & BAITERA, 1977). Furthermore, hypertrophy of the detrusor muscle can evolve due to the high voiding pressure (RÖDDER et al., 2006). Compared to a sound urethra, stricture tissue contains less elastic fibres and a reduced blood vessel density after traumatic injuries (CAVALCANTI et al., 2007). The reduced blood vessel density was also recognised in a minipig model of urethral stricture by Sievert et al. Moreover, it was observed that inflammatory reactions decreased in minipigs over a period of 12 weeks, whereas fibrosis increased. For human stricture tissue a collagen I:III ratio of 4.8:1 was found in comparison to 1.9:1 for sound urethral tissue (SIEVERT et al., 2012).

The patients are confronted with symptoms of lower urinary tract obstruction such as hesitancy, poor streaming, terminal dribbling, and/or a feeling of incomplete bladder emptying (post void residual volume). Thus, a detailed anamnesis and urine analysis are first diagnostic steps. Further diagnostic proceedings to be performed are urinary flow rate study, a symptom score system, and possibly ultrasonography, retrograde urethrogram, voiding cystogram, or cystoscopy (MUNDY & ANDRICH, 2011). Hereby not only the presence but also the localisation and length of the stricture can be specified as well as the grade of spongiofibrosis. Uroflowmetry, analysing the urine flow rate (the quantity of fluid voided per unit of time) within the urinary outflow tract during micturition is a helpful advice to classify the severity of the outlet obstruction.

2.4.2 Current therapies

2.4.2.1 Non-invasive or minimally invasive procedures

Therapeutic intervention is only necessary if the patient is notably affected by the symptoms such as severe voiding problems, pain, discomfort or recurrent urinary tract infections. In an acute inflammatory situation it can be helpful to rest the urethra by installing a suprapubic catheter for a certain period of time before definite treatment (MUNDY & ANDRICH, 2011).

The current curative and palliative treatment can be distinguished into instrumental methods and urethroplasty. **Direct vision internal urethrotomy** (urethrotomia interna according to Sachse) is the gold standard for patients being treated for urethral stricture for the first time and for short uncomplicated bulbar strictures as well as palliative treatment, though relapses are common (NAUDE & HEYNS, 2005; MUNDY & ANDRICH, 2011). On average 68% of the patients experience stricture recurrence (ENGEL & FISCH, 2010). Furthermore, urethrotomy can involve extravasation or infective complications (DESMOND et al., 1981). According to Rödder et al. 50-60% of the patients do not need further treatment after urethrotomy (RÖDDER et al., 2006). **Dilatation** of the urethra is also indicated in simple and short strictures in the bulbar urethra or can be used for palliative stricture management (MUNDY & ANDRICH, 2011). A different principle was pursued by the implantation of **urethral stents**, but in most cases they do not lead to a good long-term outcome concerning patient satisfaction (DE VOCHT et al., 2003). In a retrospective study complications like dribbling, recurrent urinary tract infections, obstruction, stent hyperplasia, stricture, stent encrustation, or urolithiasis occurred in 55% of the cases (HUSSAIN et al., 2004). For this reason they should not be part of the current therapeutic management of urethral strictures.

2.4.2.2 Open surgery

Most patients with severe strictures require open surgery as primary intervention or after failed urethrotomy to achieve freedom of affliction. Reconstructive surgery consists of excision and reanastomosis for short strictures or graft implementation (HAUSER et al., 2010). **End-to-end anastomosis** can be accomplished in bulbar or membranous strictures with a maximum of 2 cm of length and features a success rate over 85% over 10 years if performed with strict indication (RÖDDER et al., 2006). Al-Qudah and Santucci state that urethroplasty in general involves early complications in 40% and late complications in 48% of the patients though most remain minor (AL-QUDAH & SANTUCCI, 2005). This study comprised the main surgical techniques: anterior anastomosis, ventral onlay buccal mucosa, fasciocutaneous flap, and posterior anastomosis with mean follow-up of 29 months. For the **fasciocutaneous flap technique** a hairless transplant of skin and fascia is placed into the urethra in an onlay fashion. Most frequent complications after flap urethroplasty with penile shaft skin or foreskin are skin necrosis or fistulae (RÖDDER et al., 2006). While these flap techniques were routinely used in the past, today the use of **buccal mucosa** is the method of choice for long or complicated strictures. Nowadays favourable results with success rates about 85-96% (ventral vs. dorsal onlay) are achieved (BHARGAVA & CHAPPLE, 2004). However, complications can occur primarily during the first 12 postoperative months after ventral onlay graft surgery (FICHTNER et al., 2004). These comprise early complications like extravasation, inflammation, haematoma or micturition disorders and late complications like fistula or diverticulum formation, stricture recurrence, erectile dysfunction or incontinence (ENGEL & FISCH, 2010). Furthermore, donor site morbidity such as haemorrhage, infections, pain, swelling, damage to the parotid duct, reduced sensation, or numbness are common events (BHARGAVA & CHAPPLE, 2004). **Meshgraft** urethroplasty requires a two-step procedure and can be successful in complicated, long, and recurring strictures (RÖDDER et al., 2006). Combinations of different surgery procedures can be used when patients suffer from multiple disorders.

In contrast to male stricture repair females cannot be treated by stricture excision and end-to-end urethroplasty due to the shortness of the female urethra. Thus, therapeutic approaches consist in endoscopic incision or flap urethroplasty by dint of autologous fascia (ROSENBLUM & NITTI, 2011).

Beside the relatively frequent appearance of relapses, the aforementioned risks and the fact that some patients simply cannot provide an autologous graft make an alternative therapy with comparable success rates essential.

2.5 Tissue engineering for the treatment of urethral strictures

2.5.1 Different scaffolds for urethra repair

Different biomaterials are used for TE of the urethra. Depending on the respective reference and structural texture they are called scaffolds or matrices and can be of natural origin or synthetic materials. While synthetics like polyglycolic acid (PGA) can be standardised and modified according to the physician's requirements, naturally derived biomaterials are often superior regarding biocompatibility and degradability. Different scaffolds for TE of the urethra were tested by Feng et al. to evaluate their stability and biocompatibility. Bladder acellular matrix graft (BAMG), SIS, acellular corpus spongiosum matrix (ACSM), and PGA all turned out to be suitable for urethroplasty and did not cause cytotoxic effects on smooth muscle cells. Concerning stability SIS, BAMG, and PGA had similar biomechanical properties to native rabbit urethra while ACSM even proved superior. Although pore size was biggest in PGA (>200 μm) a confluent cell layer did not develop on this matrix. On the other hand pore size did not allow for a sufficient infiltration on BAMG but multilayer cell growth was observed (FENG et al., 2010).

Another study for evaluation of biocompatibility, stability, and cell morphology on commercially available biomaterials concluded that most materials showed better stability than native urothelium (WÜNSCH et al., 2005). In fact, cells grown on biogenic membranes resembled native urothelium meaning that they formed flat cell layers with many cell-cell contacts. When fibroblast and epithelial cell growth was evaluated on 13 different naturally derived scaffolds, Brehmer et al. showed that cell growth differed depending on the structure of the biomaterial used (BREHMER et al., 2007). While cells grown on carrier-type scaffolds only formed a closed superficial layer, those grown on fleece-type ones showed ingrowth into the scaffold but did not form a complete epithelium. Sponge-type scaffolds provoked both ingrowth of cells and the formation of adherent epithelium. Table 1 gives an overview of different materials for bladder repair purposes modified according to Brehmer et al.

Table 1: Overview of different scaffolds for bladder repair modified according to Brehmer et al.

Scaffold Type	Definition	Examples	Pore size [µm]	Manufacturer
Carrier-type scaffold	Small pore size, no ingrowth of cells	Equine collagen mixture	0-100	CliniCare
		Bovine collagen mixture	n.a.	Innocoll
		Porcine collagen	n.a.	Bard GmbH
		Human fascia lata explant	n.a.	Mentor
		70% collagen, 30% elastin membrane	0-25	Bioplex Medical, BV
		Small intestinal submucosa	10	Cook
Fleece-type scaffold	Fibre construction, huge pore size	PGA fleece	0-200	A. Atala, Boston Mass., USA
		Cellulose fleece	n.a.	Ethicon GmbH
Sponge-type scaffold	Pore size between 20 and 40 µm	Bovine collagen I sponge	26	Helmholtz Institute, RWTH Aachen
		Bovine mixed collagen sponge	10-60	ICN Biomedicals Inc.

2.5.1.1 Small intestinal submucosa

SIS is retrieved from porcine jejunum in which the tunica mucosa is mechanically removed from the inner surface as well as tunica muscularis and serosa from the outer surface. The product of this procedure is a thin translucent graft, mainly consisting of submucosal tissue. As SIS was shown to be non-immunogenic it was experimentally used for several urologic applications with varying success (CHENG & KROPP, 2000). While SIS was prepared autonomically in each laboratory in early studies, it is now commercially available as a solid or injectable material and has been applied in different fields of TE.

In 1998, SIS was prepared in the laboratory, used as an onlay graft in **rabbit** urethras and compared to preputial skin grafts and sham operations (urethrotomy only). All animals treated by preputial skin grafts developed urethral diverticula whereas none of the SIS treated ones did. The SIS graft group revealed superior regeneration compared to the preputial skin graft group with the regenerated urethra containing three to four layers of urothelium. The main difference of the SIS grafted urethras

from the untreated regions was the presence of less smooth muscle content (KROPP et al., 1998).
Although SIS prepared in the laboratory did not seem to induce cytotoxic effects on smooth muscle cells (FENG et al., 2010), reduced cell growth was observed when seeding urothelial cells (UC) on commercially available SIS (WÜNSCH et al., 2005). After incubation of porcine urothelial cells (PUC) with SIS conditioned medium, Feil et al. even observed cytotoxic effects. Cell viability being assessed via WST-1 assay declined to zero. In addition residual porcine DNA was discovered in this commercial SIS, which makes it ineligible for human application (FEIL et al., 2006).
When rabbits were treated by graft urethroplasty with either onlay or tubularised elastin or self-made SIS, both materials revealed superior when they were used as an onlay graft. Tubular grafts induced inflammation and fibrosis and led to a significantly reduced urethral diameter after three months (XIE et al., 2007).
Self-made SIS proved superior in animal studies, which could be due to the sterilisation or manufacturing processes. However, **clinical approaches** with commercial SIS partially showed promising outcomes: In a clinical trial 20 men suffering from a urethral stricture with a length of 2-8 cm were treated by onlay/inlay graft urethroplasty with unseeded SIS. Seventeen patients (85%) were successfully cured and did not require further treatment after surgery at a mean follow-up of 21 months whereas the remaining three displayed stricture recurrence within three months after surgery (PALMINTERI et al., 2007). In a different study with 50 patients treated by SIS graft urethroplasty and a median follow-up of 31 months results were equally promising (FIALA et al., 2007). With an 80% cure rate the outcome was similar to the Palminteri study.
SIS grafts could be a viable alternative in short and uncomplicated strictures in a one-layer design but seem to fail when the stricture length exceeds a certain calibre and the urethral bed is pathologically altered (e.g. spongiofibrosis). Sievert et al. also assessed that SIS grafts could be beneficial in selected cases and observed a positive outcome in 9 of 13 patients (SIEVERT et al., 2005). In a consecutive study with five patients with a mean stricture length of 9 cm SIS grafts did not lead to a satisfying result (HAUSER et al., 2006). Extravasation, urinary tract infections, and severe urethritis were observed in addition to recurrent stricture in four of them. When used as a tubular graft in nine patients, the procedure was not successful either (LE ROUX, 2005). Only two of them maintained urethral patency after surgery.

In summary, the success of SIS in urethroplasty seems to be heavily dependent on the initial situation regarding the stricture (length, urethral bed, spongiofibrosis, inflammation, scarring, etc.) and the surgical method (onlay vs. circumferential graft).

2.5.1.2 Acellular matrix grafts

Different animal trials as well as clinical studies have been performed on matrices derived from the bladder and urethra. For preparation of matrix grafts, the urethral or bladder tissue is retrieved from either a homologous or a heterologous source and decellularised by chemical and/or enzymatic treatment (SIEVERT & TANAGHO, 2000).

When heterologous (dog) and homologous acellular urethral matrix grafts were used for urethroplasty in **rabbits**, there was no significant difference between the two grafts and untreated controls with regard to urodynamic functionality and urethrography after eight months. Complete epithelialisation was observed in homologous grafts. Although smooth muscle content was less in dog urethras than in homologous grafts, there were no signs for significant inflammation or tissue rejection in both groups. In the tissue specimens of homologous graft treated rabbits, blood vessel and smooth muscle ingrowth was observed already after ten days (SIEVERT et al., 2000; SIEVERT et al., 2001).

In a different experimental trial urethroplasty was performed in 18 rabbits with either unseeded BAMG or seeded biomaterial with epidermal cells from the foreskin. After histological and immunohistological investigation seeded scaffolds revealed superior. Eight of nine animals that received unseeded material developed strictures at the transplantation site whereas none of the seeded group did (FU et al., 2008). The enhanced regeneration in tubularised seeded acellular matrix grafts in contrast to unseeded scaffolds was determined in an earlier study with smooth muscle and epithelial cells in ten rabbits (DE FILIPPO et al., 2002). A different study claimed that urethral repair with unseeded matrices led to a satisfying cure when the replaced segment did not exceed 0.5 cm (DORIN et al., 2008).

In a **clinical trial** of El-Kassaby et al. 28 patients suffering from a urethral stricture were treated by urethroplasty with unseeded human BAMG. The outcome was evaluated by medical history, physical examination, retrograde urethrography, cystoscopy, and uroflowmetry and revealed clinical improvement in 24 patients after surgery although urethral repair was performed in segments reaching up to 16 cm.

After a mean follow-up of 37 months urethrography showed wide patent urethras in these patients and average and mean maximum flow rates were increased considerably (EL-KASSABY et al., 2003). However, it is noteworthy that the group of patients was highly selected in this study.

A recent clinical study with 30 patients revealed that the use of acellular bladder matrix does not provide an alternative to buccal mucosa urethroplasty for patients with previous surgical interventions (EL-KASSABY et al., 2008). The patients were divided randomly into two groups receiving either buccal mucosa transplants or BAMG. The outcome was assessed depending on the number of previous interventions and therewith on the presence of spongiofibrosis and the quality of the urethral mucosa. Patients showing physiological voiding pattern with steady stream at a mean follow-up of 25 months were considered as successful outcomes. Results concerning urethrography and uroflowmetry were comparable in patients with healthy urethral beds. However, buccal mucosa transplantation was superior to BAMG in patients with previous interventions and consequential urethral damages. In this group 66.7% of BAMG surgeries were not successful and required further treatment. While the length and location as well as the duration and the aetiology of the stricture did not have an impact on the therapeutic success, the quality of the urethral bed (fresh and vascular mucosa, no signs of spongiofibrosis) seemed to be crucial for the clinical outcome.

The contrast between poor results of certain BAMG surgeries with unseeded matrices in the rabbit and good results in clinical studies may be explained by the degree of urethral damage, the surgical method, and perioperative management. Currently, there are no clinical studies using seeded BAMG. Anyhow, deductive to data of animal experiments seeded matrices might reveal superior than unseeded ones in a clinical setting.

2.5.1.3 Other collagen based scaffolds

Collagen membranes have already been discussed as graft material for urologic purposes in the 80ies (GORHAM et al., 1984). First in vitro experiments have been performed to evaluate its permeability to urine, stability, and influence on the formation of urinary crystals. Though, crystal formation was observed after six days of incubation in urine the authors assume that this could have been due to the experimental conditions and may not appear in vivo.

In a **rabbit** urethroplasty study a defined collagen biomatrix (based on bovine tendon) was compared to unseeded SIS and both turned out to be suitable materials for urethra grafting with similar results concerning urothelial and smooth muscle regeneration. The histological and immunohistological analysis was performed one, three, and nine months after the grafting procedure. Nevertheless, smooth muscle regeneration in the grafted parts was extremely poor in all groups with only single smooth muscle cells identified after nine months (NUININGA et al., 2003). In a later study urethroplasty was performed using a tubular type I collagen biomatrix with and without growth factors. Rabbits which received a graft supplemented with growth factors showed relative narrowing of the urethra or diverticula. However, the formation of organised urothelium, capillaries, and glands was superior in the growth factor group (NUININGA et al., 2010). This study advises to modify the collagen scaffold in a way that an excellent functional outcome can be merged with satisfying smooth muscle and urothelial regeneration as well as blood vessel and gland density.

Based on their comparison of different scaffolds for TE of the urethra Feng et al. performed urethroplasty in 18 rabbits with seeded and unseeded ACSM. Corpus spongiosum matrix was isolated from porcine penile tissues and a 3D neo-urethra was constructed by seeding lingual keratinocytes and smooth muscle cells. Matrices seeded with both cell types displayed a multilayer urothelium and organised muscle bundles at six months after surgery while unseeded ACSM evoked inflammation and did not induce sufficient epithelial and muscular regeneration (FENG et al., 2011).

Transplants of urothelial cells on collagen were tested in a **clinical study** for hypospadias repair in six boys (FOSSUM et al., 2007; FOSSUM & NORDENSKJÖLD, 2009; FOSSUM & NORDENSKJÖLD, 2010). In a first procedure UC were extracted by bladder washings and in a second step the boys were treated with autologous UC/collagen scaffold in an onlay graft technique. All displayed excellent results at mean follow-up time of 7.25 years with respect to cosmetic appearance, urinary flow curves, erection, and histology. Yet, postoperative complications like fistulae and strictures occurred in four of six patients.

2.5.1.4 Synthetic matrices

Synthetics feature different advantages in comparison to naturally derived materials. They can be produced according to a strict standard, do not hold the risk of infectious agents and are constructed to build an impermeable urine-blood barrier replacing the urothelium. The most commonly used and best known synthetic materials for urologic TE purposes are PGA and poly (lactic-co-glycolic acid) (PLGA).

In an **in vitro** approach of Selim et al. (SELIM et al., 2011) the best method of sterilisation for PLGA seeded with buccal mucosa cells was investigated. Although mechanical properties were impaired, regardless of the used method, fibre diameter was not significantly reduced by γ-irradiation. Treatment with both peracetic acid and γ-irradiation were suitable methods for sterilising PLGA scaffolds that remained sterile for over three months in antibiotic-free culture medium.

Kundu et al. generated thin polymer matrices of three different synthetic substances by electrospin coating directly onto thin films. These composite scaffolds with films on the luminal surface were compared to the same electrospun materials alone and commercially available SIS. Adherence and proliferation of human urothelial cells (HUC) on the composite scaffold consisting of thin films attached to a highly porous fibrous matrix turned out to prove best. Also the barrier function, which was assessed by a permeability assay, was superior than in the other two test groups (KUNDU et al., 2011).

A recent **clinical study** for urethral reconstruction in five patients resulted in satisfying outcome measurements (RAYA-RIVERA et al., 2011). Here a PLGA - PGA scaffold tube seeded with autologous urothelium and muscle cells was used for urethroplasty in five boys aged 10-14 years. Histological examination of regular biopsies revealed sound urethral architecture with epithelial and smooth muscle layers within the engineered section. Urodynamics as well as radiographic and endoscopic analysis showed wide urethral calibres without strictures for at least 12 months after surgery. Although patient satisfaction was good at a median long-term follow-up of 71 months, this study must be judged critical. Patient number was very low, the bridged lengths are unknown, and in addition regular biopsies were performed in the children.

2.5.2 Cell-based therapies

For several years UC are cultivated and stratified successfully and cell sheets have been constructed **in vitro** (MAURER et al., 2005). Cells are routinely harvested from bladder or ureter biopsies, but new findings suggest that retrieval could prospectively be realised by bladder washings, which are much less invasive (FEIL et al., 2008a; NAGELE et al., 2008).

Fossum et al. created a three-layer substitute for the lower urinary tract consisting of UC, fibroblasts, and smooth muscle cells seeded in a "sandwich manner" (FOSSUM et al., 2004). Indeed, co-culture of the three different cell types was feasible and the preservation of the respective phenotype was confirmed immunohistologically. Anyhow, animal experiments are pending and it remains open why this concept was not further pursued in ensuing approaches of this group.

After successful implementation of a porcine urethral stricture model UC suspensions have been injected into the urethra of 12 **minipigs** for stricture repair in an experimental approach (SEIBOLD et al., 2011). Histological analysis showed that the urethra healed without severe inflammation or stricture formation after surgery. Although the labelled transplanted cells could be retrieved up to eight weeks after sacrification, they did not always remain in the urothelium, but migrated throughout other penile layers. As a result of these cell-based studies, the seeding of biomaterials is an auspicious concept and accounts for a crucial part of tissue-engineered constructs.

2.6 Objectives of this study

In the present study a TE approach mainly for the therapy of urethral strictures was investigated by using a collagen cell carrier (CCC) seeded with autologous UC as a urethral transplant. It was based on a previous study where a porcine animal model of induced urethral stricture was established (SIEVERT et al., 2012). Different methods of stricture induction were tested and thermocoagulation proved to cause a stricture displaying the greatest similarity to human stricture tissue. The stricture formation was verified by urethrography and histological analysis.

As a first step towards the development of an autologous transplant urethral stricture was subsequently treated by injection of UC suspension and application of cell sheets. Although functional regeneration was not analysed, it was hereby shown that the transplantation of autologous urothelium is feasible (SELENT et al., 2008; SEIBOLD et al., 2011). However, the cells could not be recovered exclusively in the urothelium, but throughout the corpus spongiosum and cavernosum. Furthermore, handling of the cell sheets was quite delicate due to their fragility that constitutes a main disadvantage for reconstruction techniques and open surgery. Consequently, seeding of UC on a cell carrier was now favoured to overcome these hurdles.

On account of this, a collagen matrix was tested substantially to increase the stability of bioartificial urothelium and to make it suturable and more manipulable for surgical instruments. By the use of a matrix that undergoes standardised processing and sterilisation procedures the risk of infection could be considered as excluded. Moreover, it affords the possibility to design it according to the requirements of cell culture and surgery and to industrialise its production.

The following three main questions were to be addressed by this study:

1. **Does the CCC display good in vitro properties for seeding of UC?**
   Metabolic activity and proliferation of UC seeded on CCC were compared to cells seeded on plastic surface. Adherence of UC on the CCC was investigated as well.
2. **Does the seeded CCC feature good in vivo biocompatibility characteristics in rats?**
   Human urothelial cells seeded on CCC were transplanted on the musculus rectus abdominis of nude rats as a preliminary small animal approach to assess integration and differentiation of UC, degradation of the CCC and potential inflammatory reactions.
3. **Is urethral reconstruction and functional regeneration after stricture induction in minipigs feasible by application of CCC autografts?**
   In a first intervention a urethral stricture was induced and bladder tissue was extracted for UC harvest. Then urothelial CCC transplants were constructed and autologous grafts were inserted in the urethra to assess the feasibility of this approach prior to clinical application.

3 Methods

3.1 In vitro investigations

3.1.1 Isolation and culture of urothelial cells

3.1.1.1 Isolation of human urothelial cells

After approval of the local ethical committee at the University of Tuebingen and consent of patients ureter tissue samples were collected from adult patients (aged 29-74 years) undergoing open nephrectomy at the Department of Urology of the University Clinics of Tuebingen. Tissue was transported to the Laboratory for Tissue Engineering and stored at 4°C in transport medium until further processing modified according to Southgate et al. (SOUTHGATE et al., 1994). The transport medium's main component was Hank's balanced salt solution (HBSS) containing 0.35 g/l $NaHCO_3^-$ and phenol red but no Ca^{2+} and Mg^{2+} (Biochrom). Furthermore, 10 mmol/l HEPES (Gibco), 20 kIU/ml aprotinin (Bayer AG), and 1% penicillin/streptomycin (Gibco) were added.

All isolation steps for HUC were performed under sterile conditions. After fat residues and stromal tissue were removed aseptically, the ureter specimens were opened by a pair of scissors and separated into pieces of 1-2 cm^2. Tissue pieces were incubated in a 50 ml BD Falcon conical tube (BD Biosciences) filled with 15 ml of "stripping solution" consisting of HBSS buffered with 10 mmol/l HEPES, 20 kIU/ml aprotinin (Bayer AG), and 1% ethylenediaminetetraacetic acid (EDTA, Biochrom) for 3 h at 37°C and 5% CO_2. The HUC were then gently scraped off from the stroma using a cell scraper (Corning Inc.) and transferred into complete keratinocyte serum-free medium (cKSFM, see below) in a BD Falcon conical tube (BD Biosciences) followed by centrifugation at 250 g for 5 min at room temperature (RT). The cells were resuspended in cKSFM which is keratinocyte serum-free medium (KSFM), supplemented with 50 µg/ml bovine pituitary extract (BPE), 5 ng/ml human recombinant epidermal growth factor (EGF, all Gibco), and 30 ng/ml cholera toxin (LIST Biological Laboratories Inc.). Subsequently the isolated cells were seeded into 25 cm^2 culture flasks with CellBIND surface (Corning Inc.). The cultures were maintained at 37°C in a humidified atmosphere with 5% CO_2. The cell culture medium was replaced the following day and thereafter every other day.

3.1.1.2 Subculture of human urothelial cells

For further passaging medium was removed from subconfluent HUC cultures and the cells were incubated in phosphate-buffered saline (PBS) without Ca^{2+} and Mg^{2+} (Gibco) containing 0.1% EDTA (Biochrom) at 37°C for 5-10 min until the cells rounded and separated from each other. Thereafter the PBS/EDTA solution was aspirated and cells were exposed to TrypLE Express (Gibco) for one min at 37°C. By thorough agitation HUC were detached from the surface of the culture flask. After transferring the cells into cKSFM in a BD Falcon conical tube (BD Biosciences) a centrifugation step at 250 g for 5 min followed. The supernatant was aspirated and the cells were carefully resuspended in cKSFM and hereby ready to be distributed into flasks or seeded in well plates. To subculture the cell suspension was splitted at a ratio of 1/2 or 1/3 (v/v) referred to the original cell volume and seeded into new CellBIND culture flasks (Corning Inc.). At least 3 h later or on the following day when cells had attached to the flask's surface further medium was added.

3.1.1.3 Culture of porcine urothelial cells

PUC were obtained from bladder biopsies and ureter specimens of minipigs. Tissue preparation, cell isolation, and culture were performed according to HUC with modifications (table 2). Established primary PUC cultures were retained in liquid nitrogen and thawed for the in vitro assays according to requirements. After thawing (see below) PUC were cultured according to HUC.

For further cultivation subconfluent cell layers were passaged by first washing them with PBS without Ca^{2+} and Mg^{2+} and then incubating in 0.25% Trypsin (both Gibco) at 37°C for 4 min. The detached cells were collected in cKSFM supplemented by 10% fetal calf serum (FCS, Gibco) centrifuged at 250 g for 5 min and resuspended in cKSFM without FCS. Cells were seeded into CellBIND culture flasks (Corning Inc.) at a splitting ratio of 1/2 or 1/3.

Table 2: Comparison between isolation and cell culture technique of HUC and PUC

Operation step		HUC	PUC
Preparation		-	Detachment of mucosa (only porcine bladder specimen)
Incubation in stripping solution		3 h	2 h
Passaging	Preincubation/Washing	PBS w/o Ca^{2+} and Mg^{2+}/ 0.1% EDTA	PBS w/o Ca^{2+} and Mg^{2+}
	Cell Detaching	TrypLE Express	0.25% Trypsin
	Trypsin Neutralisation	-	cKSFM/10% FCS

3.1.2 Cryoconservation of urothelial cells

All urothelial cells, which have been used for in vitro assays, were frozen after isolation and thawed according to requirements. For freezing cells were detached from the culture flasks as described in chapter 3.1.1. After centrifugation at 250 g for 5 min cells were resuspended in ice-cold freezing medium containing 50% cKSFM, 40% FCS (Gibco), and 10% dimethylsulphoxide (DMSO, Sigma-Aldrich Chemie GmbH).

Cells harvested from one 75 cm^2 tissue culture flask were distributed into three cryo tube vials (Nunc GmbH & Co. KG) at 1 ml each. After resuspending the cells in freezing medium the vials were immediately transferred in a freezing container (Thermo Fisher Scientific GmbH) containing isopropanol at -80°C overnight to be placed in liquid nitrogen on the next day.

For thawing, vials were placed in a water bath at 37°C until defrosting and cells were suspended in cKSFM in a BD Falcon conical tube (BD Biosciences). After centrifugation at 250 g for 5 min cells were resuspended in cell culture medium and seeded into CellBIND culture flasks (Corning Inc.). Two vials were seeded into one 75 cm^2 flask. Further medium was added on the following day.

3.1.3 Counting of living cells by trypan blue staining

Trypan blue is a vital stain that allows to distinguish dead cells from living cells. As a diazo dye it incorporates selectively into the cell membrane of dead cells while intact membranes are not coloured.

Cells were harvested as described before (see chapter 3.1.1), transferred in a BD Falcon conical tube (BD Biosciences), centrifuged at 250 g for 5 min and resuspended in cKSFM. An aliquot of cell suspension was diluted 1/2 (v/v) in trypan blue (Lonza Walkersville Inc.) in a 96-well Cellstar round bottom TC-plate (Greiner Bio-One GmbH). A Neubauer counting chamber (Glaswarenfabrik Karl Hecht GmbH&Co KG "Assistent") was loaded with the stained cells. The uncoloured living cells of the four edge quadrants were counted with a binocular microscope. After calculation of the average number of cells per quadrant and multiplication by the correction factors for chamber size (10^4) and dilution (2), the total number of viable cells per ml was determined as final value.

3.1.4 Seeding of cells on collagen cell carrier

The scaffold used in this study is an ultra-thin (20 µm in air-dried condition) collagen cell carrier (CCC, Viscofan Bioengineering) which features a biocompatible material derived from pure bovine collagen type I. It is produced on a large scale under highly standardised procedures minimising batch-to-batch variations. The mechanical stability and excellent suturability make it suitable for surgical application. Furthermore, due to its high transparency and its low autofluorescence it is the ideal material for the envisaged investigations.

For the in vitro experiments and the rodent model urothelial cells were seeded on CCC of a cross section dimension of 14 mm fitting into the wells of a 24-well plate (Fig. 1). The CCC membranes were washed three times for 5 min at 37°C in 250 µl of pre-warmed Dulbecco's phosphate buffered saline (DPBS, Biochrom) in a CellBIND 24-well plate (Corning Inc.). Then DPBS was aspirated and the scaffolds were centred flatly in the well without any wrinkles and air bubbles underneath. After overnight drying in the operating laminar flow hood with plate lid left ajar, the CCC was ready for seeding.

Prior to cell seeding the CCC was incubated in pre-warmed cKSFM for at least 30 min at 37°C. HUC or PUC were detached from the flasks as described above and seeded on the CCC in defined densities. For the in vitro assays - three parallels each - cells were seeded on CCC and on standard plastic surface as control.

For the large animal model and immunofluorescence analysis of cell-seeded CCC, UC were seeded on 6-well CCC inserts of a cross section dimension of 34 mm (Fig. 1). The preparation of the CCC 6-well inserts was conducted according to the 24-well inlays without overnight drying. The inserts were placed in a CellBIND 6-well plate (Greiner Bio-One GmbH) and washed three times with DPBS (see above). DPBS was filled in the insert (1.5 ml) and into the well (2.6 ml). Immediately after washing inserts were pre-incubated in cell culture medium and 3-4 x 10^5 cells/cm^2 were seeded on the insert-CCC.

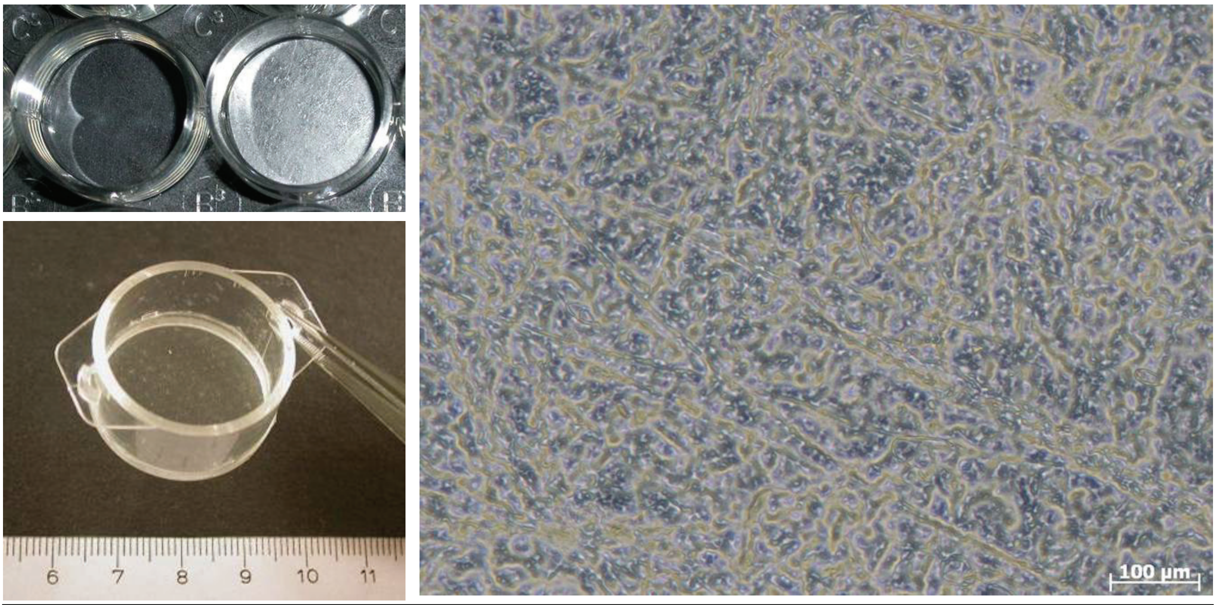

Fig. 1: CCC membrane sample in a well plate (left, top) and CCC inserts (left, below), unseeded CCC in phase contrast microscopy (right)

3.1.5 Stratification of urothelial monolayer cultures

Established monolayer UC cultures were microscopically observed for growth behaviour. The quality of the cell culture was documented photographically prior to induction of multilayer formation with the Axiovert 200 M microscope and the integrated AxioCam HRc colour camera (both Zeiss) in 10-fold magnification. At a confluence state of 100%, defined as a gap-free cell monolayer, stratification was induced by increasing the calcium concentration of the cell culture medium as follows:

For preparation of the stratification medium, the cell culture medium was supplemented with 5.5% $CaCl_2$ (Baxter Deutschland GmbH) to the final concentration of 1.09 mM/l $CaCl_2$ for cKSFM or 1.07 mM/l $CaCl_2$ for CnT-02. The proliferation medium was then removed and stratification medium was added. For ongoing cultivation the stratification medium was changed every other day. Stratification morphology was recorded photographically as described above. After app. eight days the cell sheets were ready to be used.

For harvesting multilayered human urothelial sheets from plastic surface of 6-well plates, the following procedure was performed: Dispase (BD Biosciences) was diluted in PBS w/o Ca^{2+} und Mg^{2+} (Gibco) in a ratio of 1/2 (v/v) to generate a dispase working solution of 25 U/ml. The culture medium was aspirated and 4 ml of PBS w/o Ca^{2+} und Mg^{2+} (Gibco) were added for washing. After aspiration of the washing medium the urothelial sheet was bordered with a cell scraper and swung gently in 0.5 ml dispase working solution. After incubation at 37°C and 5% CO_2 for 7-8 min the dispase solution was aspirated. The sheet was finally washed three times in 3 ml of PBS.

For harvesting cell-seeded CCC, the seeded membrane was lifted out of the well with the aid of a forceps or the matrix was cut from the insert plastic holder, respectively.

3.1.6 In vitro assays

Ten different thawed HUC lines and four different thawed PUC lines were used for all the in vitro assays while for each of the eight experimental groups at least three different primary cultures were used. Bromodeoxyuridine (BrdU) assay was performed to evaluate proliferation and water-soluble tetrazolium salt (WST)-1 assay to evaluate metabolic activity of HUC and PUC in culture passages 2-7 seeded on CCC in comparison to cells seeded on standard plastic surface.

For HUC thirteen experiments were performed in four different experimental groups: WST-1 and BrdU assay was performed on three or four primary cultures each to examine the cellular behaviour of HUC cultures. These two groups were further divided into experiments in the proliferative status (Prol, low seeding density; 2.5×10^4 cells/cm^2) as well as cell behaviour after induction of stratification (Strat, high seeding density; 4×10^5 cells/cm^2). Regarding PUC the same principle was pursued with the respective four experimental groups including three different primary cultures each (see table 3). For experiments in high seeding density stratification was induced as soon as the cultures were confluent.

The assays were always performed with UC cultures seeded in CellBIND 24-well plates (Corning Inc., Corning, NY, USA) in the respective seeding density. HUC or PUC of one cell line were seeded in three parallels on CCC and on standard plastic as a control. Another three wells served as blanks without cells to take account of background absorbance in the measurement. Consequently, each assay experiment was performed for three parallels at four days after cell seeding or after induction of multilayer formation, respectively.

Before performing BrdU or WST-1 assay, the status of the primary cultures was always documented photographically as described above.

Table 3: Primary cultures used for the BrdU and WST-1 assays, HL = human ureter specimen, MSBL = minipig bladder specimen, MSHL = minipig ureter specimen, P = passage

HUC assays				
BrdU Prol	HL 10/18 P4	HL 10/19 P3	HL 10/26 P2	HL 07/49 P4
BrdU Strat	HL 10/3 P5	HL 04/005 P7	HL 10/21 P3	
WST-1 Prol	HL 10/17 P3	HL 10/18 P3	HL 10/19 P3	
WST-1 Strat	HL 07/47 P4	HL 07/14 P5	HL 10/21 P3	
PUC assays				
BrdU Prol	MSBL 79930 P7	MSBL 79939 P5	MSHL 106597 P7	
BrdU Strat	MSBL 79930 P7	MSBL 79939 P5	MSHL 106597 P6	
WST-1 Prol	MSBL 79930 P4	MSHL 106597 P4	MSBL 79939 P7	
WST-1 Strat	MSBL 79930 P6	MSHL 106597 P6	MSBL 200201 P5	

3.1.6.1 BrdU assay for evaluation of proliferation

BrdU is a synthetic nucleoside that is an analogue of thymidine and therefore integrates into the cells' DNA during mitosis. It is commonly used as a labelling reagent for in vitro and in vivo examinations. BrdU test is a fast, precise, and simple colorimetric method to evaluate proliferating cells. The test principle consists of the following steps: 1. BrdU is incorporated into the newly synthesised DNA of replicating cells (during the S phase of the cell cycle), substituting for thymidine. 2. After denaturation and fixation, specific anti-BrdU antibodies can be used to detect the incorporated chemical, thus indicating cells that were actively replicating their DNA. 3. Finally these immune complexes can be recovered through a substrate reaction and quantification of the absorbance of reaction products. The developing colour and resultant optical density values directly correlate to the amount of DNA synthesised and thus to cell proliferation.

In the present study cell proliferation was quantified with the Cell Proliferation ELISA BrdU (Roche Diagnostics Deutschland GmbH). The cell culture medium was removed from the wells, 300 µl cKSFM were filled into each well and 30 µl BrdU labelling reagent were added. After gentle shaking, the cells were incubated at 37°C for 2 h to allow the BrdU to incorporate into the cells' DNA. After removing the well content, 300 µl fixation and denaturation reagent was added followed by another 30 min incubation period at RT. After removal of the fixation reagent, 250 µl of BrdU-peroxidase solution were added to bind to the incorporated BrdU during another 45 min of incubation at RT. Three washing steps with 300 µl washing buffer followed to remove the remaining free BrdU-peroxidase. Substrate solution (250 µl) was added to the wells for 5 min to be converted by the BrdU-peroxidase for colorimetric measurement. The reaction was then stopped by addition of 75 µl of 1 M sulfuric acid. Twice 100 µl of the content of each well was transferred to a 96-well ELISA microplate (Greiner Bio-One GmbH) to get doublets of each well resulting in 18 wells for the measurement. Optical density of the developed colour was quantified at 450 nm with a kinetic ELISA microplate reader (Milenia Biotec GmbH) and analysed with SoftMax Pro software (Molecular Devices Inc.).

3.1.6.2 WST-1 assay for evaluation of metabolic activity

WST-1 is a tetrazolium salt that is cleaved to formazan by mitochondrial dehydrogenases when it gets in contact with metabolically active cells. The formazan concentration thus correlates indirectly with the total number of viable cells. The formazan dye is measured using a scanning spectrophotometer. The greater the number of metabolically active cells, the darker the formazan dye, the higher the optical density measured. The WST-1 test provides a spectrophotometric assay for measurement of viability, growth, chemo sensitivity, and proliferation in cell culture. It has evolved from the MTT [3(4,5-dimethyl-thiazoyl-2-yl)2,5 diphenyl-tetrazolium

bromide] colorimetric assay in the nineties. Being more rapid and easier to perform WST-1 test has frequently been used for evaluation of cytotoxic effects of viruses or drugs (FRANCOEUR & ASSALIAN, 1996). It displays sufficient reproducibility and can be completely automated (NISSEN et al., 1997).
Hence the test provides evidence for viability of the cells seeded on CCC. WST-1 assay was performed with the Cell Proliferation Reagent WST-1 (Roche Diagnostics Deutschland GmbH). First the cell culture medium was removed from the wells. For the assays in the proliferative status 400 µl of cKSFM were added to the wells together with 40 µl cell proliferation reagent WST-1 and for the assays in the stratifying status 600 µl of cKSFM together with 20 µl cell proliferation reagent WST-1. After incubation at 37°C for 3 h triplets of 100 µl of the content of each well were transferred to a 96-well ELISA microplate (Greiner Bio-One GmbH) to get 27 wells ready to be measured. The measurement of optical density was performed as described above for BrdU assay at 450 nm.

3.1.7 Investigations on cell adherence

Analogous to the WST-1 and BrdU assays cell adherence was determined for cultures in low seeding density (analysis of proliferative phase, seeding density 2.5×10^4 cells/cm^2) and in high seeding density (analysis of stratifying phase, seeding density 4×10^5 cells/cm^2). One day after seeding the supernatants from CCC seeded cells as well as from cells seeded on plastic were removed and pooled, three wells each in safe-lock tubes (Eppendorf AG). If necessary it was stored on ice until cell counting. After quick-centrifugation at 16000 g (Eppendorf centrifuge 5415C, Eppendorf AG) for 10 s, the supernatant was removed and the decanted cells were adjusted to 100 µl final volume. Living and dead cells in the supernatant were counted as described under 3.1.3. Cell adherence was investigated in different passages in 12 HUC experiments (6 in low seeding density, 6 in confluence, 11 different primary cultures) and 12 PUC experiments (6 in low seeding density, 6 in confluence, 4 different primary cultures).

3.1.8 Quality control: Immunocytochemistry

For quality control expanded HUC and PUC were seeded on eight chamber Lab-Tek Permanox Chamber Slides (Nunc GmbH & Co. KG) in a density of 5 x 10^4 cells/cm^2 and incubated in humidified atmosphere at 37°C and 5% CO_2 until they reached 80-90% confluence.
Immunocytochemistry was performed with mouse monoclonal anti-cytokeratin cocktail AE1/AE3 (Millipore) to determine the epithelial phenotype, anti-fibroblasts monoclonal antibody clone TE-7 (Millipore), and anti-smooth muscle α-actin antibody clone 1A4 (Sigma-Aldrich Chemie GmbH) to demonstrate the absence of fibroblasts and smooth muscle cells, respectively. Negative controls were performed omitting the primary antibody. Washing steps in between every part of the following procedure were performed with PBS powder (bioMérieux Deutschland GmbH) dissolved in Ampuwa (Fresenius Kabi Deutschland GmbH). Reagents for immunocytochemical staining were taken from the EnVision+ System-HRP (DAB) kit (Dako Deutschland GmbH) working with a streptavidin-biotin method.
Cells were fixed at 90-100% confluence by incubation in 3.7% paraformaldehyde (PFA) for 10 min. Slides were then stored in PBS solution at 4°C until further processing.
For AE1/AE3 and 1A4 staining urothelial cells had to be permeabilised by addition of 0.1% saponin solution as a mild detergent for 10 min. Saponin solution was prepared from saponin stock solution (see annexe) diluted in PBS solution. AE1/AE3 antibody was diluted in saponin working solution whereas TE-7 and 1A4 were diluted in antibody diluent (Dako Deutschland GmbH) according to table 4. The chambers on the slide were incubated with the different unconjugated primary antibodies or antibody diluent for negative controls for 30 min. Horseradish peroxidase (HRP) labelled polymer was added and the cells were incubated another 30 min. HRP labelled polymer is conjugated to goat anti-mouse immunoglobulins and therefore binds to mouse primary antibodies. After incubation in DAB (3,3'-diaminobenzidine)+substrate chromogen for 3 min an Ampuwa (Fresenius Kabi Deutschland GmbH) bath followed. The conversion of DAB (3,3'-diaminobenzidine)+substrate chromogen by bound HRP lead to the brown dyeing. Counterstaining was performed with haematoxylin (Vector Laboratories Inc.) for 1 min followed by 10 min of rinsing with tap water for blueing. Binding to the primary antibody was detected as a brown colouration whereas negative cells only

showed blue haematoxylin nucleus staining. When the slide was dried, it was mounted in glycerol gelatine (Merck KGaA), covered with a microscope cover slip (R. Langenbrinck Labor- und Medizintechnik) and stored at RT.

The slides were evaluated qualitatively for positive or negative antigen expression being visible by brown dyeing with the microscope Axiovert 200M (Zeiss) and photographed.

Table 4: Antibodies for immunocytochemical staining

Identification	Antibody specificity	Clone	Dilution	Company
epithelial phenotype	pancytokeratin	AE1/AE3	1/500	Millipore
fibroblasts	fibroblasts	TE-7	1/2000	Millipore
smooth muscle	smooth muscle α-actin	1A4	1/10000	Sigma-Aldrich Chemie GmbH

3.1.9 PKH26 staining

PKH26 is a red fluorescent cell linker for in vitro cell labelling, in vitro proliferation studies, and long term in vivo cell tracking. The half-life for elution of PKH26 from labelled rabbit red blood cells is greater than 100 days (see product description Sigma-Aldrich Chemie GmbH). It integrates into the cell membrane lipid layer and enables the experimenter to retrieve the sought cells and tissue in vitro and in vivo by fluorescence microscopy. In this study it served as a tracking system to detect the transplanted cells in vivo in the extracted tissue. PKH26 Red Fluorescent Cell Linker Kit (Sigma-Aldrich Chemie GmbH) including PKH26 cell linker and corresponding diluent was used. Two different staining protocols were applied:

a) For the in vitro studies and the nude rat model UC were stained in suspension: Cells were detached from the culture flasks and counted (see above). As app. 50% of the cells were lost during the staining procedure double of the favoured final cell number had to undergo the procedure. 5 x 10^6 cells were transferred in a BD Falcon conical tube (BD Biosciences) and centrifuged at 250 g for 5 minutes. The supernatant was aspirated and the pellet was resuspended in 300 µl of diluent.

285 µl of diluent was mixed with 15 µl of PKH26 cell linker. The cell suspension was gently added to the staining solution and was incubated for 8 min (handwarm) by gentle agitation. The reaction was stopped by addition of 2 ml cell culture medium supplemented with 20% FCS (Gibco) and incubation for 1-2 min followed by centrifugation. After two washing steps with culture medium w/o FCS, successful staining was checked by fluorescence microscopy (Axiovert 200M, Zeiss) with the integrated red fluorescence filter F41-027 (AHF Analysentechnik).

b) For the minipig model the staining protocol has been improved to increase the yield of stained cells. Here UC were stained as an adherent confluent cell layer in 6-well inserts: Therefore, 300 µl of diluted PKH26 cell linker were mixed with 1 ml of the respective culture medium. After removal of the medium the insert was filled with 1.3 ml staining solution while the bottom of the well was filled with 1.3 ml of medium. The cells were stained for 1 h at 37°C and 5% CO_2. The reaction was then stopped by adding 3 ml of culture medium supplemented with 20% FCS into the insert and into the well. After 2 min of incubation the well and the insert were washed twice with culture medium w/o FCS and the staining success was checked as described above.

3.1.10 Immunofluorescence of stratified human urothelial cells

For the confirmation of urothelial phenotype, differentiation and the formation of cell-cell junctions immunofluorescent staining was performed with the antibodies against AE1/AE3 (pancytokeratin; epithelial phenotype), CK-20 (cytokeratin 20; urothelial differentiation marker), p63 (urothelial marker), E-Cadherin (epithelial adherence junctions), and ZO-1 (tight junctions) in stratifying HUC cultures. The cells were seeded on CCC inserts and plastic culture plates as a control. Specifities of the used primary antibodies, company, and dilution are listed in table 5. Negative controls were performed omitting the primary antibody.

3.1.10.1 Cell culture preparations

HUC were labelled with PKH26 (see 3.1.9) and 1.6 x 10^5 cells/cm^2 were seeded on CCC 6-well inserts as described before (see 3.1.4). In addition, 2.8 x 10^5 cells/cm^2 were seeded on plastic surface of a CellBIND 6-well plate (Corning Inc.) as a control. Cells were cultured until formation of a confluent cell layer and stratification was induced. After eight days of stratification the matrix-free cells were detached as described (see 3.1.5).

The cells on CCC were washed three times with PBS solution and subsequently fixed in 3.7% PFA for 10 min, before they were washed twice again with PBS solution. The seeded matrix was cut from the insert's plastic holder and placed flatly on tissue freezing medium (Leica microsystems Nussloch GmbH) analogous to the control. At -20°C cryostat sections of 5 µm thickness were cut perpendicular to the matrix surface, placed on SuperFrost microscope slides (R. Langenbrinck Labor- und Medizintechnik) and dried overnight at RT in the dark.

3.1.10.2 Immunofluorescent staining procedure

All washing steps throughout the immunofluorescence procedure were performed with PBS (bioMérieux Deutschland GmbH) dissolved in Ampuwa (Fresenius Kabi Deutschland GmbH) for 3-5 min.

As p63 constitutes intranuclear staining the respective tissue sections had to undergo a citrate buffer treatment for cell permeabilisation prior to further antibody incubation steps. Therefore, a 10 mM citrate buffer of citric acid and sodium citrate diluted in Ampuwa (Fresenius Kabi Deutschland GmbH) was adjusted to pH 6.0. Then the slides were heated in the microwave thrice for 3 min with intermittent addition of Ampuwa. After 20 min of cooling in the citrate buffer the staining procedure was started.

As the first step of immunofluorescent staining procedure the tissues were heated at 40°C for 30 min on a heating plate to make the tissues stick to the slides. After cooling, the tissue section was encircled with the Dako Pen (Dako Deutschland GmbH) and washed twice. Unspecific binding was blocked with 5-10% rabbit IgG normal serum (Dako Deutschland GmbH) for 30 min. Incubation was performed in the dark in a humid chamber at RT as for all the following steps. The primary antibodies were diluted in antibody diluent (Dako Deutschland GmbH) according to table 5 and added to the tissue slides for 60 min. Two washing steps followed prior to addition of the secondary antibody rabbit anti-mouse IgG F(ab)$_2$ Fluorescein isothiocyanate (FITC) which was diluted in antibody diluent (both Dako Deutschland GmbH) in a ratio of 1/40. Thirty min of incubation were followed by two more wash cycles. After drying, the slides were mounted in Vectashield (Vector Laboratories

Inc.) containing DAPI (4',6-diamidino-2-phenylindole), a cell nucleus fluorescent dye and stored at -20°C.

The slides were evaluated qualitatively for positive or negative antigen expression using the microscope Axiovert 200M (Zeiss) and the integrated fluorescence filters of appropriate wavelengths (AHF Analysentechnik). The immunofluorescence results for urothelial sheets on CCC were compared to the dyeing of urothelial multilayer constructs seeded on standard plastic (controls).

Table 5: Antibodies for immunofluorescent staining of multilayer sheets

identification	antibody specificity	clone	dilution	company
epithelial phenotype	pancytokeratin	AE1/AE3	1/100	Millipore
urothelial differentiation (surface marker)	cytokeratin 20 (CK-20)	K_S20.8	1/50	Dako Deutschland GmbH
urothelial differentiation	p63	4A4	1/50	DIANOVA GmbH
epithelial adherence junctions	E-Cadherin	D33	1/100	Dako Deutschland GmbH
tight junctions (zonula occludens)	ZO-1	ZO1-1A12	1/25	Invitrogen GmbH

3.2 Animal models

3.2.1 Nude rat model

3.2.1.1 Study design and conditions

The rodent experiments were performed according to the approval of the Regional Administrative Authority of Tuebingen (CU 1/10) with athymic nude rats (Crl:NIH-Foxn1nu, Charles River Laboratories). Twelve rats underwent surgery for the evaluation of biocompatibility of urothelium-CCC-constructs. Featuring reduced immunocompetence they are the ideal animal model for transplantation experiments in general. Female animals at the age of five weeks and with a body weight of app. 130 g at the beginning of the experiment were used. They were kept in groups of four animals in Sealsafe individually ventilated makrolon cages (IVC) type IV (TECNIPLAST S.p.A.) at a temperature of 22 +/-2°C, 55 +/-10% relative humidity, and physiological day-night rhythm (12 h light/12 h dark) at a research animal facility of the University of Tuebingen. The cages were filled with litter (aspen) and cleaned weekly. The animals were given vegetal commercial laboratory animal food (ssniff Spezialdiäten GmbH) and water ad libitum. Environmental enrichment measurements were undertaken.

Prior to the beginning of the experiment, the animals were allowed to adapt to the surrounding conditions for one week. Each animal underwent transplantation of urothelium-CCC-constructs onto the rectus abdominis to prove biocompatibility. After surgery carprofen (Rimadyl, Pfizer Deutschland GmbH) was injected daily at 5 mg/kg as an analgetic for the first three postoperative days. The physical condition of the rats as well as the wound healing was checked daily. Twice a week the body weight was determined as an evidence for potential suffering. The four animals each were sacrificed after one, two, and four weeks and the extracted rectus muscle was analysed histologically and immunohistologically.

3.2.1.2 Preparation of the urothelial-collagen cell carrier transplants

Thawed HUC were cultured as described above, labelled by PKH26 in suspension and seeded onto CCC in a CellBIND 24-well plate (Corning Inc.). On stratification day eight urothelium-CCC-constructs were ready to be transplanted (Fig. 2). They were transported to the animal facility in an insulated polystyrene box.

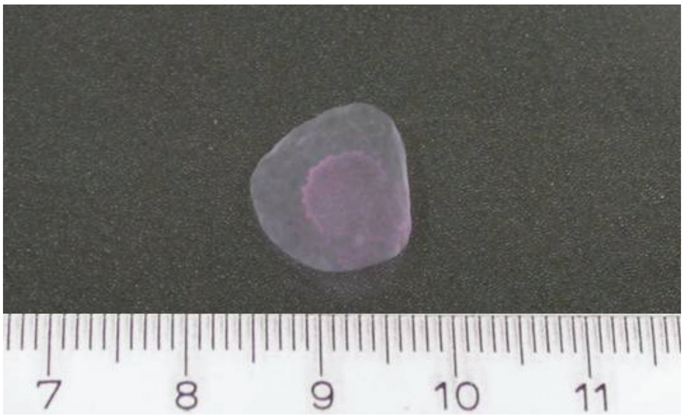

Fig. 2: CCC seeded with PKH26 labelled HUC prior to transplantation.

3.2.1.3 Surgery

The urothelial cell-matrix-transplants were placed in an incubator at 37°C and 5% CO_2 under humidified atmosphere during the preparation of the surgery. The animals were anaesthetised by intraperitoneal injection of Xylazin 2% at 4 mg/kg and

Fig. 3: Application of cell seeded CCC onto the rectus abdominis muscle, transplant lying on the abdominal wound prior to transplantation (arrow indicates CCC)

Ketamin at 100 mg/kg (both Albrecht GmbH) mixed in a syringe. The depth of anaesthesia was checked by the negative righting reflex and negative interdigital reflex. After supine positioning, application of eye ointment, fixation of the animal and spacious skin disinfection, the rectus muscle was exposed by a midline abdominal incision of app. 2 cm. The superficial abdominal fascia was lifted from the subjacent muscle to build a pocket. Each transplant was washed in 0.9% NaCl (Fresenius Kabi Deutschland GmbH) prior to application. With a forceps, it was carefully placed flatly into the pocket between muscle and fascia (Fig. 3). With two to three single stitches the fascia was adapted prior to the skin closure in buried suture using the surgical suture Coated Vicryl (Ethicon Inc.). The rats were placed in a warm environment and monitored until they were conscious. The duration of the complete procedure was app. 30 min.

3.2.1.4 Euthanasia procedure and tissue retrieval

After the scheduled periods of one, two, and four weeks the animals were euthanised by intraperitoneal injection of pentobarbital-sodium 500 mg/kg (Narcoren, 160 mg/ml, Merial GmbH). The tissue of the transplantation site including skin, rectus abdominis muscle and serosa was removed spaciously (app. 3 x 3 cm) for histological work-up. Tissue from the non-transplanted side was taken as well to serve as control tissue. The tissue shrank to half of the original size after extraction.

The tissue samples were placed in a BD Falcon conical tube (BD Biosciences) with saccharose solution 18% directly after extraction and stored at 4°C overnight. Saccharose served as a cryoprotective agent.

The following day tissue samples were divided into pieces of app. 1.5 cm of length and placed in embedding moulds (Thermo Fisher Scientific GmbH) filled with tissue freezing medium (Leica microsystems Nussloch GmbH). The moulds were plunged in liquid nitrogen until they were completely frozen. Tissue samples were then stored at -80°C until further processing.

3.2.2 Minipig model

3.2.2.1 Study design and conditions

The pig represents a common and appropriate large animal model for transplantation research in preclinical studies because its anatomy and physiology are well known and the proportions are similar to humans (DEHOUX & GIANELLO, 2007). Eight male castrated Göttingen Minipigs at the age of app. nine months and of app. 20-25 kg of weight at the beginning of the experiment were used for the syngenic animal study. The barrier-bred pigs were obtained from Ellegaard, Denmark and kept in the centre for experimental medicine of the University Clinics of Tuebingen at RT and physiological day-night rhythm. The animals were fed once a day with conventional minipig fodder (SDS Diets) and received water ad libitum. They were merged in one group in a compartment of 19 m^2. Prior to the beginning of the experiment, the animals were allowed to adapt to the surrounding conditions for one week.

Each animal underwent two surgical interventions. Prior to anaesthesia a fasting period of 24 h was kept. In a first approach the urethral stricture was induced by thermocoagulation, bladder tissue was harvested for the retrieval of autologous cells, and a vesicostomy was established. In a second intervention three weeks later the autologous urothelium-CCC-construct was applicated at the stricture site. After the respective observation periods euthanasia and extraction of the urethra for histological and immunohistological work-up were performed. Two animals each were put down after one, two, and four weeks after transplantation of seeded CCC transplants. The anaesthesia regime, perioperative medication, and euthanasia are listed in the annexe. All doses are approximate values and were adapted by the responsible veterinarian according to interindividual differences.

3.2.2.2 Surgical procedures

The porcine urethral stricture model was implemented at the Department of Urology of the University Clinics of Tuebingen in previous studies (SEIBOLD et al., 2011; SIEVERT et al., 2012). The large animal trial was recognized by the Regional Administrative Authority of Tuebingen (CU 1/08).

The surgical procedure comprised two interventions. Blood samples were taken prior to any intervention to confirm good health status of all six minipigs. Prior to the first intervention urine was analysed per Combur Test M sticks (Roche Diagnostics Deutschland GmbH). Prior to the manipulation of the urethra urethrography was performed with a c-arm X-ray unit at every intervention to record the physiological condition, the stricture formation or the stricture healing.

a) First intervention:

The minipigs were sedated by intramuscular injection in the housing compartment and were transported to the operating room. After installing a venous catheter into the auricular vein, general anaesthesia was induced and the animals were intubated. They were placed on the operation desk in supine position and the surgical field was cleaned, disinfected, and covered. The abdominal cavity was opened and the bladder was exposed (Fig. 4).

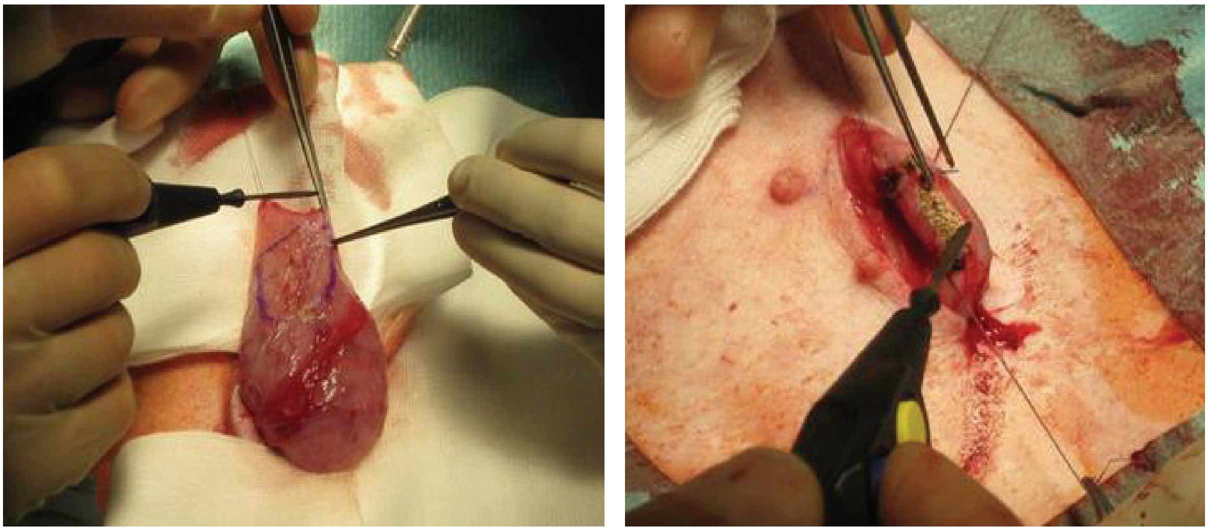

Fig. 4: In the first surgical intervention the bladder was exposed to harvest urothelial cells. The tissue to be excised is marked (left). Urethral damage was induced by superficial circumferential electro coagulation (right).

After drawing 5-10 ml of urine for analysis a bladder specimen of app. 2 x 2 cm was excised, transferred into transport medium (see 3.1.1) and kept at 4°C until further work-up. The bladder was fixed to the abdominal wall and a vesicostomy was installed to allow free flow of urine during the stricture formation.

Fig. 5: The completed vesicostomy after the first surgery procedure.

The freed urethra was opened distal to the future stricture site and contrast medium (Peritrast Infusio 31%, Dr. Franz Köhler Chemie GmbH) was instilled for contrast x-ray by a ureteric catheter CH04 (Coloplast GmbH). Urethrography was performed to document the normal urethral lumen prior to stricture induction. Afterwards the urethra was closed again with 5/0 Vicryl sutures (Ethicon Inc.). The urethral stricture was induced by circumferential electro coagulation (Fig. 4). The location of the lesion was marked by non-resorbable 0 Prolene sutures (Ethicon Inc.) prior to adaptation of fascia and skin (Fig. 5).

b) <u>Second intervention:</u>

Three weeks after stricture induction procedure the minipigs were pre-medicated as in the first intervention. Anaesthetisation and urethrography were performed as described above.

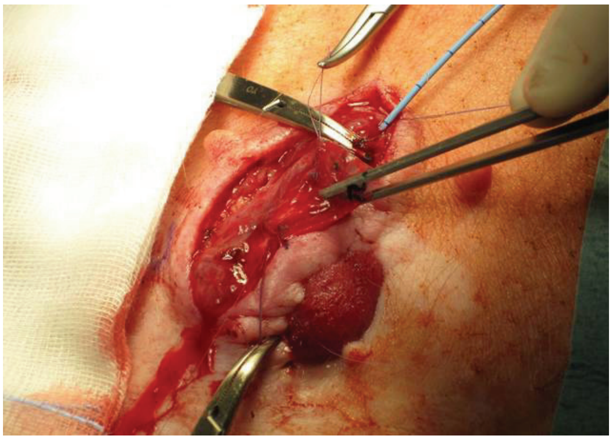

Fig. 6: Autologous cell seeded CCC was held by forceps during transplantation into the porcine urethra.

The urethra was exposed at the stricture site which was retrieved by the previously attached marking sutures. Cell seeded CCC was washed in NaCl. The construct was then sutured flatly to the urothelium with single stitches with the cells facing the lumen (Fig. 6). Finally the urethra and the abdomen were closed.

3.2.2.3 Construction of autologous transplants

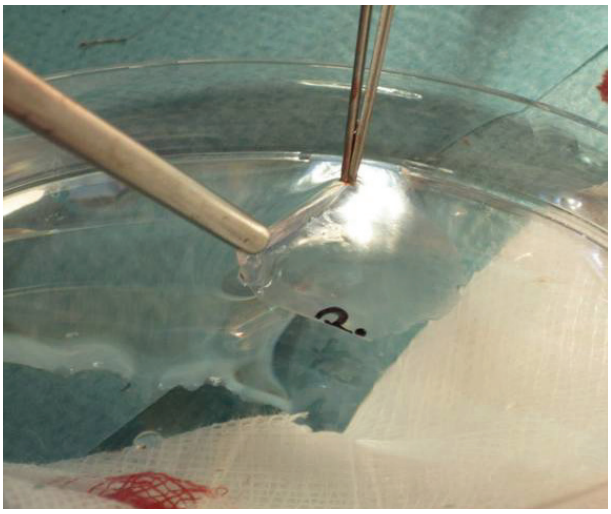

Fig. 7: Seeded CCC (with the letter "R" indicating rear unseeded side of the transplant) was taken out of the Petri dish prior to transplantation.

On the day of the first surgery bladder samples were transferred to the cell culture laboratory in transport medium and PUC were isolated according to the established protocol (see 3.1.1). Primary cell culture and subculture were performed as described. In contrast to the in vitro assays a different medium was used for cultivation. PUC were cultured in supplemented CnT-07 for proliferation or CnT-02 with 1.07 mM/l $CaCl_2$ for stratification (both CELLnTEC Advanced Cell Systems AG). Cells were cultivated for app. two weeks including one passage and finally 3 x 10^5 cells/cm^2 were seeded on the upper side of CCC inserts (see 3.1.4). On the subsequent day seeded cells were labelled with PKH26 (see 3.1.9) and stratification was induced 4 h later by changing the culture medium to CnT-02 and increasing the calcium concentration. On day seven to eight of stratification autologous urothelial cell-CCC-constructs were ready to be applied (Fig. 7).

3.2.2.4 Urethral tissue retrieval

After the determined periods of one, two, and four weeks blood samples were analysed again and two animals each were sacrificed according to the protocol (see annexe) by intravenous injection into the V. cava cranialis (Fig. 8). Briefly, the animals were pre-medicated and sedated by application of Azaperone 4.0 mg/kg, Midazolam 0.5 mg/kg, and Ketamin 14 mg/kg. Anaesthesia was deepened by application of pentobarbital and finally KCl (B. Braun Melsungen AG) until cardiac arrest. After a third urethrography large parts of the urethra surrounding the stricture site (app. 10-12 cm) were excised and transferred in a BD Falcon conical tube (BD Biosciences) with 18% saccharose solution directly after extraction and stored at 4°C overnight.

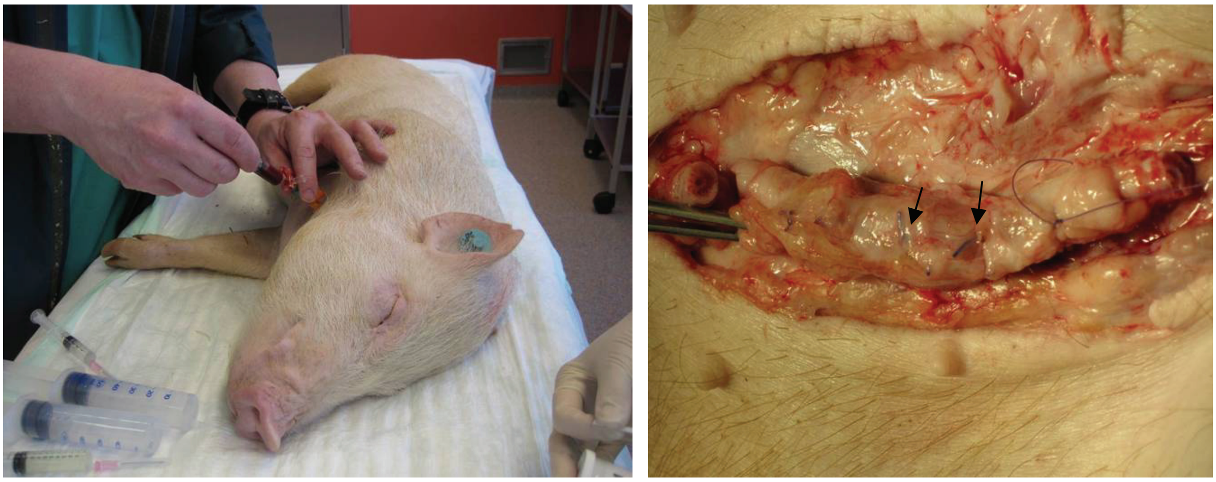

Fig. 8: Euthanasia by intravenous injection of the drugs into the V. cava cranialis (left). Extraction of urethral tissue with unresorbable sutures (arrows) confining the transplantation site (right)

The following day connective tissue of the urethra was removed, the area around the transplant was divided into five sections of app. 1 cm length (Fig. 9) and placed in embedding moulds (Thermo Fisher Scientific GmbH) filled with tissue freezing medium (Leica microsystems Nussloch GmbH). The moulds were plunged in liquid nitrogen until they were completely frozen. Tissue samples were then stored at -80°C until further processing.

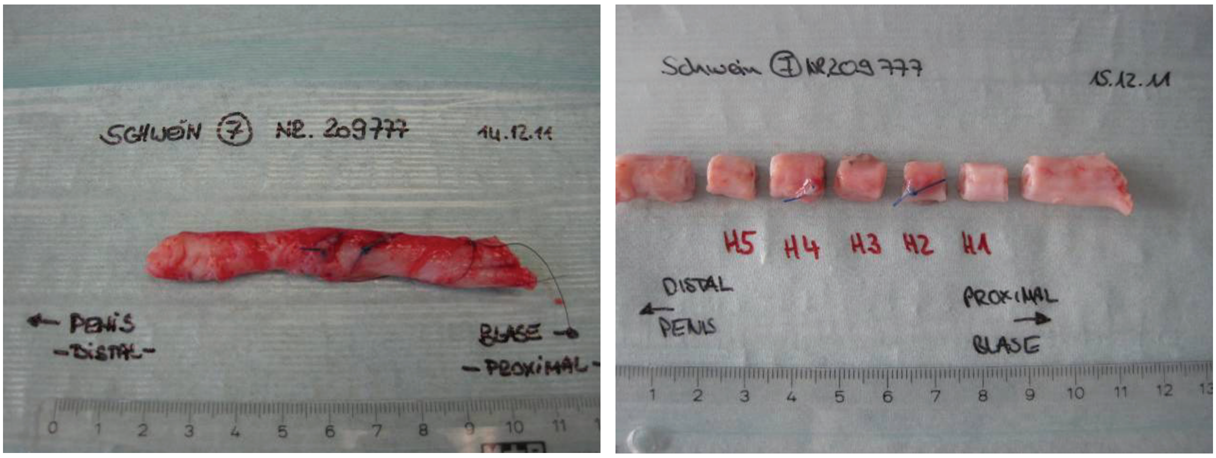

Fig. 9: The extracted urethra was divided into five sections. Section three contained the main part of the transplant site.

3.2.3 Tissue processing, staining, and microscopic evaluation

3.2.3.1 Cryotome cutting

App. 200 cryostat sections of 5 µm thickness were made of each tissue with a Leica CM1900 cryotome (Leica microsystems Nussloch GmbH) at -20°C. They were placed on SuperFrost microscope slides (R. Langenbrinck Labor- und Medizintechnik) and dried overnight in the dark at RT. Slides were then stored at -20°C.

3.2.3.2 Haematoxylin-eosin staining

For histologic evaluation haematoxylin-eosin (HE) staining was performed on at least one tissue slide of every rat and on control tissue. Concerning minipigs' tissues several slides were stained. First a 0.1% eosin solution was prepared: Therefore, Certistain Eosin G (Merck KGaA) was diluted in 90% ethanol and a drop of glacial acetic acid.

Tissues to be stained were heated at 56°C for 30 min on a heating plate and then incubated in haematoxylin (Vector Laboratories Inc.) for 20 s. This step was followed by 10 min of watering under running water and 5 s of dipping in Ampuwa (Fresenius Kabi Deutschland GmbH). Eosin staining was performed with the aforementioned 0.1% eosin solution for 5 min. After a final wash under running water for 10 min, stained slides were dried at 37°C in a drying cabinet (BE 200, Memmert GmbH und Co. KG) and then mounted in Vectamount (Vector Laboratories Inc.).

3.2.3.3 Immunofluorescence

Concerning the investigation in rats immunofluorescent staining was performed on tissue slides of each animal with the primary antibodies specific for pancytokeratin, CK-20, p63, E-Cadherin, and ZO-1 according to the procedure described under 3.1.10. Negative controls were performed omitting the primary antibody. The following modifications were made: As secondary antibodies Cy2 conjugated donkey anti-mouse IgG F(ab')2 was used in a dilution of 1/50 and Cy2 conjugated goat anti-mouse IgG (H+L) in a dilution of 1/100 (both DIANOVA GmbH). Due to the different host species donkey IgG normal serum and goat serum (both Dako Deutschland GmbH) were used as blocking serum.

Immunofluorescent staining of minipig tissues was also performed for all animal samples with the identical panel of primary antibodies. Here goat anti-mouse IgG (H+L) Cy2 conjugated antibody (DIANOVA GmbH) was used in a dilution of 1/100 as secondary antibody and goat serum (Dako Deutschland GmbH) was used for blocking. Furthermore, ZO-1 was diluted at a ratio of 1/40 in contrast to the previous investigations. Processed slides were mounted in Immunoselect (DIANOVA GmbH), containing DAPI, and covered with cover slips (R. Langenbrinck Labor- und Medizintechnik).

3.2.3.4 Microscopic evaluation

Microscopic evaluation was performed with a fluorescence microscope (Axiovert 200M, Zeiss) with the red fluorescence filter F41-027, green fluorescence filter F41-020, and blue DAPI fluorescence filter F31-000 (all AHF Analysentechnik). The results were recorded with AxioCam HRc (Zeiss).

Native tissue slides and HE stained slides were analysed microscopically with regard to the survival and integration of the transplanted cells as well as the degradation of the CCC and potential inflammatory reactions. The applicated cells were detected by red PKH26 fluorescence.

For evaluation of the immunofluorescent stainings, green fluorescence was assessed distinguishing between positive or negative expression of the different antigens. Tissues were assessed with regard to double fluorescence showing urothelial phenotype (green fluorescence) of the transplanted cells (red fluorescence).

4 Results

4.1 In vitro results

4.1.1 Cell culture of urothelial cells

Primary isolated HUC and PUC were adherent to the plastic surface or to the CCC 24 h after being seeded. The growth behaviour of PUC differed significantly depending on the primary culture. After thawing (two vials in a 75 cm^2 flask) HUC required app. five days to achieve confluence while PUC required app. two weeks. Altogether, PUC grew slower than HUC throughout the whole culture period. Moreover, the yield of PUC after detachment of the flask's surface was much poorer. A confluent culture flask provided a yield of app. 4-6 x 10^4 HUC/cm^2 or 2.5 x 10^4 PUC/cm^2. All cells showed typical morphology for urothelial cells, though, PUC morphology was not as uniform as HUC morphology. Figure 10 shows PKH26-labelled HUC on plastic surface in comparison to HUC seeded on CCC.

The CCC was easy to handle, to stick to the well plate, and to remove. It did not break, shrink or crack during thorough manipulation, but stayed in its original shape. Due to its excellent handling characteristics and its stability it was judged as a suitable material for the projected in vivo investigations.

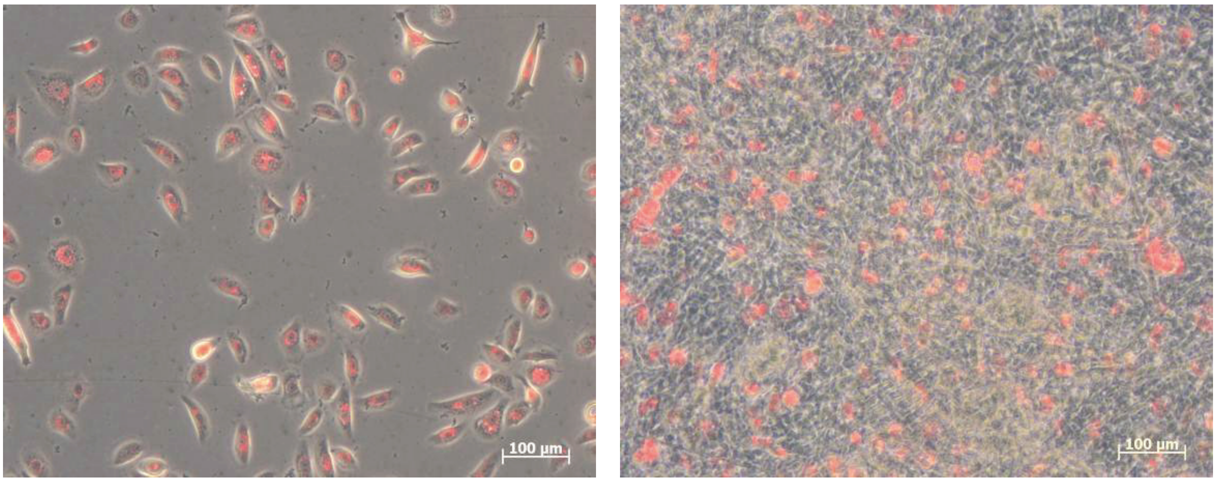

Fig. 10: HUC grown on standard plastic (left) and on CCC (right) at day 1 after seeding. PKH26-labelled HUC show red fluorescence. Phase contrast microscopy

4.1.2 Proliferation and metabolic activity of HUC on CCC

BrdU and WST-1 assays were performed to evaluate proliferation and metabolic activity of HUC in proliferating and stratifying cultures.

For each experiment the optical density measured in the control wells was set as 100% and optical density of CCC seeded cells was set in relation to the control value. The results of BrdU and WST-1 assays were comparable concerning the kinetic development of proliferating and stratifying cultures on CCC compared to controls on standard plastic surface. While HUC showed reduced proliferative and metabolic capacity on the first two measuring points (24-25% for BrdU and 38-45% for WST-1) in low seeding density compared to controls, they approached values for HUC seeded on plastic on test days 3 and 4 (99-103% for BrdU and 70-91% for WST-1, Fig. 11 and 12). When seeded in confluence and stratification was induced HUC on CCC revealed 111-139% for BrdU and 89-91% for WST-1 and therewith corresponded to controls on all four measurement points or even revealed superior (Fig. 13 and 14).

Altogether, HUC seeded on CCC, whether on later culture days in the proliferation phase or in the stratification phase, showed similar or even better proliferation and metabolic activity than controls seeded on plastic surface. Early HUC cultures (until day 4 after seeding) in the proliferating state revealed proliferation and metabolic activity rates considerably lower than controls. Table 6 and 7 show the data of optical density measurements in percentage of the controls. Definite test days after seeding for proliferation experiments (Prol, low seeding density: 2.5×10^4 cells/cm^2) or after induction of stratification for stratification experiments (Strat, high seeding density: 4×10^5 cells/cm^2) are further presented in tables 6 and 7.

For each of the eight experimental groups three different primary cultures were used except for BrdU assay on proliferating HUC which was performed on four different cell lines. Figure 11 demonstrates mean values of four independent BrdU experiments and figure 12 shows mean values of three independent WST-1 experiments. Figures 13 and 14 demonstrate mean values of independent BrdU and WST-1 experiments on three stratifying HUC cultures each. Figure 15 shows a representative example of one WST-1 assay on a proliferating HUC culture to demonstrate development of optical density measurements over four test days.

Table 6: Percentage of optical density compared to controls of different primary cell lines (BrdU: n = 4, WST-1: n = 3) showing growth development of proliferating HUC in an experimental period of seven days including four different test days (measurement time points days 1, 2, 4, and 7 after seeding)

HUC Proliferation	**Day after seeding**			
	1	**2**	**4**	**7**
BrdU Prol	17%,20%, 34%,30%	21%, 23%, 21%, 32%	81%, 48%, 183%, 82%	129%, 128%, 91%, 65%
Mean	25%	24%	99%	103%
WST-1 Prol	35%, 53%, 47%	18%, 67%, 30%	85%, 90%, 34%	63%, 135%, 75%
Mean	45%	38%	70%	91%

Table 7: Percentage of optical density compared to controls of different primary cell lines (n = 3) showing growth development of stratifying HUC in an experimental period of eight days including four different test days (measurement time points days 0, 1, 4, and 8 of stratification)

HUC Stratification	**Day of stratification**			
	0	**1**	**4**	**8**
BrdU Strat	148%, 149%, 119%	127%, 113%, 108%	109%, 129%, 94%	106%, 123%, 123%
Mean	139%	116%	111%	117%
WST-1 Strat	90%, 95%, 86%	87%, 97%, 88%	102%, 86%, 82%	84%, 93%, 89%
Mean	90%	91%	90%	89%

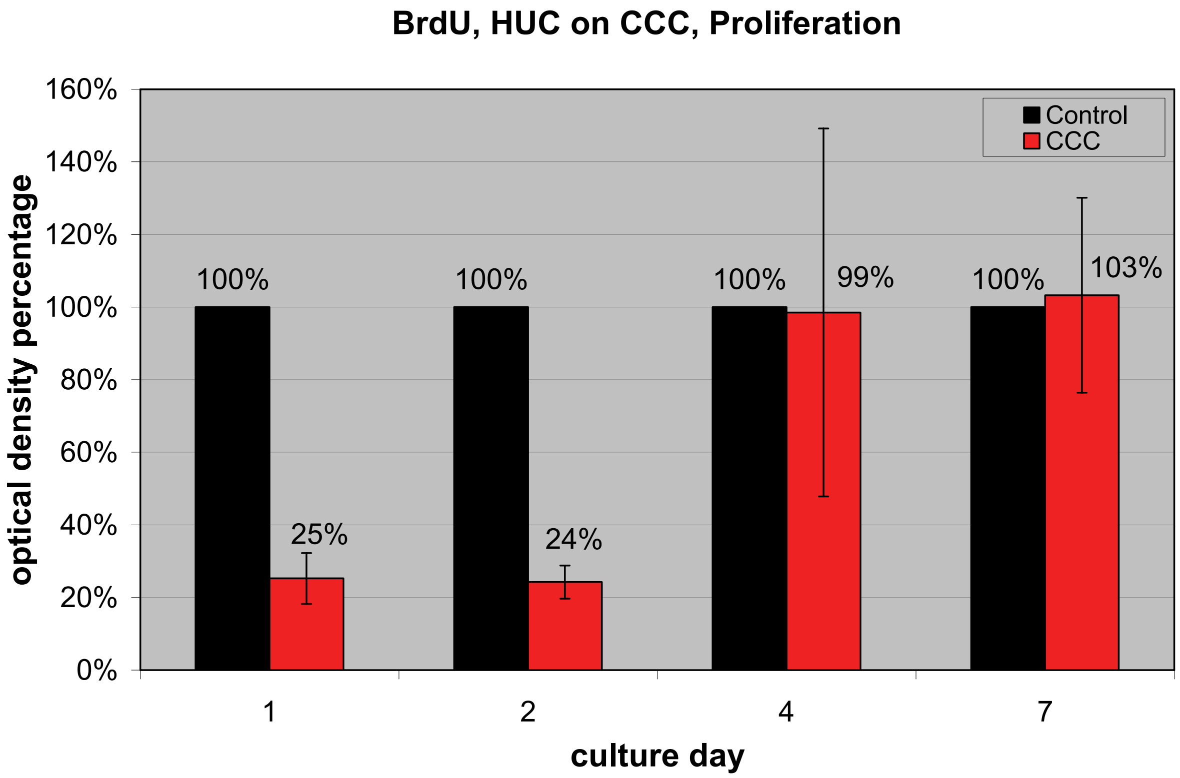

Fig. 11: BrdU assay: mean values of proliferating HUC cultures (n = 4) seeded on CCC, optical densities as percentage of the control which was set as 100% for each experiment. Seeding density 2.5 x 10^4 cells/cm^2

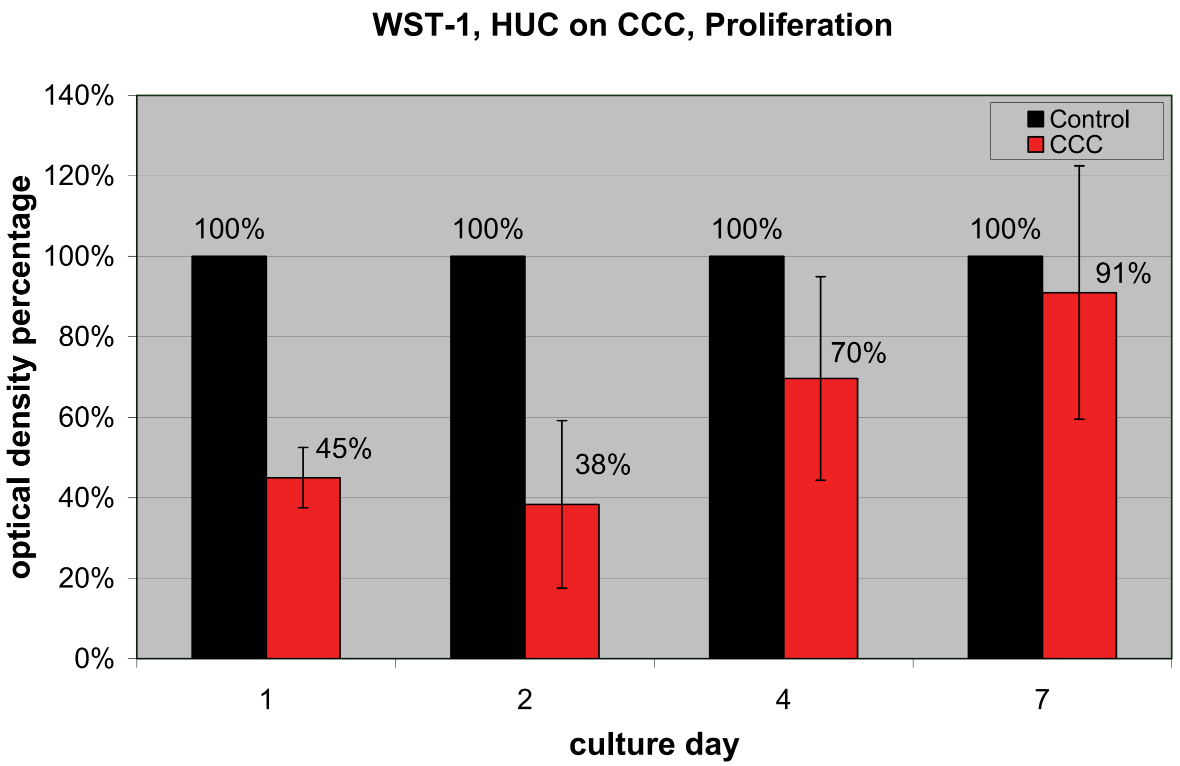

Fig. 12: WST-1 assay: mean values of proliferating HUC cultures (n = 3) seeded on CCC, optical densities as percentage of the control which was set as 100% for each experiment. Seeding density 2.5 x 10^4 cells/cm^2

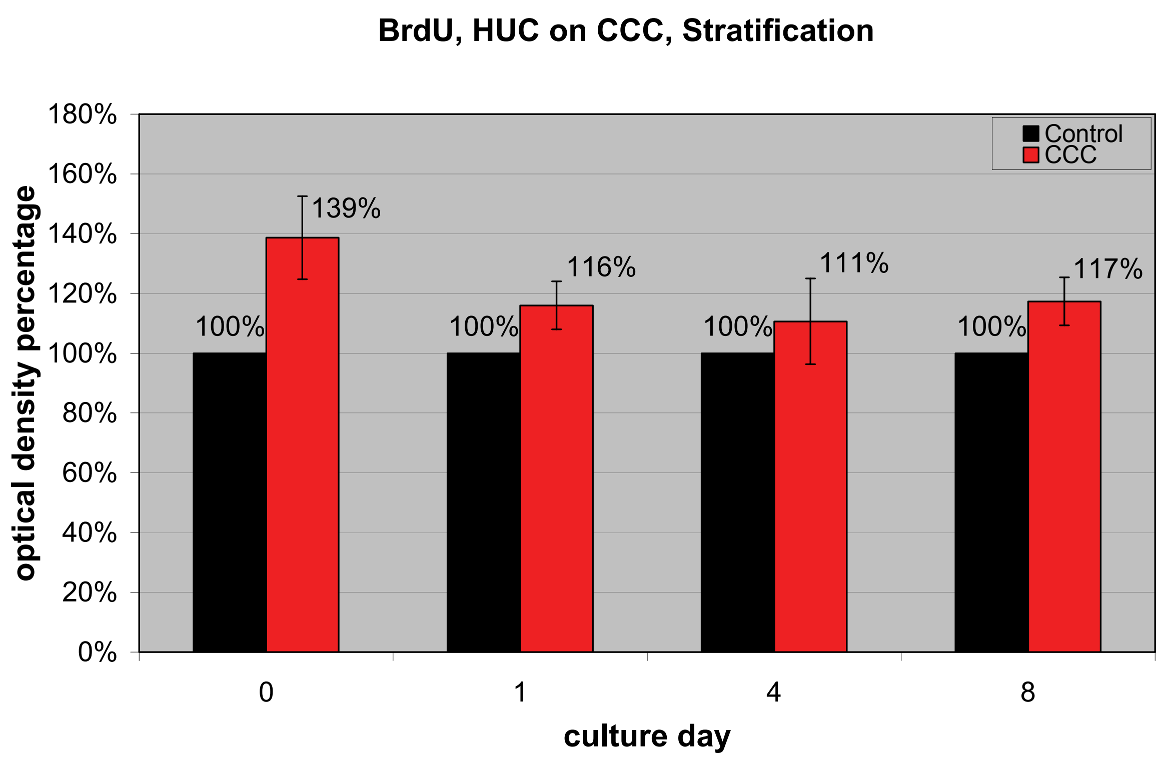

Fig. 13: BrdU assay: mean values of proliferating HUC cultures (n = 3) seeded on CCC, optical densities as percentage of the control which was set as 100% for each experiment. Seeding density 4 x 10^5 cells/cm^2

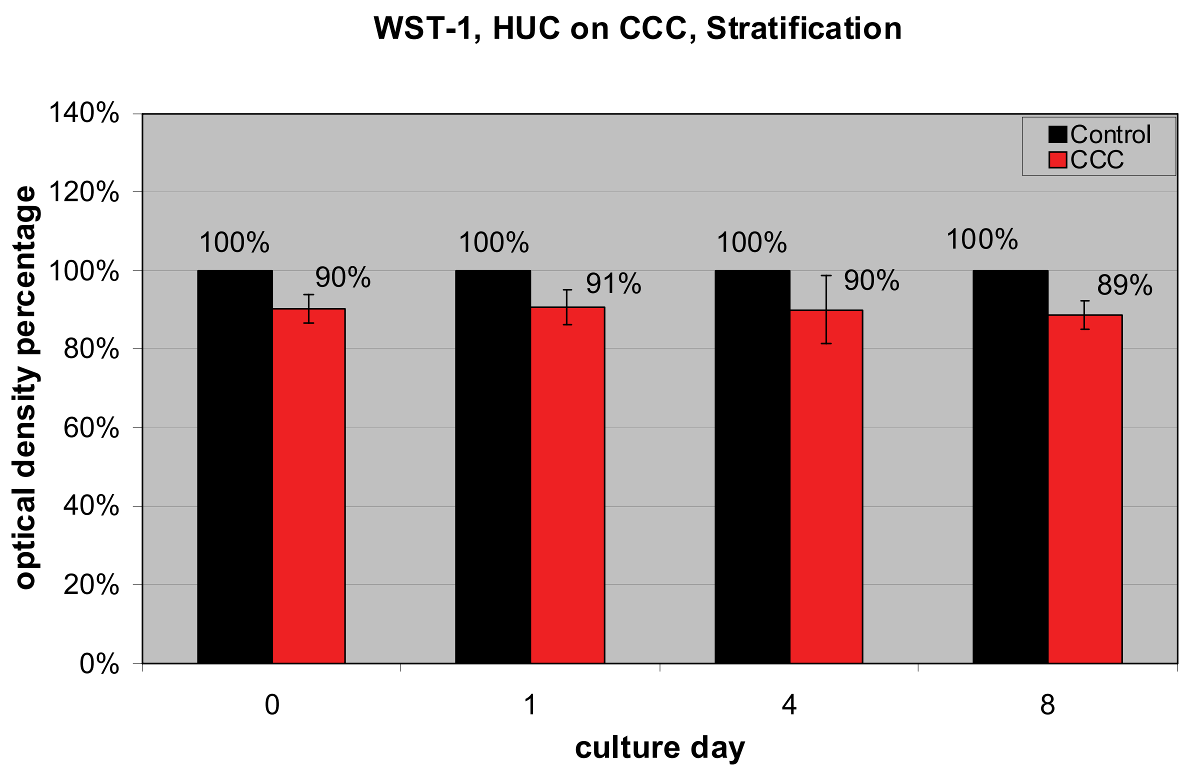

Fig. 14: WST-1 assay: mean values of stratifying HUC cultures (n = 3) seeded on CCC, optical densities as percentage of the control which was set as 100% for each experiment. Seeding density 4 x 10^5 cells/cm^2

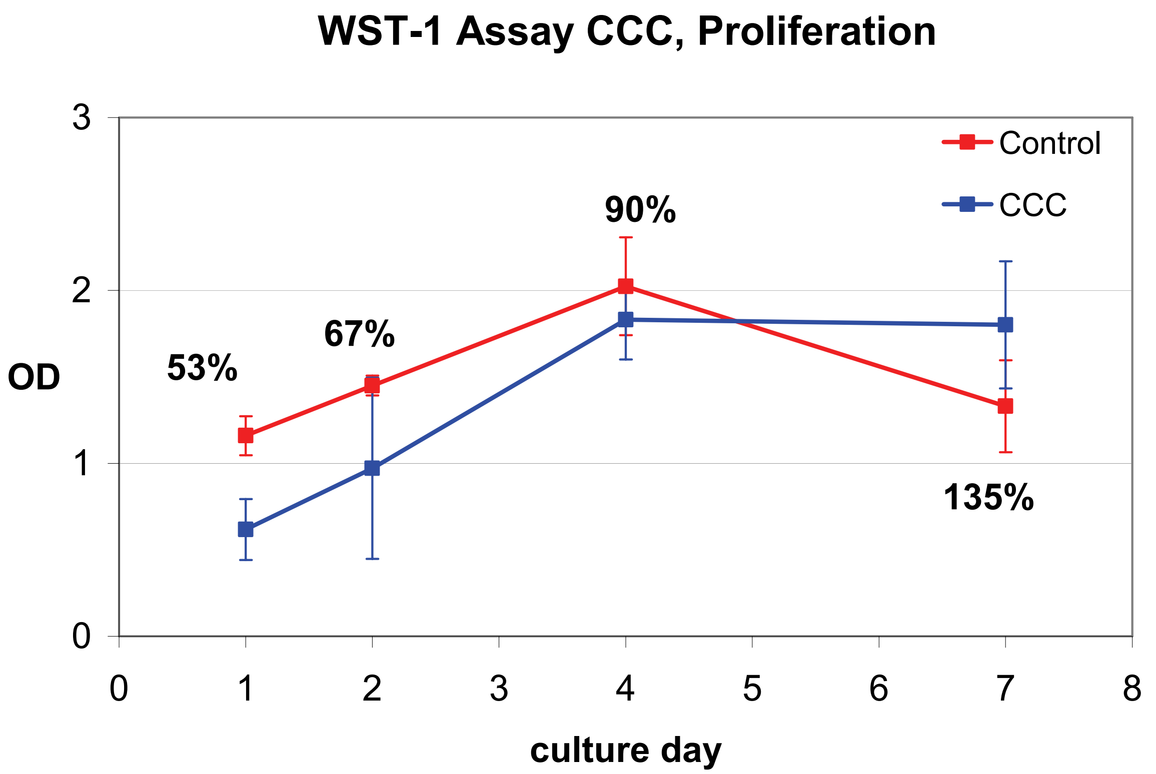

Fig. 15: Representative WST-1 assay: Development of optical density (OD) in a WST-1 assay experiment of a proliferating HUC culture (2.5 x 10^4 cells/cm^2, human ureter cell line HL 10/18 in culture passage 3). Red curve represents control (HUC on plastic surface), blue curve represents HUC on CCC.

4.1.3 Proliferation and metabolic activity of PUC on CCC

BrdU and WST-1 assays were performed to evaluate proliferation and metabolic activity of PUC in proliferating and stratifying cultures.

The results of BrdU assay for the different PUC lines were greatly varying. For PUC seeded in low density the proliferative capacity and metabolic activity decreased slightly over the four test days from mean value of 109% (WST-1 assay) and 102% (BrdU assay) on day one to 95% and 73% on day seven in comparison to controls. For stratifying PUC the general kinetic did not show considerable differences to the control group over the four test days but fluctuated slightly.

The development of results of WST-1 assay resembled the ones for BrdU. PUC cultures in the proliferating and stratifying state revealed results similar or even superior to controls. Anyhow, for proliferating cultures metabolic activity and proliferation rates decreased throughout the culture period after seeding on CCC in comparison to the controls. Table 8 and 9 show the data of optical density measurements in percentage of the controls. Definite test days after seeding for proliferation experiments (Prol, low seeding density: 2.5 x 10^4 cells/cm^2) or after induction of stratification for stratification experiments (Strat, high seeding density: 4 x 10^5 cells/cm^2) are further presented in tables 8 and 9. For all eight experimental groups three different primary cultures were used. Figure 16 and 17 demonstrate mean values of three independent BrdU and WST-1 experiments. Figures 18 and 19 demonstrate mean values of independent BrdU and WST-1 experiments on three stratifying PUC cultures each. Figure 20 shows a representative example of one BrdU test on a stratifying PUC culture to demonstrate development of optical density measurements over four test days.

Table 8: Percentage of optical density compared to controls of different primary cell lines (n = 3) showing growth development of proliferating PUC in an experimental period of seven days including four different test days (measurement time points days 1, 2, 4, and 7 after seeding)

PUC Proliferation	Day after seeding			
	1	2	4	7
BrdU Prol	97%, 145%, 65%	71%, 103%, 66%	86%, 104%, 68%	88%, 89%, 42%
Mean	102%	80%	86%	73%
WST-1 Prol	66%, 133%, 128%	54%, 124%, 124%	79%, 97%, 83%	89%, 100%, 95%
Mean	109%	101%	86%	95%

Table 9: Percentage of optical density compared to controls of different primary cell lines (n = 3) showing growth development of stratifying PUC in an experimental period of eight days including four different test days (measurement time points days 0, 1, 4, and 8 of stratification)

PUC Stratification	Day of stratification			
	0	1	4	8
BrdU Strat	171%, 130%, 64%	133%, 104%, 68%	109%, 107%, 77%	104%, 114%, 70%
Mean	122%	102%	98%	96%
WST-1 Strat	88%, 88%, 135%	103%, 93%, 107%	122%, 100%, 109%	137%, 96%, 123%
Mean	104%	101%	110%	119%

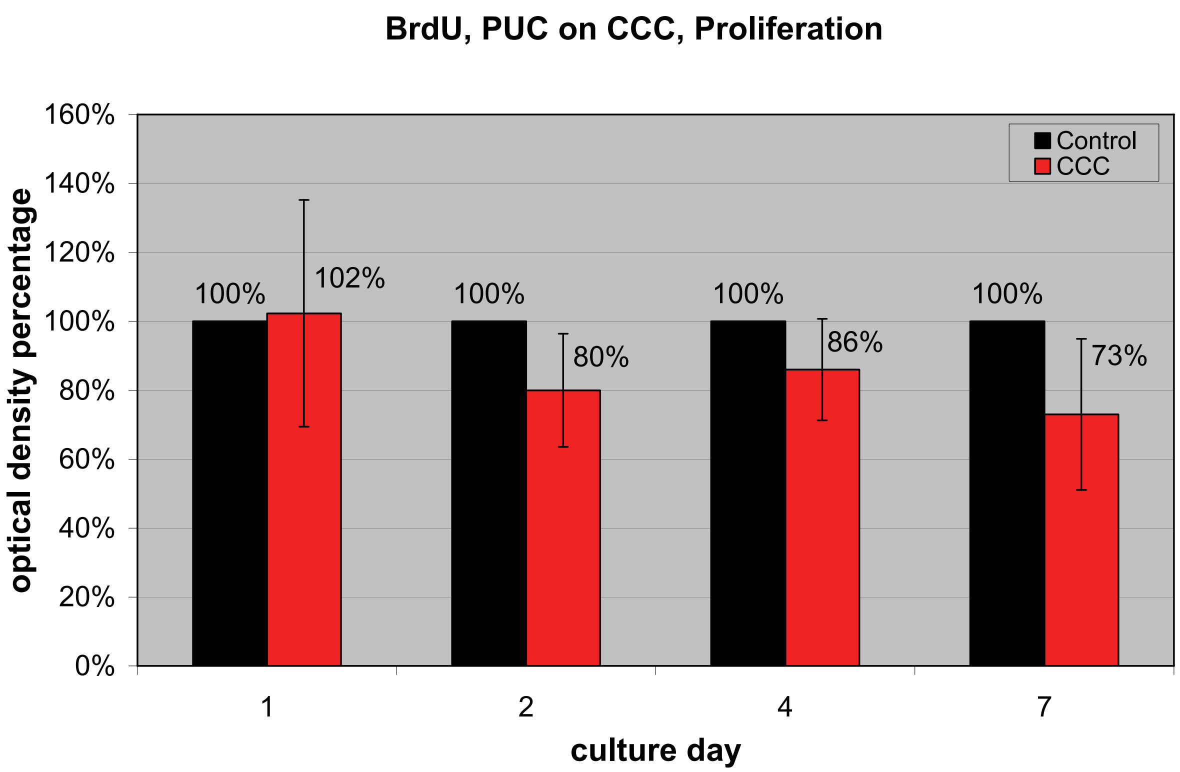

Fig. 16: BrdU assay: mean values of proliferating PUC cultures (n = 3) seeded on CCC, optical densities as percentage of the control which was set as 100% for each experiment. Seeding density 2.5 x 10^4 cells/cm^2

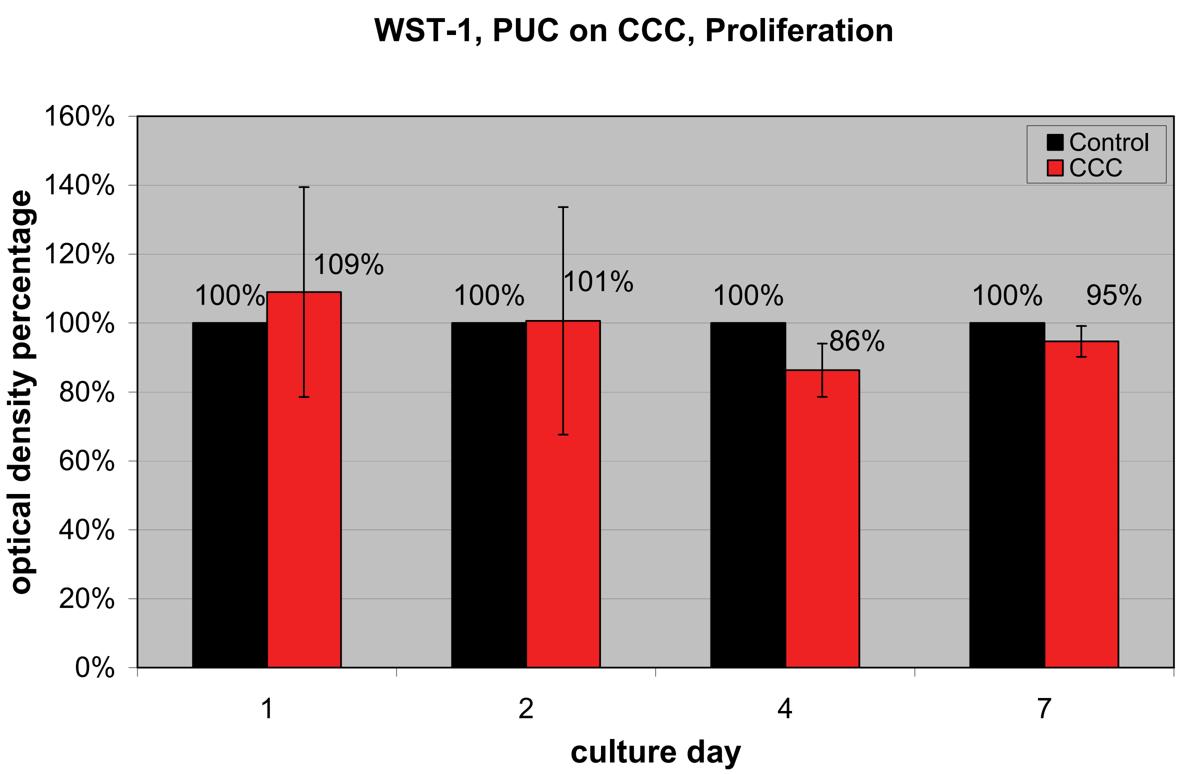

Fig. 17: WST-1 assay: mean values of proliferating PUC cultures (n = 3) seeded on CCC, optical densities as percentage of the control which was set as 100% for each experiment. Seeding density 2.5 x 10^4 cells/cm^2

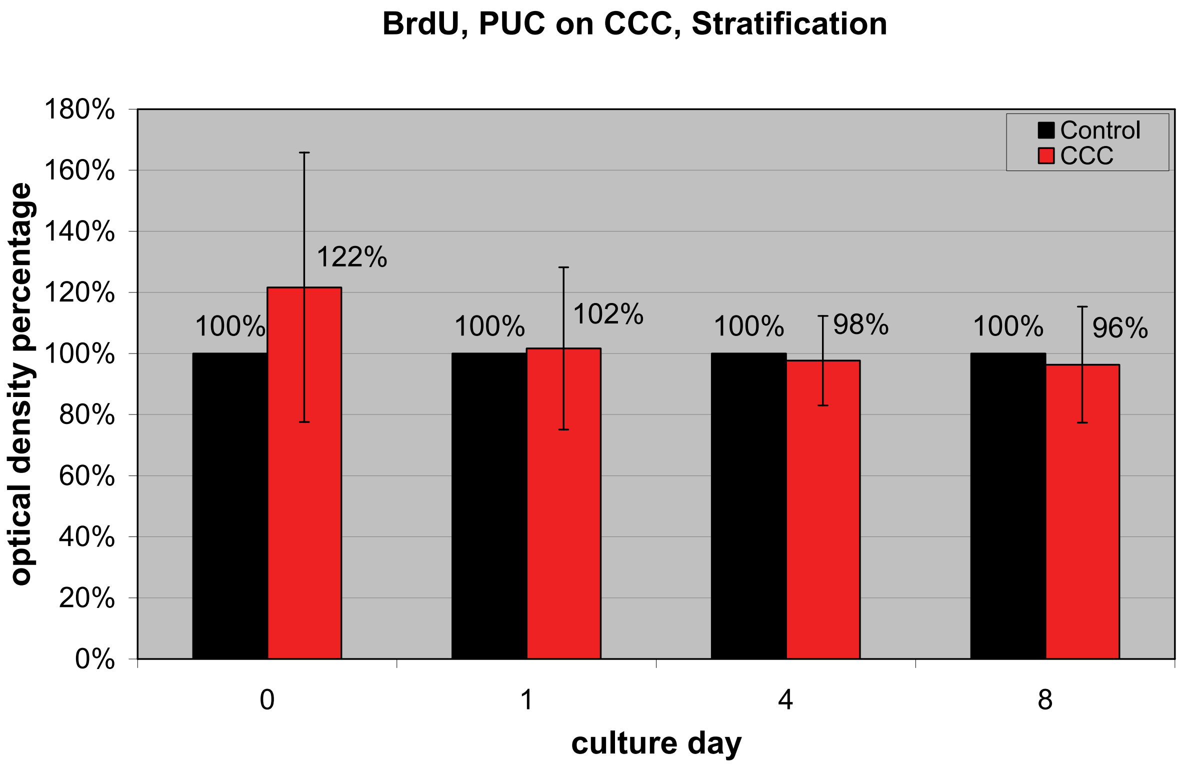

Fig. 18: BrdU assay: mean values of stratifying PUC cultures (n = 3) seeded on CCC, optical densities as percentage of the control which was set as 100% for each experiment. Seeding density 4 x 10^5 cells/cm^2

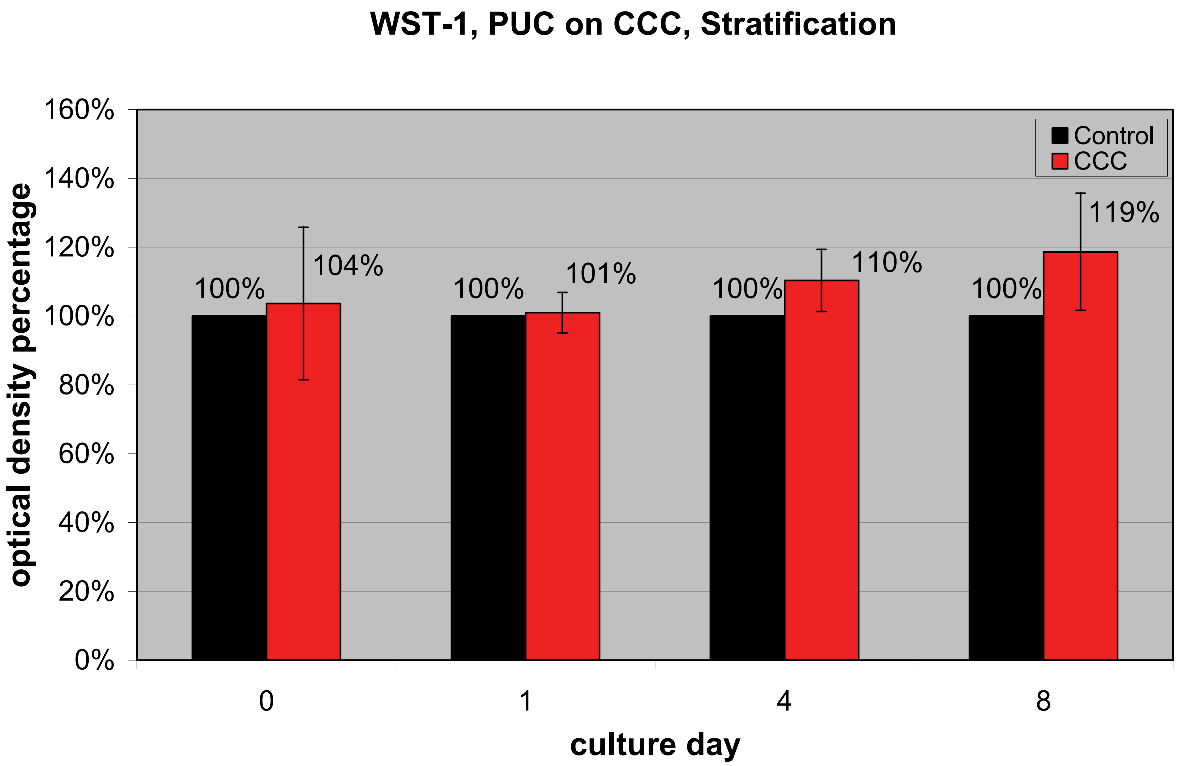

Fig. 19: WST-1 assay: mean values of stratifying PUC cultures (n = 3) seeded on CCC, optical densities as percentage of the control which was set as 100% for each experiment. Seeding density 4 x 10^5 cells/cm^2

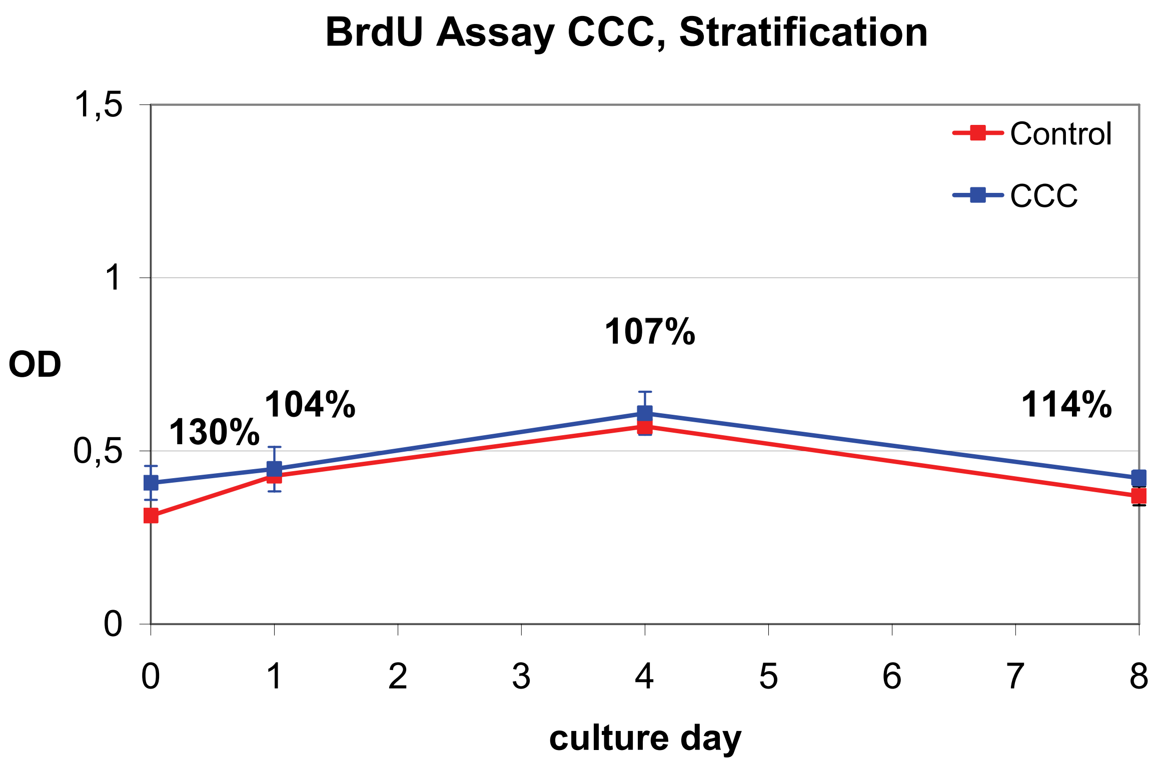

Fig. 20: Representative BrdU assay: Development of optical density (OD) in a BrdU assay experiment of a stratifying PUC culture (4 x 10^5 cells/cm^2, minipig bladder cell line MSBL 79939 in culture passage 5). Red curve represents control (PUC on plastic surface), blue curve represents PUC on CCC.

4.1.4 Cell adherence

Primary cell adherence was indirectly ascertained by counting the non-adherent cells in the culture supernatant one day after initial cell seeding. Data were determined for six HUC and six PUC cultures each seeded in low (Prol = 2.5 x 10^4 cells/cm^2) and high (Strat = 4 x 10^5 cells/cm^2) density. Altogether, 12 HUC and 12 PUC supernatant cell countings revealed the mean values presented in table 10.
Based on the total number of seeded cells the following mean value data were achieved: When seeded in high density 2.2% of HUC did not adhere to the scaffold compared to 2.0% on plastic surface. For PUC 13.6% of the cells were counted compared to 12.7% of controls. Experiments in low seeding density revealed a greater difference in HUC and PUC seeded on CCC vs. on plastic. While 16.2% of HUC and 15.3% of PUC did not adhere to the CCC, it was only 2.2% and 6.6% on plastic, respectively (Fig. 21 and 22).
Cells seeded in low density adhered to the CCC weaker than to plastic surface. In contrast, when seeded in confluence they revealed adherence to the CCC

comparable to plastic seeding. Furthermore, PUC showed inferior adherence to plastic and to CCC than HUC did.

Table 10: Mean values in percentage of total number of seeded cells. Non-adherent cells counted in the culture supernatant one day after seeding in low (Prol = 2.5 x 10^4 cells/cm^2) and high (Strat = 4 x 10^5 cells/cm^2) density on CCC and on plastic surface as a control, n = 6

		Control	CCC
HUC	Prol	**2.2%**	**16.2%**
	Strat	**2.0%**	**2.2%**
PUC	Prol	**6.6%**	**15.3%**
	Strat	**12.7%**	**13.6%**

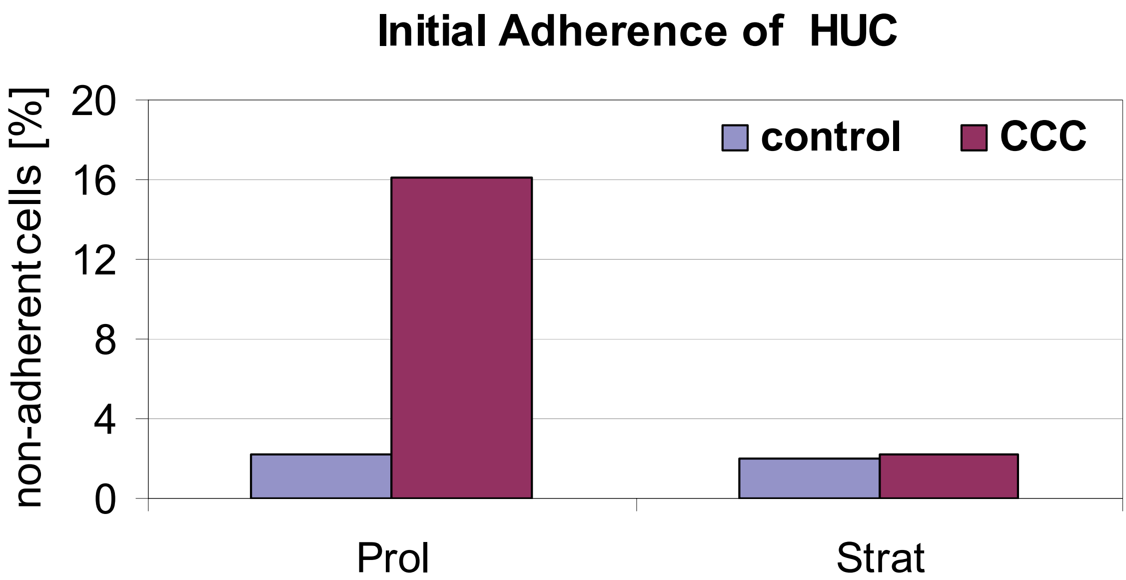

Fig. 21: Initial adherence of HUC: Mean values in percentage of total number of seeded cells. Non-adherent cells counted in the culture supernatant one day after seeding in low (Prol = 2.5 x 10^4 cells/cm^2) and high (Strat = 4 x 10^5 cells/cm^2) density on CCC and on plastic surface as a control, n = 6

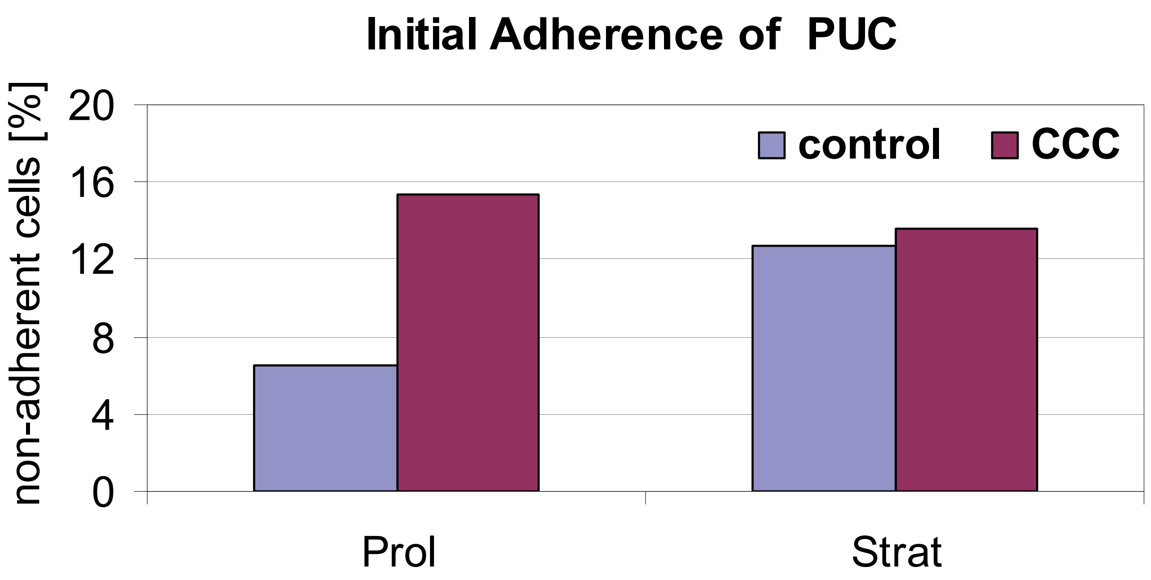

Fig. 22: Initial adherence of PUC: Mean values in percentage of total number of seeded cells. Non-adherent cells counted in the culture supernatant one day after seeding in low (Prol = 2.5×10^4 cells/cm^2) and high (Strat = 4×10^5 cells/cm^2) density on CCC and on plastic surface as a control, n = 6

4.1.5 Immunocytochemistry

Immunocytochemistry was performed with anti-pancytokeratin marker for epithelial phenotype (clone AE1/AE3), anti-fibroblast marker (clone TE-7), and anti-smooth muscle α-actin marker (clone 1A4). Positive staining was evident by brown colour development of substrate chromogen. Negative controls did not show brown staining. All HUC and PUC seeded on chamber slides stained positive for AE1/AE3 and negative for both TE-7 and 1A4 (Fig. 23 and 24). Thus, epithelial phenotype was confirmed by the specific positive and negative staining which is typical for urothelial cells.

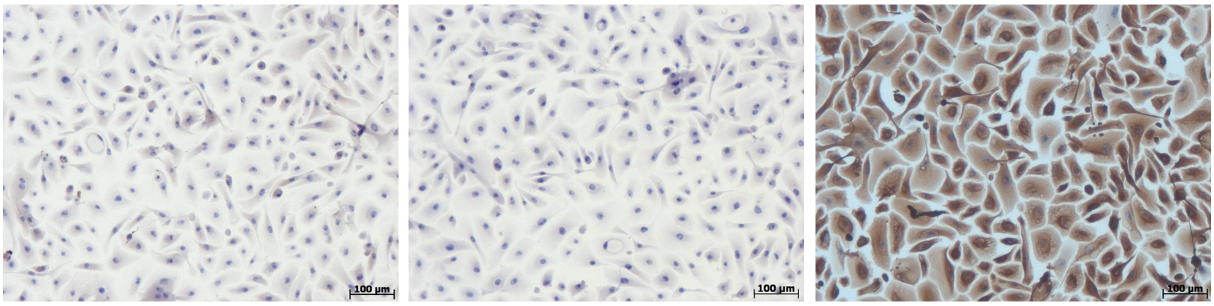

Fig. 23: Immunocytochemical staining of HUC in culture passage 4 for smooth muscle α-actin (left), fibroblast marker (centre), and pancytokeratin cocktail (right). Brown colour indicates positive staining. Bright field

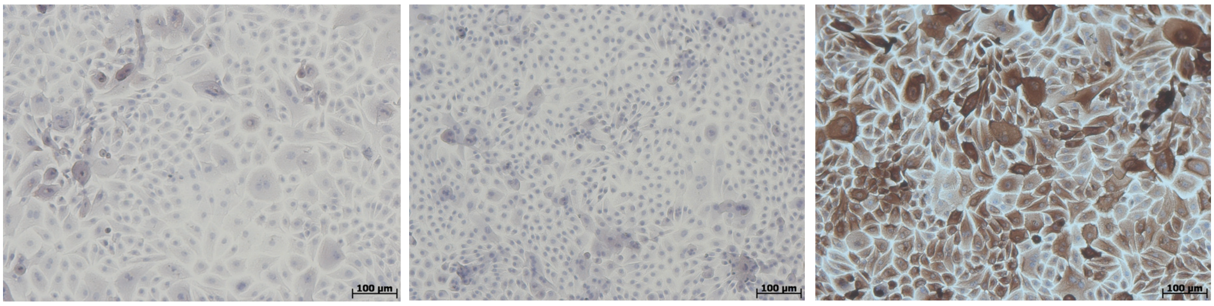

Fig. 24: Immunocytochemical staining of PUC in culture passage 7 for smooth muscle α-actin (left), fibroblast marker (centre), and pancytokeratin cocktail (right). Brown colour indicates positive staining. Bright field

4.1.6 Immunofluorescence on cryostat sections

Immunofluorescent staining showed that UC seeded on CCC inserts in 6-well plates did not form a stratifying cell sheet displaying an equal morphology as on plastic. In plastic seeded cultures cell layers resembled more compact and thick whereas on CCC the cell layers appeared thinner (Fig. 25 and 26).

Negative controls did not show green fluorescence. All investigated antigens were detected by positive staining with pancytokeratin (epithelial phenotype) showing strong green fluorescence but slightly reduced in comparison to the control (Fig. 25 and 26). CK-20 (ongoing urothelial differentiation) was detected in single superficial cells (Fig. 27). Anti-p63 (urothelial phenotype) was bound throughout the basal cells of the urothelium and showed strong fluorescence comparable to the control (Fig. 28). E-Cadherin and ZO-1 (cell-cell junctions) were partially verified and were found weaker in signals than in the control tissue (Fig. 29 and 30). Altogether, stainings on CCC resembled minimally reduced compared to plastic seeded urothelium.

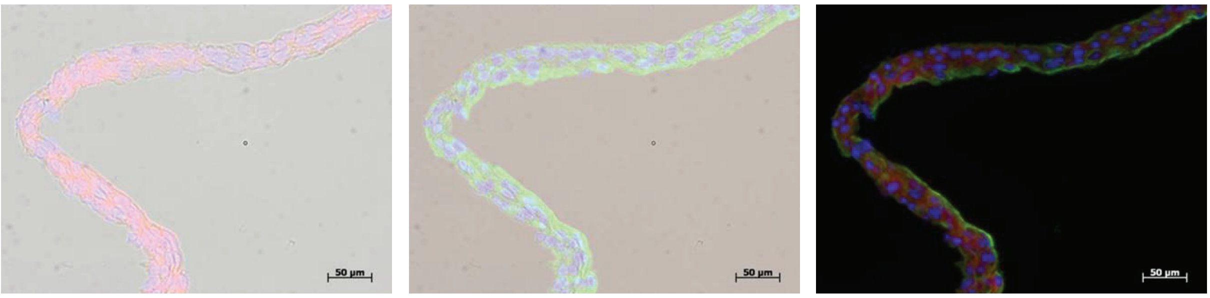

Fig. 25: Positive **pancytokeratin** staining of HUC seeded on **plastic surface**. Merged red fluorescence of PKH26, blue cell nucleus fluorescence of DAPI and bright field (left); merged green fluorescence of AE1/AE3, blue fluorescence of DAPI and bright field (centre); composite image w/o bright field (right)

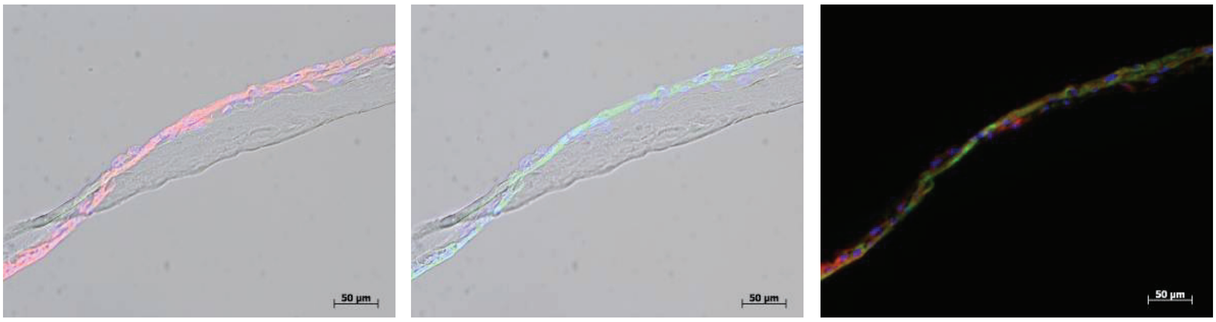

Fig. 26: Positive **pancytokeratin** staining of HUC seeded on **CCC**. Merged red fluorescence of PKH26, blue cell nucleus fluorescence of DAPI and bright field (left); merged green fluorescence of AE1/AE3, blue fluorescence of DAPI and bright field (centre); composite image w/o bright field (right)

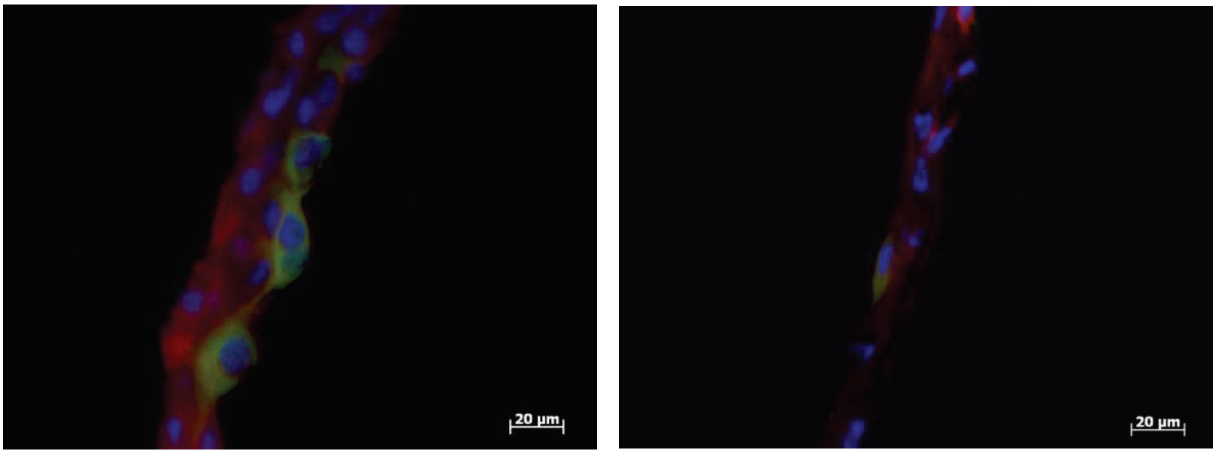

Fig. 27: Positive **CK-20** staining of HUC seeded on plastic surface (left) and on CCC (right); red fluorescence (PKH26) of HUC, blue fluorescence (DAPI) of cell nuclei and green fluorescence of CK-20 expression as a composite

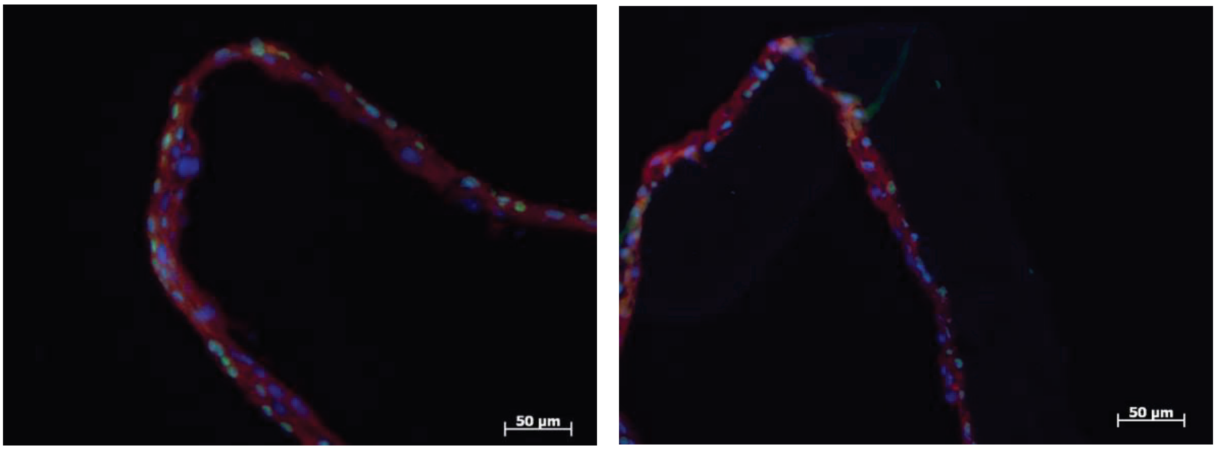

Fig. 28: Positive **p63** staining of HUC seeded on plastic surface (left) and on CCC (right); red fluorescence (PKH26) of HUC, blue fluorescence (DAPI) of cell nuclei and green fluorescence of p63 expression as a composite

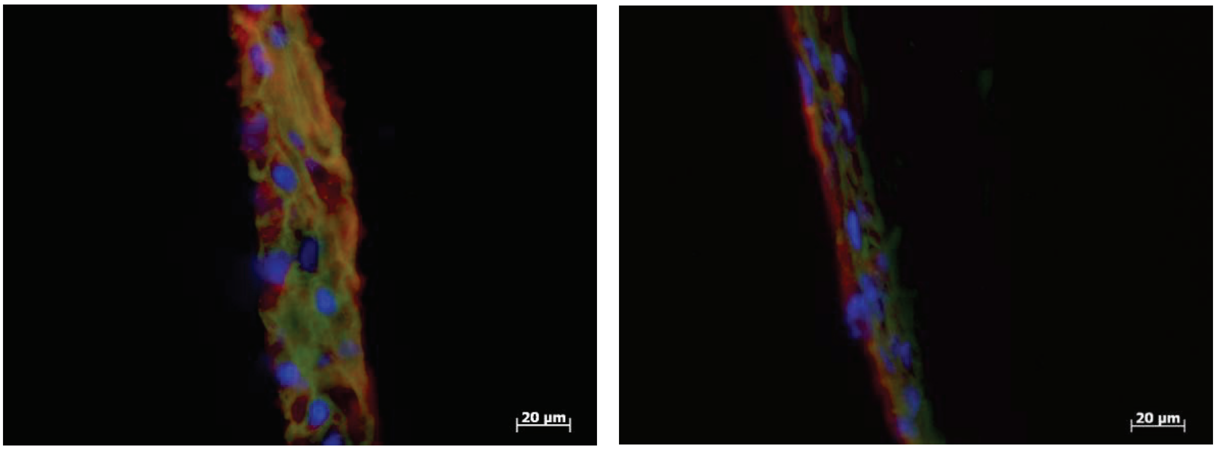

Fig. 29: Positive **E-Cadherin** staining of HUC seeded on plastic surface (left) and on CCC (right); red fluorescence (PKH26) of HUC, blue fluorescence (DAPI) of cell nuclei and green fluorescence of E-Cadherin expression as a composite.

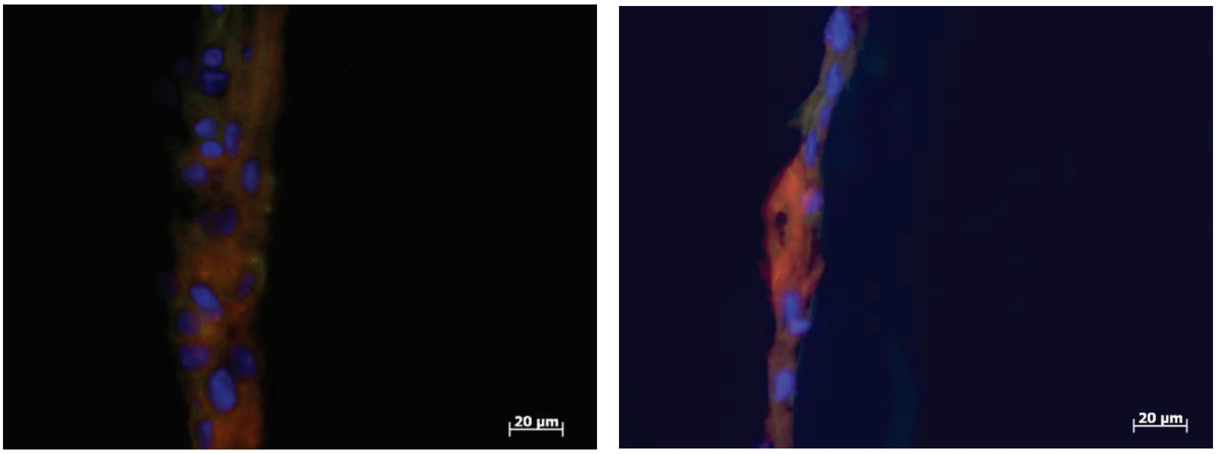

Fig. 30: Positive **ZO-1** staining of HUC seeded on plastic surface (left) and on CCC (right); red fluorescence (PKH26) of HUC, blue fluorescence (DAPI) of cell nuclei and green fluorescence of ZO-1 expression as a composite

4.2 Results from animal experiments

4.2.1 Nude rat model

4.2.1.1 Surgery outcome and follow-up

HUC were seeded on CCC and transplanted on the rectus abdominis muscle of 12 nude rats. All animals survived anaesthesia and the respective experimental periods without incidents. They did not show any physical impairments or inflammatory reactions on the transplantation site throughout the experimental period. The wound healing proceeded without inflammation or apparent rejection reactions. The rats' behaviour did not reveal any signs for discomfort like isolation, apathy or inappetence. The body weight developed analogous to reference data obtained from Charles River.

Muscle tissue was extracted spaciously after euthanisation of the rats one, two, and four weeks after surgery. When extracted after one week, the transplant could be assumed gleaming slightly on the rectus muscle. After two weeks the transplant could be recovered as a white solid object resembling connective tissue in two animals (Fig. 31). In the other two animals the transplant could not be detected macroscopically. Four weeks after surgery the transplant was not visible anymore.

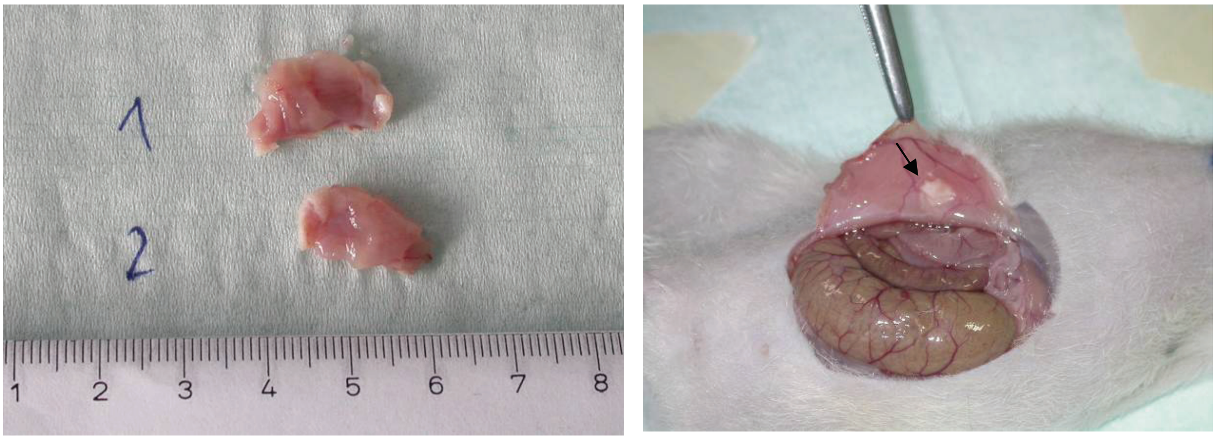

Fig. 31: Tissue sample extracted one week after surgery was divided into two pieces. Transplant is not visible macroscopically (left). Tissue extraction two weeks after surgery with connective tissue formation (right). Arrow indicates transplant position

4.2.1.2 Histologic evaluation

The transplanted HUC could be detected by red PKH26 fluorescence in all animals (Fig. 32-34). The seeded CCC was lying folded between the skin and the rectus muscle in eight animals and reached into the muscle tissue in four of them. It showed excellent integration into the host tissue in eight animals, while four revealed additional tissue formation around the transplant. None of them showed severe inflammatory signs in the HE stained tissue slides. The CCC could be located easily, showing different states of degradation and different morphologies throughout the experimental period. In four animals the CCC appeared as a dark dense structure whereas it was light and homogeneous in the remaining ones. The CCC was almost completely degraded in two animals four weeks after transplantation (Fig. 34).

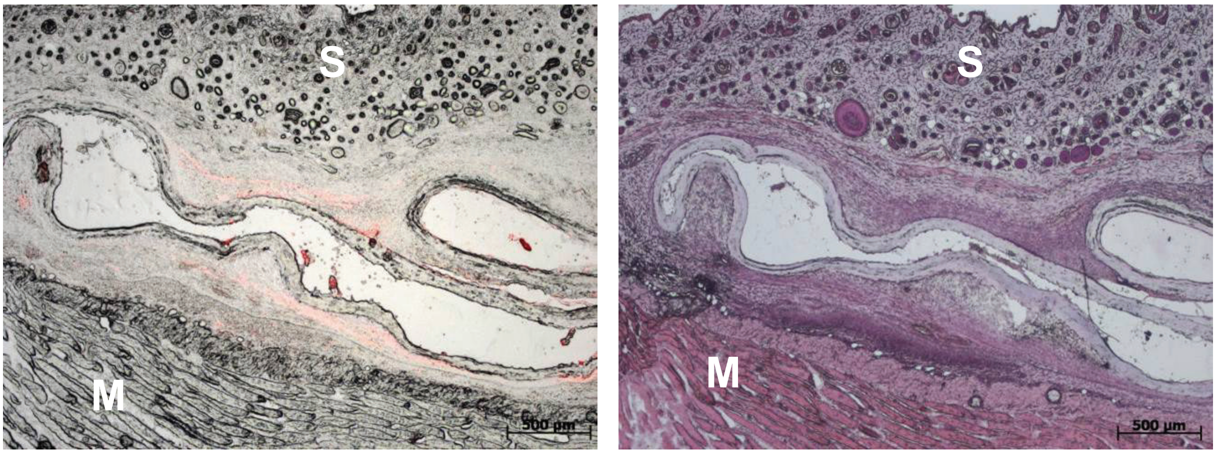

Fig. 32: Cryostat section **one week after transplantation**. Unstained section showing red fluorescence of PKH26-labelled transplanted HUC (left). HE-stained section (right). S = skin, M = rectus abdominis muscle. Bright field

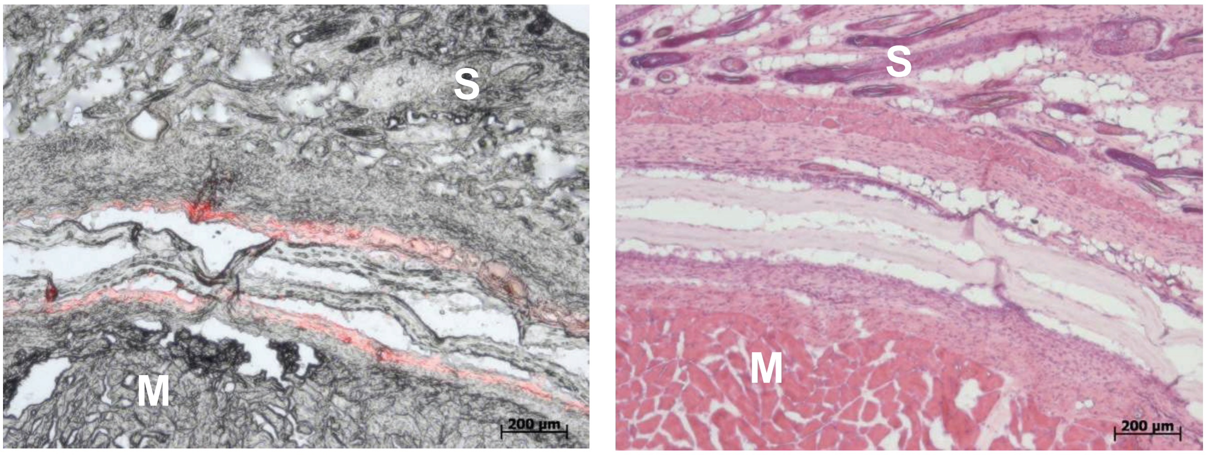

Fig. 33: Cryostat section **two weeks after transplantation**. Unstained section showing red fluorescence of PKH26-labelled transplanted HUC (left). HE-stained section (right). S = skin, M = rectus abdominis muscle. Bright field

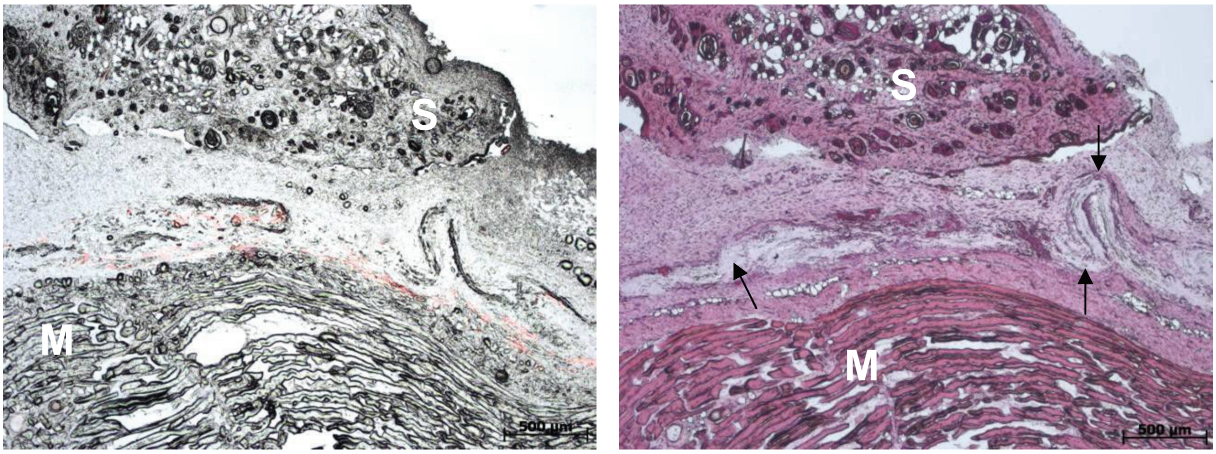

Fig. 34: Cryostat section **four weeks after transplantation** Unstained section showing red fluorescence of PKH26-labelled transplanted HUC (left). HE-stained section (right). Transplant almost vanished in the subcutaneous tissue. S = skin, M = rectus abdominis muscle. Arrows indicate CCC in degeneration. Bright field

4.2.1.3 Evaluation of immunohistological staining

Cryostat tissue sections of CCC constructs in rectus muscle of nude rats were characterised via immunofluorescence. Negative controls did not show green fluorescence. None of the used primary antibodies showed unspecific binding to muscle and subcutaneous tissue surrounding the transplant.

Positive pancytokeratin expression was assessed at the transplant position for all animals one week and for two animals two weeks after surgery (Fig. 35). Expression of CK-20, p63, E-Cadherin, and ZO-1 was verified in the groups one and two weeks after surgery (Fig. 36-39). Four weeks after surgery anti-pancytokeratin, the most sensitive antibody for epithelial phenotype, was not bound (Fig. 40).

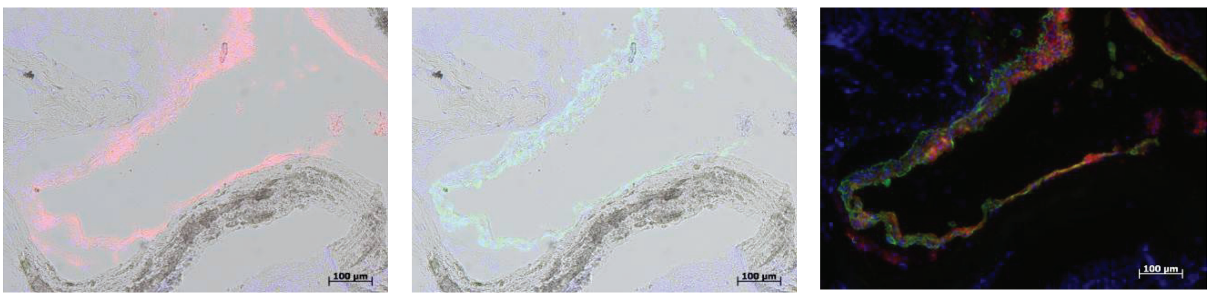

Fig. 35: Positive pancytokeratin expression of cryostat section two weeks after transplantation. Merged red fluorescence of PKH26-labelled transplanted HUC, blue cell nucleus fluorescence of DAPI and bright field (left). Merged green fluorescence for pancytokeratin, blue cell nucleus fluorescence of DAPI and bright field (centre). Composite image w/o bright field (right)

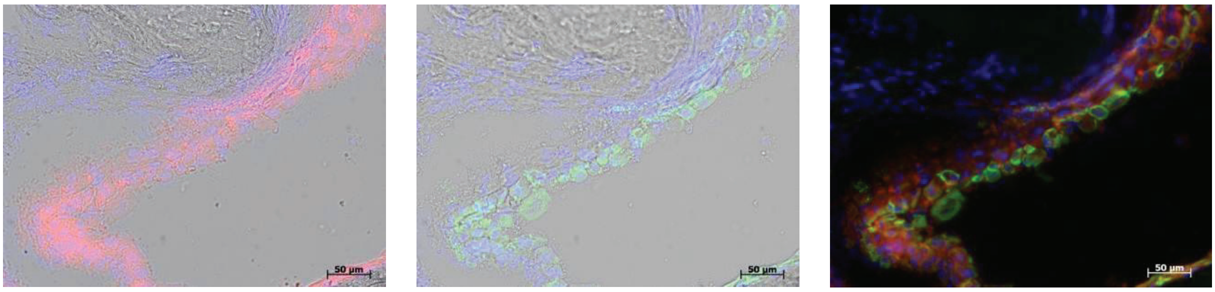

Fig. 36: Positive CK-20 expression of cryostat section two weeks after transplantation. Merged red fluorescence of PKH26-labelled transplanted HUC, blue cell nucleus fluorescence of DAPI and bright field (left). Merged green fluorescence for CK-20, blue cell nucleus fluorescence of DAPI and bright field (centre). Composite image w/o bright field (right)

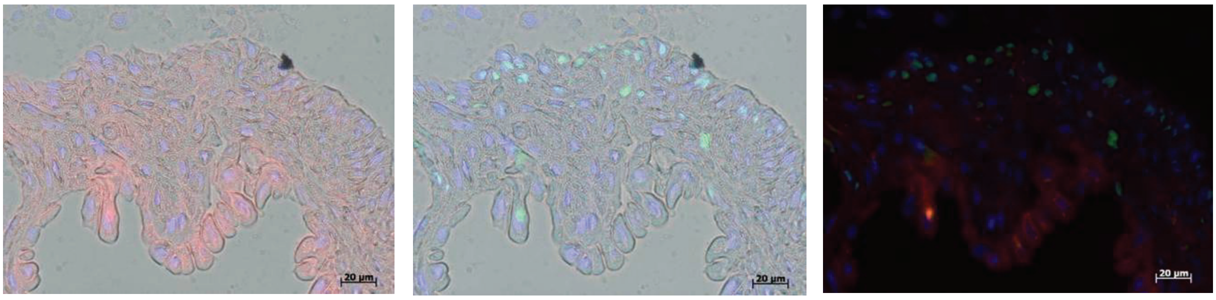

Fig. 37: Positive p63 expression of cryostat section two weeks after transplantation. Merged red fluorescence of PKH26-labelled transplanted HUC, blue cell nucleus fluorescence of DAPI and bright field (left). Merged green fluorescence for p63, blue cell nucleus fluorescence of DAPI and bright field (centre). Composite image w/o bright field (right)

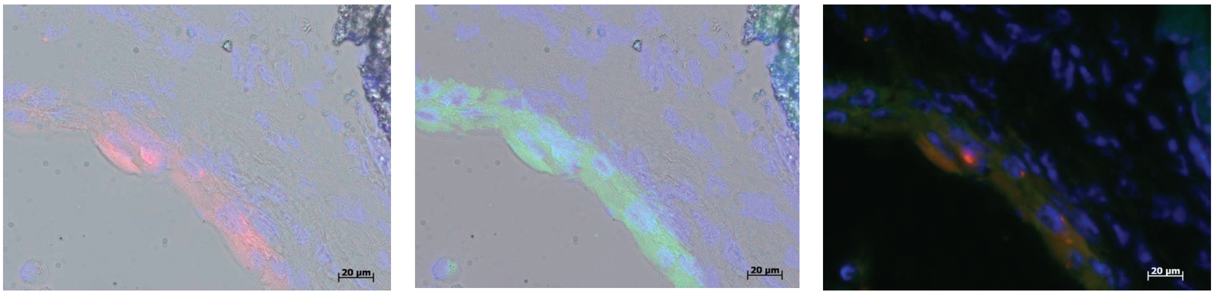

Fig. 38: Positive E-Cadherin expression of cryostat section two weeks after transplantation. Merged red fluorescence of PKH26-labelled transplanted HUC, blue cell nucleus fluorescence of DAPI and bright field (left). Merged green fluorescence for E-Cadherin, blue cell nucleus fluorescence of DAPI and bright field (centre). Composite image w/o bright field (right)

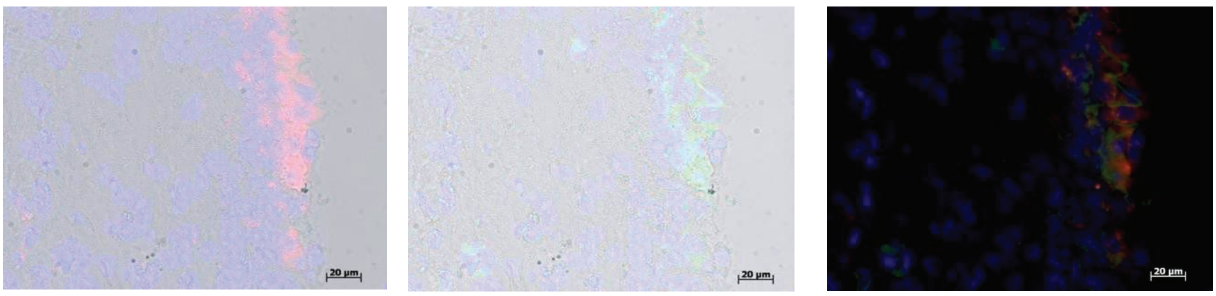

Fig. 39: Positive ZO-1 expression of cryostat section two weeks after transplantation. Merged red fluorescence of PKH26-labelled transplanted HUC, blue cell nucleus fluorescence of DAPI and bright field (left). Merged green fluorescence for ZO-1, blue cell nucleus fluorescence of DAPI and bright field (centre). Composite image w/o bright field (right)

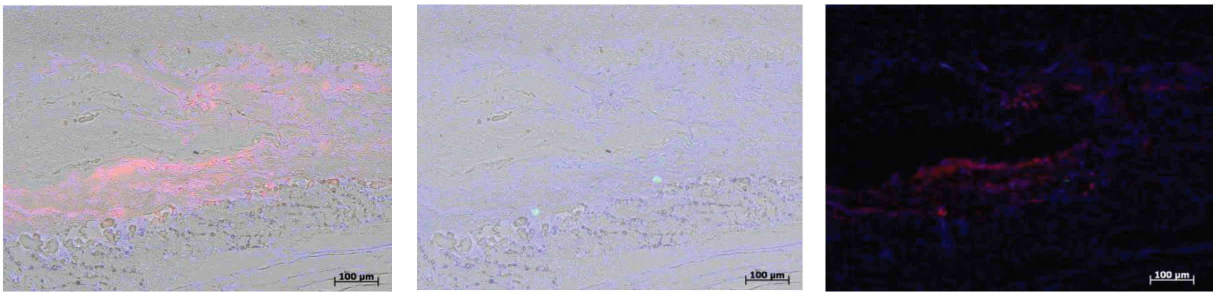

Fig. 40: Negative pancytokeratin expression of cryostat section four weeks after transplantation. Merged red fluorescence of PKH26-labelled transplanted HUC, blue cell nucleus fluorescence of DAPI and bright field (left). Merged green fluorescence for pancytokeratin, blue cell nucleus fluorescence of DAPI and bright field (centre). Composite image w/o bright field (right)

4.2.2 Minipig model

4.2.2.1 Cell culture, surgery outcome, and follow-up

All animals survived anaesthesia well and did not show impairments during the complete experimental period. White blood counts did not reveal systemic inflammation or rejection reactions. The vesicostomy healed well and all animals passed urine without complications.

When the bladder was opened initially, two animals showed hyperaemia and swelling of the bladder wall as well as opaque and smelling urine. As these animals were in good general condition, they were set under the same antibiotic regime like all other animals after surgery. Cell culture success was suboptimal in these two animals, meaning that PUC were growing slowly and stratified cultures showed inhomogeneous morphology. In one of these animals urothelial cells only formed a thin urothelium while cells of the other animals formed thicker cell sheets.

When the animals were sacrificed and the urethra removed, no inflammatory signs or stricture formation could be verified macroscopically.

4.2.2.2 Urethrographic evaluation

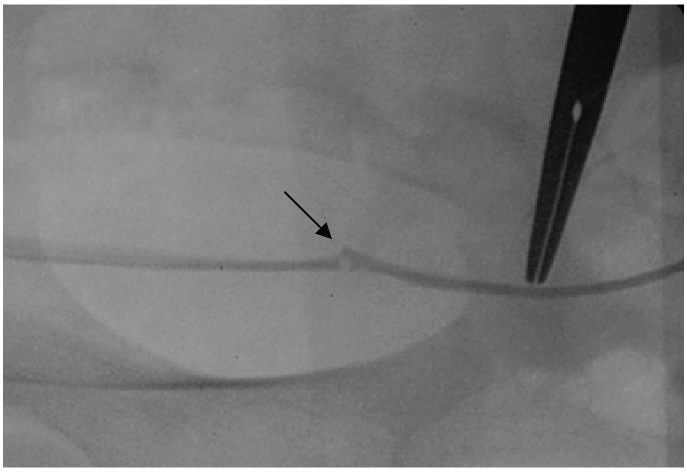

Fig. 41: Preoperative status of the urethra determined by urethrography demonstrating a physiological urethral lumen. Arrow indicates the end of the urethral catheter.

Prior to surgery all animals showed urethral lumens without any signs of stricture or other impairments (Fig. 41). A defined stricture formation after thermocoagulation could not be demonstrated by contrast x-ray, but slight narrowing was observed in single minipigs (Fig. 42). More important, none of the animals showed stricture formation after transplantation of cell seeded CCC (Fig. 43).

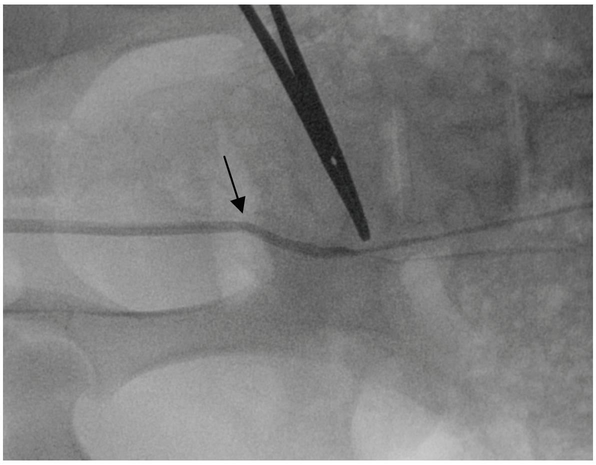

Fig. 42: Urethral status three weeks after stricture induction by thermocoagulation. Arrow indicates potential stricture site with slight narrowing.

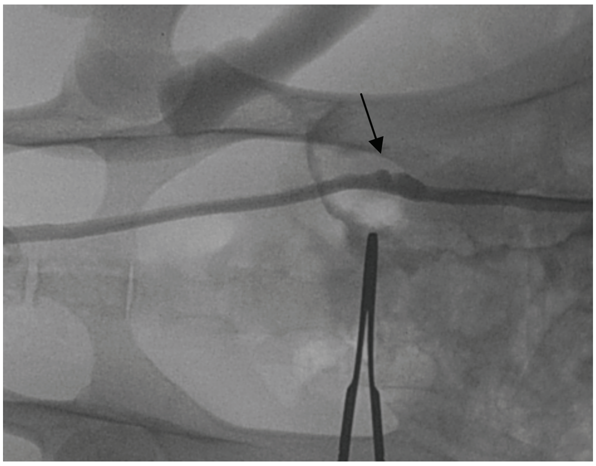

Fig. 43: Urethral status four weeks after urethroplasty. Urethral patency is established. Arrow indicates former stricture site.

Evaluation of urethrographic photographs did not reveal a considerable difference in urethral morphology prior to surgery and after transplantation.

4.2.2.3 Histologic evaluation

The seeded CCC could be detected until four weeks after surgery though there were only small pieces of the CCC left due to degradation. It showed good tissue integration without signs of inflammation in HE-stained sections. The red fluorescence of PKH26 was reduced in course of time meaning that strong fluorescence was detected after one and two weeks whereas it slightly decreased after four weeks. The red fluorescent cells were mostly lying in direct contact to native urothelium. However, in animals where the CCC was still intact, it was visible that the cells were shifted off in large part (Fig. 44-46).

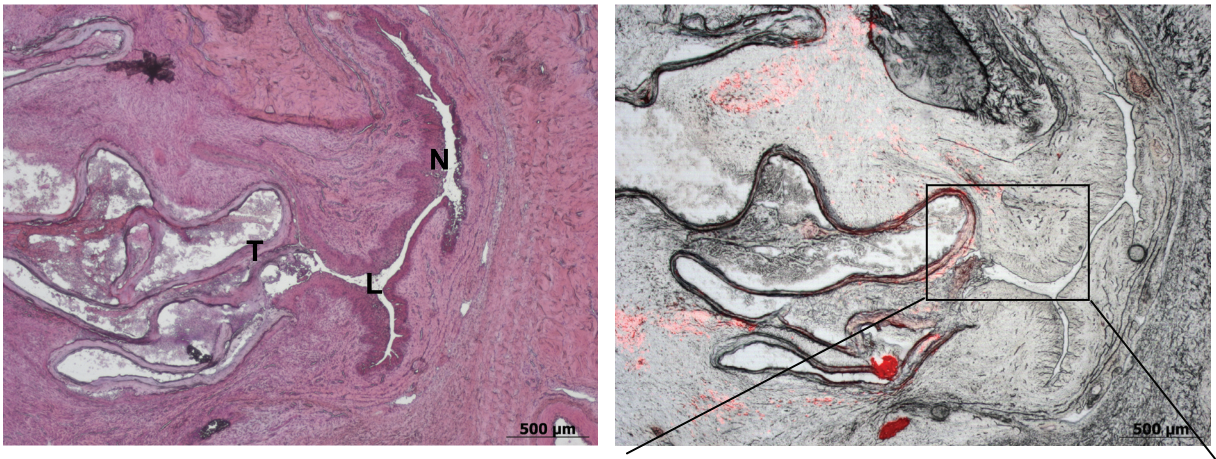

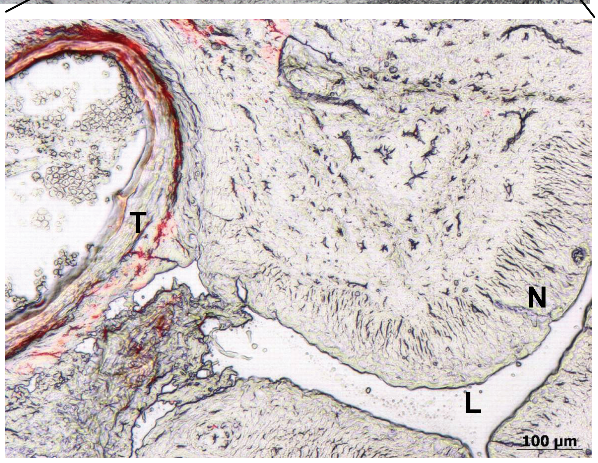

Fig. 44: Cryostat section at **one week after transplantation**. CCC can be located clearly in HE-stained section (top left). Parts of the transplanted cells (red fluorescence) are lying in direct contact to the native urothelium and to the matrix (top right and enlarged section below). L = urethral lumen, N = native urothelium, T = transplant; Bright field

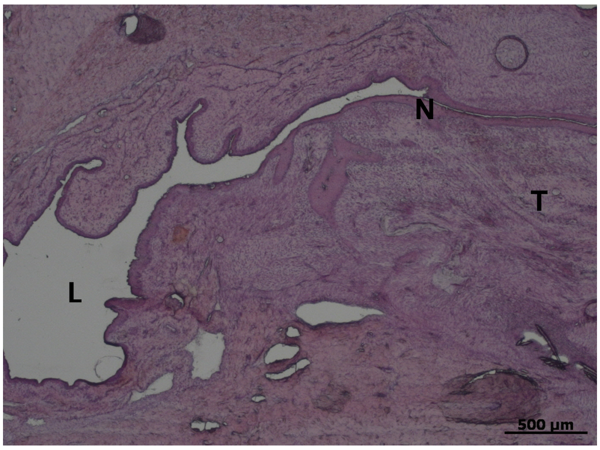

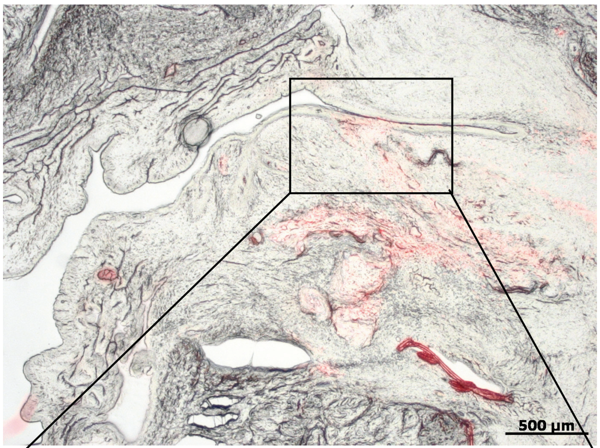

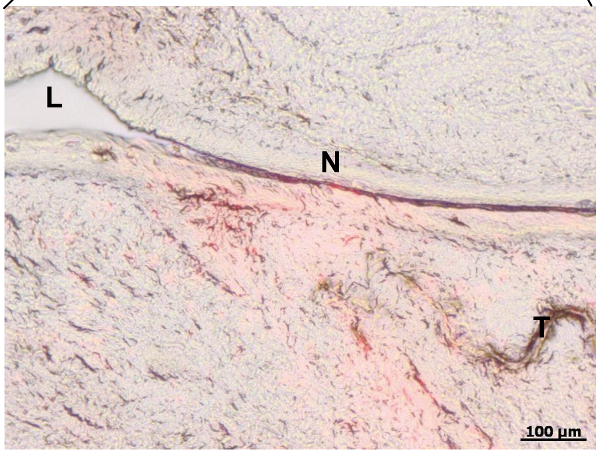

Fig. 45: Cryostat section at **two weeks after transplantation**. Pieces of the CCC can be located in HE-stained section (top left). Parts of the transplanted cells (red fluorescence) are lying in direct contact to the native urothelium (top right and enlarged section below). L = urethral lumen, N = native urothelium, T = transplant; Bright field

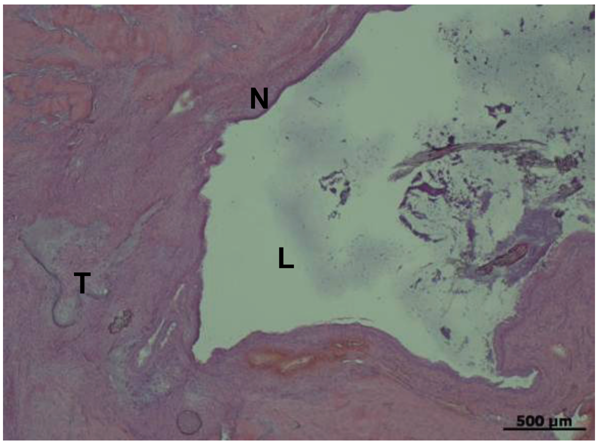

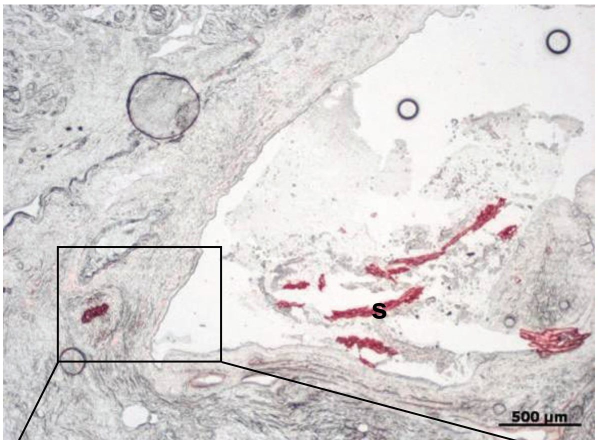

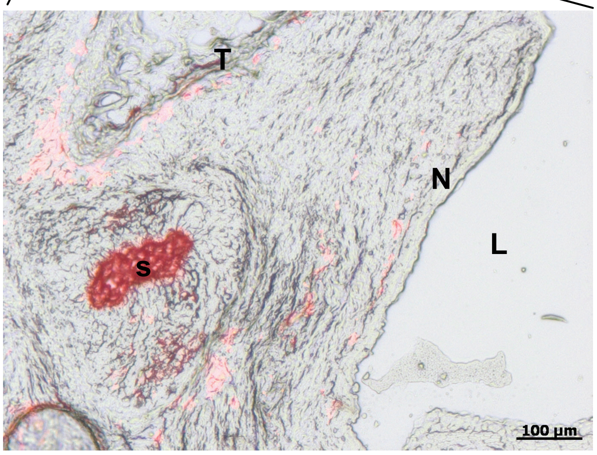

Fig. 46: Cryostat section at **four weeks after transplantation**. Pieces of the CCC can be located in HE-stained section (top left). Parts of the transplanted cells (red fluorescence) are lying in direct contact to the native urothelium (top right and enlarged section below). Strong red fluorescence of suture material (s). L = urethral lumen, N = native urothelium, T = transplant; Bright field

4.2.2.4 Evaluation of immunohistological staining

Immunohistologically stained sections were checked for red PKH26 and green antibody fluorescence. Native urothelium stained positive for the tested markers pancytokeratin, CK-20, p63, ZO-1, and E-Cadherin and served as a positive control to confirm the methodical approach.

Urothelial phenotype of the transplanted cells in vivo was proved by red PKH26 and green antibody double fluorescence. Pancytokeratin verified positive epithelial phenotype by double fluorescent areas in all animals though only weak fluorescence was detected after four weeks in contrast to native urothelium (Fig. 47-49). For CK-20 verification double fluorescence indicating the formation of umbrella cells was detected over the period of two weeks in single cells as well as for ZO-1 and E-Cadherin, both indicating cell-cell junctions. P63 was detected in PKH26 positive areas until two weeks after cell application (Fig. 50-53).

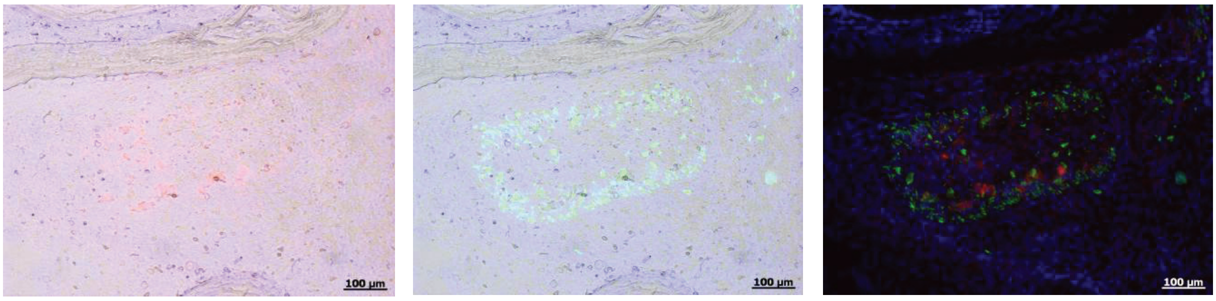

Fig. 47: Positive **pancytokeratin expression** proven by double fluorescence of cryostat section **one week after transplantation**. Merged red fluorescence of PKH26-labelled transplanted HUC, blue cell nucleus fluorescence of DAPI and bright field (left). Merged green fluorescence for pancytokeratin, blue cell nucleus fluorescence of DAPI and bright field (centre). Composite image w/o bright field (right)

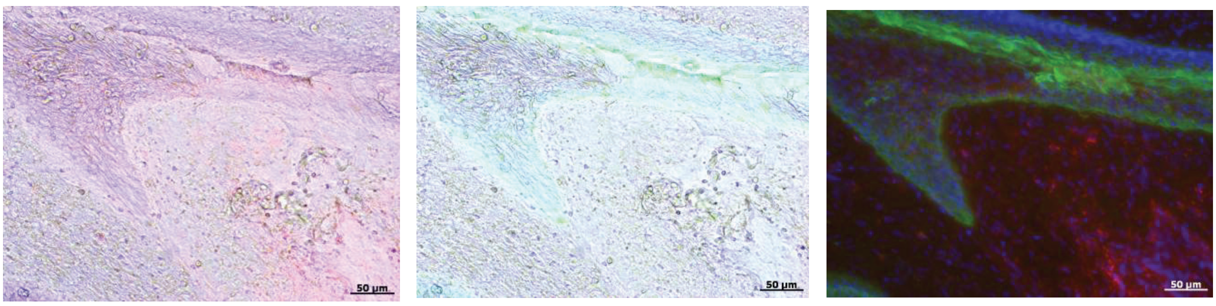

Fig. 48: Positive **pancytokeratin expression** proven by double fluorescence of cryostat section **two weeks after transplantation**. Merged red fluorescence of PKH26-labelled transplanted HUC, blue cell nucleus fluorescence of DAPI and bright field (left). Merged green fluorescence for pancytokeratin, blue cell nucleus fluorescence of DAPI and bright field (centre). Composite image w/o bright field (right)

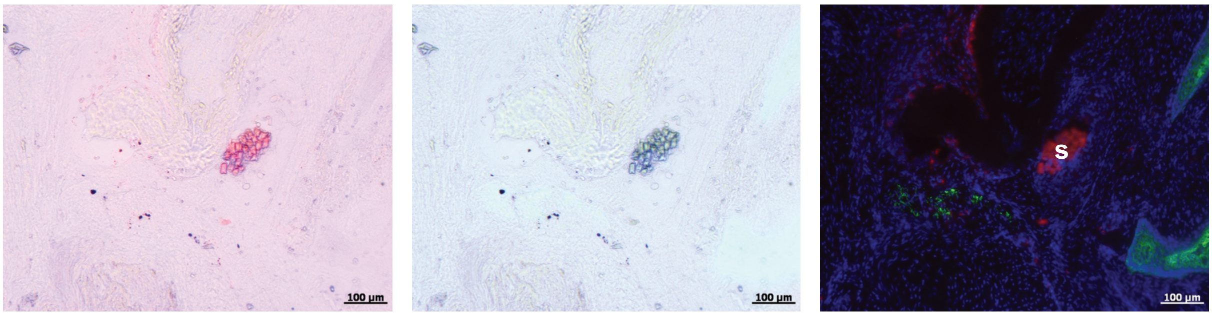

Fig. 49: Weak **pancytokeratin expression** proven by double fluorescence of cryostat section **four weeks after transplantation**. Merged red fluorescence of PKH26-labelled transplanted HUC, blue cell nucleus fluorescence of DAPI and bright field (left). Merged green fluorescence for pancytokeratin, blue cell nucleus fluorescence of DAPI and bright field (centre); Composite image (right). s = suture material

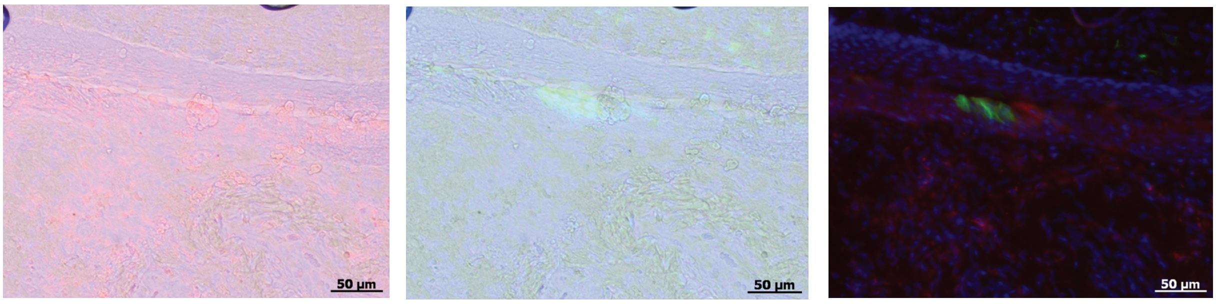

Fig. 50: Positive **CK-20 expression** proven by double fluorescence of cryostat section **two weeks after transplantation**. Merged red fluorescence of PKH26-labelled transplanted HUC, blue cell nucleus fluorescence of DAPI and bright field (left). Merged green fluorescence for CK-20, blue cell nucleus fluorescence of DAPI and bright field (centre). Composite image (right)

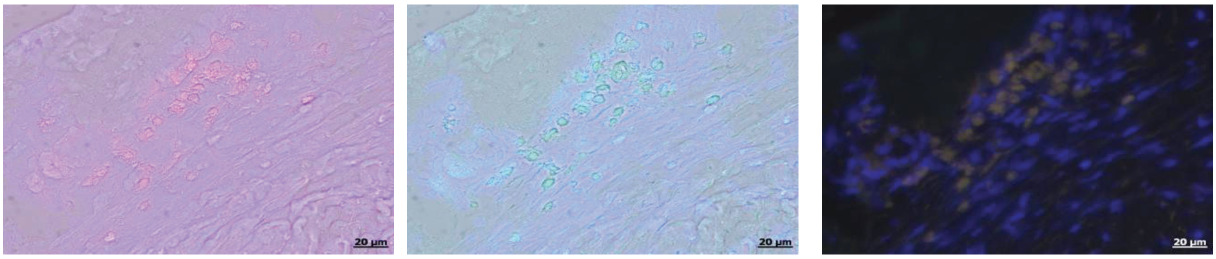

Fig. 51: Positive **p63 expression** proven by double fluorescence of cryostat section **two weeks after transplantation**. Merged red fluorescence of PKH26-labelled transplanted HUC, blue cell nucleus fluorescence of DAPI and bright field (left). Merged green fluorescence for p63, blue cell nucleus fluorescence of DAPI and bright field (centre). Composite image (right)

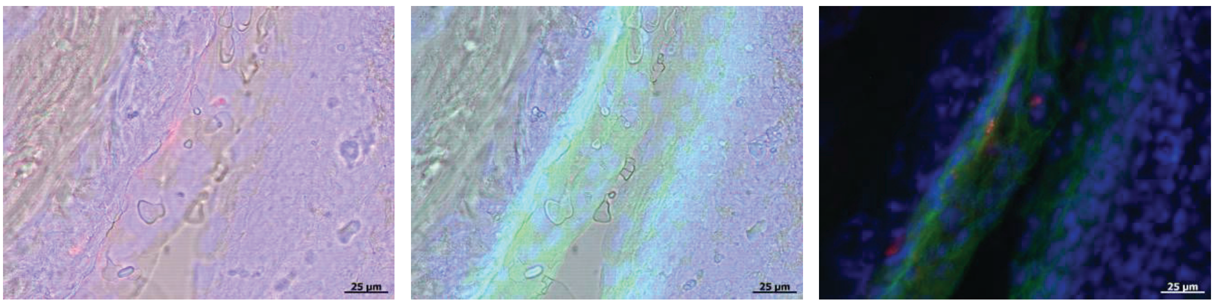

Fig. 52: Positive **E-Cadherin expression** proven by double fluorescence of cryostat section **one week after transplantation.** Merged red fluorescence of PKH26-labelled transplanted HUC, blue cell nucleus fluorescence of DAPI and bright field (left). Merged green fluorescence for E-Cadherin, blue cell nucleus fluorescence of DAPI and bright field (centre). Composite image (right)

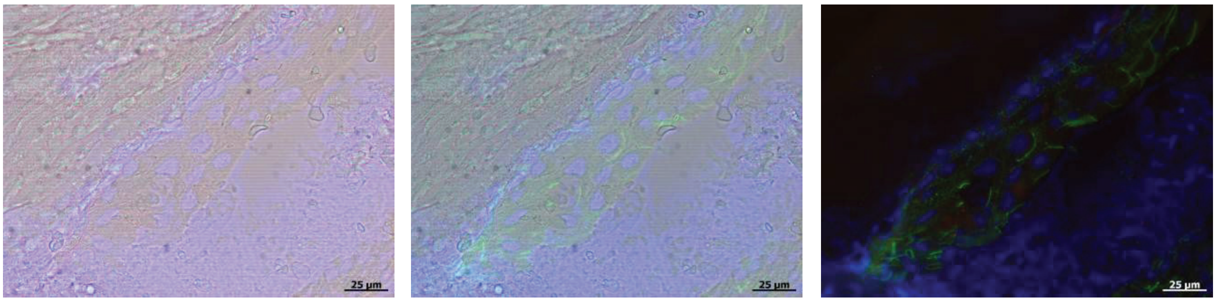

Fig. 53: Positive **ZO-1 expression** proven by double fluorescence of cryostat section **one week after transplantation**. Merged red fluorescence of PKH26-labelled transplanted HUC, blue cell nucleus fluorescence of DAPI and bright field (left). Merged green fluorescence for ZO-1, blue cell nucleus fluorescence of DAPI and bright field (centre). Composite image (right)

5 Discussion

5.1 In vitro properties of the CCC for seeding of HUC and PUC

5.1.1 Cell culture and multilayer growth

HUC and PUC showed good growth behaviour in all in vitro settings. Although cell culture was performed in cKSFM successfully in other studies and for all in vitro tests in this study, a different GMP-compliant medium is beneficial with regard to clinical application (WÜNSCH et al., 2005; FEIL et al., 2006; NAGELE et al., 2008; TURNER et al., 2011). As cKSFM contains ingredients of animal origin, it is not in accordance with the quality criteria of EU GMP guidelines and therewith German pharmaceutical law. Consequently, the culture medium was switched for the minipig model and PUC were then cultured in CnT medium prior to the in vivo application. In comparison to the culture of PUC in cKSFM they showed better growth behaviour and a more solid cell sheet on CCC. On account of this, CnT medium is preferred for future investigations on UC adapting cell culture conditions to current regulatory requirements.

In cryostat sections of HUC and PUC grown on CCC it was observed that cells formed a sheet of thick layers on plastic but built up a thinner layered sheet on CCC. This was most likely due to physiological change of the cell formation when they were detached from the bottom of the culture dish or well plate. In this way the cell sheets contracted and appeared as a more compact tissue. In contrast, when cells stayed attached on the CCC, they remained in a stretched shape leading to plain cell sheets.

Different approaches were pursued in the past to enforce the formation of compact multilayered cell sheets for TE purposes: As a previous study of Davis et al. discovered, UC show enhanced proliferation and viability when grown in a bioreactor system. For construction of artificial bladder tissue UC were seeded on acellular matrix scaffolds and grown under static conditions and in a bioreactor system mimicking varying bladder pressure. After three days the number of viable cells was significantly greater in the bioreactor group compared to the static culture (DAVIS et al., 2011). This indicates that UC require dynamic conditions for optimal proliferation and viability. Hence dynamic culture conditions could lead to an improved multilayer formation on CCC.

Furthermore, the effect of growth factors was analysed in order to possibly accelerate growth and improve the morphology of UC sheets. To increase blood supply of tissue-engineered urethral substitutes Guan et al. transduced rabbit urothelial cells with vascular endothelial growth factor (VEGF) gene-modified retrovirus and seeded them on decellularised rabbit artery. After subcutaneous transplantation in a nude mouse model VEGF modified cells formed a solid organised urothelium with similar morphology like native rabbit urethra and revealed stronger expression of urothelial differentiation markers in comparison to non-modified UC. Furthermore, a better microvessel formation and vascularisation of the tissue engineered constructs was observed (GUAN et al., 2008). Altogether, cell growth and multilayer formation on CCC could be improved under dynamic culture conditions or by addition of growth factors for example by special CCC coatings.

5.1.2 Analysis of cell proliferation via BrdU assay

BrdU assay was performed to evaluate proliferation of HUC and PUC on CCC in two different seeding densities in comparison to plastic seeded cells. This assay was estimated to be a reliable method for quantification of cell growth in preceding studies (MAGHNI et al., 1999). BrdU test was used to evaluate the proliferation of canine lymphocytes in comparison to MTT, XTT, and radioactive thymidine incorporation assay. BrdU turned out to correlate strongly with the previous gold standard, the thymidine incorporation assay and was therefore judged to be the most suitable non radioactive alternative (WAGNER et al., 1999).

In the present study proliferation of HUC in low density was considerably below the controls while in higher density and stratification HUC demonstrated proliferation rates similar to or even higher than controls. PUC on CCC also revealed good proliferation rates in comparison to controls but a decrease over seven days when seeded in low density. In stratifying cultures PUC also reached higher proliferation rates than controls. Anyhow, all tests showed high variations between different primary cultures. This could be due to variabilities in substrate absorbance, growth behaviour or simply proliferative capacity. The differing morphology of the different primary cultures, especially in PUC cultures indicated these differences. More tests with a greater diversity of primary cultures could be performed to increase the validity of the results and minimise the effect of donor variabilities.

Investigations on PUC were relevant with regard to the preclinical setting in minipigs. But with regard to clinical application proliferation of HUC on CCC is of greater interest because retrieval from an autologous cell source is intended. As it is advisable to seed HUC in high density to induce stratification shortly afterwards, the results of HUC in the stratifying phase are most important. Compared with the other three experimental groups HUC in stratification revealed the best proliferation rates on CCC. This result is of utmost significance in the context of translational research and emphasises the excellent qualities of the CCC for urogenital reconstruction.

5.1.3 Analysis of cell metabolic activity via WST-1 assay

In the present study the WST-1 assay was used to analyse the viability by quantifying the metabolic activity of HUC and PUC on the collagen membrane in low and high seeding density. PUC seeded on CCC revealed equal or superior viability compared to controls independent of the cell density. Analogous to the BrdU assay viability of HUC seeded on CCC in lower density was slightly reduced compared to controls on standard plastic surface. When seeded in or grown to high density, HUC showed values of optical density close to the controls. Apparently HUC seeded on CCC required a longer period to develop the same viability like on plastic. Furthermore, the inferior adherence after low density seeding of UC on CCC may have led to inferior results also for viability.

The high donor variabilities for single test days can be due to the different behaviour of the primary cultures in general and on CCC. The results also displayed internal variances in the experiments, which might be due to bias promoted by differing absorbance of the CCC samples alone. Sources of assay variation can generally result from differences between absorbance of plastic of different wells on the microplate and between two different microplates or the presence of small air bubbles (FRANCOEUR & ASSALIAN, 1996). Still, it remains unclear why some primary cultures display the same or even superior metabolic activity on CCC than on plastic while others remain lower.

In general, the development of metabolic activity of HUC seeded on CCC corresponded to the proliferation rates determined by BrdU assay. HUC in high density showed excellent metabolic activity when seeded on CCC and after induction of stratification. As already quoted above, viability of HUC is of major importance for clinical application and underlines the suitability of the CCC for the intended purpose.

5.1.4 Cell adherence on CCC

There are different methods to determine cell adherence on scaffolds. Most authors just give a subjective assessment of the microscopic picture (WÜNSCH et al., 2005; BREHMER et al., 2007); others evaluate proliferation by different assays shortly after seeding (SABBAGH et al., 1998; MONTZKA et al., 2011). Hodde et al. used liquid scintillation counting to assess the cell adherence on the scaffolds and investigated its relation to the method of scaffold sterilisation (HODDE et al., 2002).

In this present study the principle of counting supernatant cells one day after seeding was chosen. It is an easy, systematic, and direct approach excluding many influencing variables possibly promoting bias. When HUC or PUC, respectively, were seeded in high cell numbers onto the scaffold and on plastic surface in parallel, the percentage of adherent cells was almost equal, whereas there was a considerable difference in experiments performed with low density seeding. In these cases UC did not adhere to the collagen surface as good as to the plastic. The histological analysis of the minipigs' tissue sections showed that fractions of PUC did not remain on the CCC and therewith on the luminal side of the urethra but were spread in the corpus spongiosum (see 4.2.2.3). Hence, the results of the minipig study are in line with the in vitro results as PUC partly detached from the collagen surface under mechanical influence possibly resulting from animal movements.

Other studies, where cell adherence of UC on different scaffolds was investigated did not use plastic adherence as a control level but just compared the different materials: Wünsch et al. equally assessed good cell adherence on special collagen matrices in comparison to synthetics when they seeded 1×10^5 PUC/cm^2 (WÜNSCH et al., 2005). Although keratinocytes and fibroblasts were used, Brehmer et al. performed a large study on cell growth on 13 different scaffolds, most of them collagen-based. They concluded that independent of the chemical composition of the biomaterial, a sponge type matrix has the best structure concerning ingrowth of cells and build-up of a complete epithelium (BREHMER et al., 2007). This was also found in an earlier study of Sabbagh et al., who assessed in vitro characteristics of a collagen sponge as urothelial graft material (SABBAGH et al., 1998). Multilayer urothelium was constructed successfully and there was also an ingrowth of cells into the sponge. Montzka et al. compared different collagen matrices with and without pores and could not find any difference with regard to the adherence of UC and smooth muscle cells, which might be due to an inconvenient pore size. Nevertheless, ingrowth of cells into the scaffold was observed in scanning electron microscopy in 3D matrices (MONTZKA et al., 2011). In general, most authors support the notion that an adequate pore size would lead to an enhanced cell adherence (MURPHY & O'BRIEN, 2010). O’Brien et al. determined cell adherence and permeability of a collagen-glycosaminoglycan matrix and concluded that increasing the pore size leads to a decrease in specific surface area and increased permeability (O'BRIEN et al., 2007). In their previous approach they had shown that cell adherence of osteogenic cells increased with increasing surface area (O'BRIEN et al., 2005). This investigation underlines the importance of creating a matrix featuring optimal pore size.

In conclusion, best results were achieved with HUC and PUC seeded on the scaffold in high density and after early induction of stratification. This practice allowed for best results concerning cell adherence on the CCC. Coating of the CCC with special growth factors, fibronectin or rather laminin could promote better adherence as it was shown in a previous study (KLEINMAN et al., 1981). Furthermore, a modification of the CCC in order to create pores on the surface may promote better ingrowth and therewith improve cell adherence. Further studies regarding the improvement of cell adherence on CCC are necessary and should be object of future research.

5.1.5 Quality control of urothelial cell cultures

HUC and PUC underwent immunocytochemical staining to prove urothelial phenotype and to exclude the presence of other cell types with antibodies detecting the following markers: AE1/AE3 (pancytokeratin), TE-7 (fibroblasts), and 1A4 (smooth muscle). As expected HUC and PUC revealed positive staining for AE1/AE3 and negative staining for both TE-7 and 1A4.

AE1/AE3 staining was performed to prove the typical cytokeratin pattern of urothelial cells. Cytokeratins are a heterogeneous group of polypeptides. As each type of epithelial cell expresses its own characteristic cytokeratin expression pattern, it can be used to evaluate the specific phenotype and simultaneously the degree of potential malignancy (SOUTHGATE et al., 1999). Hence, cytokeratins serve as differentiation markers being associated with the maturation of the cell.

In line with an earlier study on HUC TE-7 and 1A4 detection was performed to exclude possible impurities by the associated cell types. Nagele et al. isolated HUC from bladder washings and investigated the expression of the respective markers in monolayer and stratified cultures (NAGELE et al., 2008). Though, only monolayer cultures were used in contrast to the previous study immunohistological results were equal. This quality control verified the used protocol for isolation and culture of pure urothelial cell cultures.

5.1.6 Immunofluorescence analysis of urothelial cells seeded on CCC

Multilayer sheets of HUC seeded on standard plastic surface as well as on CCC were investigated for specific urothelial marker expression by immunofluorescent staining. For human urothelium CK-7, CK-8, CK-18, and CK-19 are expressed throughout all urothelial cell layers, CK-5 and CK-17 in basal cells, CK-13 in all except the basal cells and CK-20 in the superficial umbrella cells (SOUTHGATE et al., 1999). Hence, constituting a mixture of specific CK antigens pancytokeratin proves the epithelial character and CK-20 is a marker for final urothelial differentiation.

Feil et al. inquired the immunoreactivity of p63 in monolayer and multilayer UC cultures in addition to other markers (AE1/AE3, CK-20, uroplakin III, fibroblast surface antigen) and found that p63 is crucial for the final differentiation in stratified urothelium. The results were similar to native urothelium: pancytokeratin (AE1/AE3) positive, fibroblast surface antigen negative, CK-20 positive in superficial cells and p63 positive in basal cells of multilayer constructs. Only uroplakin III did not show positive staining in contrast to native urothelium (FEIL et al., 2008b). In a different approach the presence of these markers was investigated in urothelium isolated from bladder washings and revealed identical results (NAGELE et al., 2008).

In the present study five different markers served as a confirmation of urothelial character of the expanded cells. Pancytokeratin (AE1/AE3), CK-20, and p63 were used to demonstrate urothelial phenotype, ZO-1 and E-Cadherin to verify cell-cell contacts in stratified urothelium in vitro. The terminal differentiation suggests that the urothelium-CCC-construct can behave and function physiologically in vivo. Thus, the results of this study correspond to investigations of other authors (see above) and verify the expression pattern being in accordance with native urothelium. The continuous observation that the dyeings were slightly reduced on CCC seeded cells in comparison to cell sheets grown on standard plastic surface can be ascribed to the deformation of the cell sheet when it was detached from the plastic surface. The compact structure of the contracted matrix-free cell sheet led to an optical impression of a stronger fluorescence signal.

Although the marker pattern for urothelial differentiation in this present study was confirmed, aforementioned studies indicated that the antigenic environment of in vitro cultures urothelium does not completely correspond to native urothelium (e.g. uroplakin III detection) (FEIL et al., 2008b; NAGELE et al., 2008). Therefore, further efforts to enforce urothelial differentiation are crucial in order to bridge this gap. Cattan et al. investigated the construction of a human tissue-engineered tubular genitourinary graft consisting of fibroblasts and UC under dynamic (hydrostatic pressure and dynamic flow) and static conditions. When compared with regard to histology and their expression of uroplakins, CK-20, and tight junction protein ZO-1 only the dynamically cultured graft showed multilayer formation and final differentiation. The authors reasoned that mechanical stimuli contribute to the differentiation process (CATTAN et al., 2011). Consequently, dynamic culture conditions could support both multilayer growth on CCC but also urothelial differentiation.

Due to the similar antigen expression urothelium expanded in vitro will most probably behave like naturally grown tissue in vivo. The specific marker pattern indicates its resistance to aggressive urine components and the construction of a functional urine-blood barrier. This was to be proved subsequently after in vivo application in both rat and minipig tissues.

5.2 In vivo biocompatibility of the seeded CCC after application in nude rats

HUC were seeded on CCC and transplanted on the rectus muscle of nude rats to prove cell survival, integration in the surrounding tissue, biodegradation of the CCC and potential inflammatory reactions. The health status of nude rats having received a human urothelial CCC transplant was not impaired at any time point of the experiment. The histological analyses revealed excellent biocompatibility of the cell carrier. It integrated well in the subcutaneous tissue and was almost completely degraded after four weeks. Only parts of the CCC were recovered in HE-stained sections. Nevertheless, slight additional tissue formation was observed when the transplants were placed deeply in the muscular tissue and moderate injury has been caused.

This particular matrix was tested on biocompatibility also by other authors. Schmidt et al. seeded human osteosarcoma cell line Saos-2, human mesenchymal stem cells, and rodent cardiomyocytes for in vitro biocompatibility testing. In comparison to other collagen matrices the CCC revealed superior growth of all three cell types (KNOELLER et al., 2010; SCHMIDT et al., 2011). After subcutaneous implantation of the unseeded CCC in rats, Knoeller et al. also reported excellent tolerability and the same group revealed good suitability as wound coverage (HELD et al., 2010). The degradation time of 42 days and the absence of inflammatory signs are in line with the in vivo results of the present study.
For immunohistological investigation sections were stained with antibodies detecting AE1/AE3, CK-20, p63, E-Cadherin and ZO-1. All markers were verified after one and two weeks but considerably reduced after four weeks. The changes in the expression profile of urothelial antigens four weeks after surgery can most likely be attributed to the untypical tissue surrounding the transplanted UC and the absence of urine specific factors. It is reported that the specific differentiation of mesenchymal stem cells (MSC) is strongly influenced by direct cell-cell contact and paracrine effects (WANG et al., 2005; WANG et al., 2006). To a certain degree these results can probably be transferred to the differentiation mechanism of other cell types like UC. For those reasons the absence of urothelium specific antigens after four weeks seems to be perspicuous. With regard to the large animal model and to clinical use it can be expected that the urothelial phenotype will be confirmed when the transplants are placed in their definite target organ, the urethra.

5.3 Feasibility of urethroplasty in the minipig model

All six minipigs that underwent two surgical procedures were at good health during the whole experimental period. The removed tissues were analysed histologically and immunohistologically and showed excellent integration of the autologous CCC construct, the degradation of the matrix, no inflammatory reactions and the expression of urothelial markers. Contrast x-ray confirmed the absence of stricture formation after urethroplasty.
Large animal studies for regeneration of urinary tract organs are rare and mainly concentrate on composite cystoplasty procedures (FRASER et al., 2004); (TURNER et al., 2011). This present urethroplasty study constitutes the first preclinical minipig trial using a tissue engineered construct based on a collagen membrane seeded with

UC. The methodology was implemented in a past study of Sievert et al., who compared three different stricture induction models in minipigs: ligation, urethrotomy and thermocoagulation (SIEVERT et al., 2012). Collagen I:III ratio, microvessel density and stricture histology were determined in human and porcine urethral stricture tissue to find the stricture model most similar to human pathology. Compared to other procedures thermocoagulation resulted in stricture formation histologically most resembling human stricture tissue. After urethral stricture induction a slight narrowing was observed by contrast x-ray. The urethral patency was fine before stricture induction and after urethroplasty. For future approaches it might be advisable to induce a more severe trauma to the urethral tissue or extend the period between stricture induction and transplantation to generate a definite stricture. As iatrogenic strictures can often be ascribed to thermocoagulation damage in the course of genitourinary surgery and due to the histological similarity this model appeared to be most suitable for imitating human stricture aetiology.

Based on the detection of PKH26 fluorescence the transplanted cells could be located in all animals and were found partly shifted off the CCC in the course of time. Moreover, the transplants did not all remain at the urothelial site but were also detected in the corpus spongiosum tissue. This might be associated to different mechanical conditions (urine contact and streaming, tissue reorganisation, animal movements, etc.), deficiencies of cell adherence on CCC in vivo and the urothelial turnover. Although Wu et al. indicate ~200 days as turnover rate for bladder urothelium, the urethral urothelium especially after surgery most probably displays a much higher rate (WU et al., 2009). In the end it remains unclear why the seeded CCC could not be located directly at the lumen in histological sections. A better fixation to the native urothelium would be beneficial for future approaches and could be achieved by running sutures. Seibold et al. likewise used autologous PUC which were labelled by PKH26 for stricture therapy but this approach was matrix-free (SEIBOLD et al., 2011). After endoscopic application of PUC suspension with hyaluronic acid, the labelled cells could be retrieved up to eight weeks after application but were distributed throughout different penile layers. When epithelial phenotype was assessed by AE1/AE3, positive cells could only be detected in the urothelium. Cells which were integrated in the corpus spongiosum lost their epithelial phenotype. This is completely in accordance with the results of the present study.

Immunofluorescence analysis revealed that native urothelium showed strong fluorescence for all the tested markers: Pancytokeratin (AE1/AE3), CK-20 and p63 (urothelial phenotype), ZO-1, and E-Cadherin (cell-cell junctions): This on the one hand confirms the methodical approach and serves as a positive control but on the other hand hampers evaluation of positive fluorescence. Therefore, only double fluorescence confirmed urothelial phenotype of the transplanted cells in this tissue surrounding. Evaluation was very demanding because strong PKH26 fluorescence was required as a precondition to confirm double fluorescence. However, it was reduced considerably in course of time. Anyhow, urothelial phenotype proven by AE1/AE3, CK-20, and p63 detection could be verified in single areas one and two weeks after transplantation as well as adherens and tight junction specific markers (E-Cadherin and ZO-1). After four weeks PKH26 fluorescence was rather weak and only pancytokeratin was detected in single cells. Green fluorescence of other markers could not be clearly assigned to the transplanted cells. Due to mechanical noxes (see above) only few of the transplanted cells were directly facing the lumen and were recovered as double fluorescent. Other cells located in the corpus spongiosum were exposed to untypical tissue surrounding and therefore probably lost urothelial phenotype. By considerably improving the adherence of the cells on CCC and the fixation of the transplant, it might remain close to the lumen and thereby be exposed to urine, native urothelium and urothelium-specific factors. This could in consequence lead to maintenance of urothelial phenotype.

5.4 Assessment and consequences for future investigations

5.4.1 Recommendations for further cell culture and animal experiments

With regard to clinical application the in vitro data resulting from HUC experiments are of paramount importance because an autologous approach is favoured for clinical application. Results of WST-1 and BrdU assays revealed an excellent suitability of the CCC for constructing urothelial CCC transplants. Both assays showed that HUC display excellent proliferation and metabolic activity when seeded in high numbers on the collagen membrane followed by direct induction of stratification. Likewise, the adherence of HUC and PUC on CCC was much superior when cells were seeded in high numbers. Consequently, it is advisable for further investigations to perform the CCC seeding in the described way. Yet, the available cell number could be limited depending on the cell source. Multilayer formation and urothelial differentiation could be supported by the construction of CCC-cell transplants under dynamic culture conditions. Studies performed on different cell types showed improved multilayer growth and differentiation behaviour when cells were grown in a bioreactor (see 5.1.1 and 5.1.6).

The nude rat model served as a preliminary experiment with respect to the minipig model in order to prove in vivo biocompatibility of HUC-CCC constructs. Cells were recovered in all animals after application on rats' rectus muscles without inflammatory reactions. Therefore, this small animal model laid the foundations for proceeding with investigations in the large animal. In minipigs, the cells and matrix could also be located until four weeks after urethroplasty with autologous PUC seeded on CCC. The urethral patency after transplantation was verified by contrast x-ray and suggests functional regeneration of the urethra. All in all, future investigations in the minipig should account for:

1. Induction of a definite and manifest urethral stricture verified by urethrography
2. Firm fixation of the CCC to the native urothelium by running sutures
3. Improvement of cell adherence on CCC

With regard to these aspects a xenogenic minipig model should be performed with transplantation of HUC. As HUC show better in vitro characteristics concerning adherence and uniform multilayer growth, xenogenic in vivo experiments will probably result in an excellent regeneration.

5.4.2 Prospects for clinical application in human and veterinary medicine

The present study showed that:

1. The CCC displays good in vitro properties for seeding of HUC and PUC including viability, proliferation, adherence and maintenance of urothelial phenotype.
2. The CCC seeded with UC features excellent in vivo biocompatibility characteristics proven in a rodent model.
3. Urethral reconstruction and functional regeneration after induction of a urethral stricture in minipigs is feasible by application of CCC autografts.

Hitherto urethral reconstruction does not play an important role in routine veterinary practice. Strictures are rather uncommon and sophisticated surgical procedures e.g. after traumatic urethral damage are often limited by financial considerations. Nevertheless, this innovative regenerative concept could offer a new therapeutic option for selected patients, first of all horses and dogs. Moreover, animal models are essential for the introduction of new surgical methods in human medicine.

After thorough assessment of this innovative therapy concept in a xenogenic large animal model, this particular knowledge is supposed to be transferred into the clinic to perform first-in-human trials. As mentioned before there is temporarily no adequate therapy for many patients suffering from complicated urethral strictures. Buccal mucosa urethroplasty is the gold standard, but comes along with high donor site morbidity and early complications. A new therapeutic approach being less invasive and displaying a better long-term outcome would be of utmost significance. The therapeutic procedure for selected cases could be the following: HUC are harvested non-invasively by bladder washings. After isolation, cultivation, and seeding of autologous HUC on CCC in high density, stratification should be induced the following day. App. four weeks later an autologous urothelial transplant can be provided for urethroplasty. This cell-based collagen transplant could be a beneficial alternative not only for stricture therapy but also for other urological disorders requiring bladder or urethra repair e.g. for hypospadias reconstruction.

6 Annexe

6.1 Materials

6.1.1 Consumables

Adhesive tape Fixomull stretch	BSN medical GmbH, Hamburg, Germany
Canullas 20 G, 23 G, 25 G, 27 G	B. Braun Melsungen AG, Melsungen, Germany
Cell scraper	Corning Inc., Corning, NY, USA
Chamber slides 8-well	Nunc GmbH & Co. KG , Langenselbold, Germany
Collagen cell carrier (inlays for 24-well plate and inserts for 6-well plate)	Viscofan Bioengineering, Weinheim, Germany
Combur Test M	Roche Diagnostics Deutschland GmbH, Mannheim, Germany
Conical tube BD Falcon 15 ml/ 50 ml	BD Biosciences, San Jose, CA, USA
Counting chamber Neubauer	Glaswarenfabrik Karl Hecht GmbH&Co KG "Assistent", Sondheim/Rhön, Germany
Cryo tube vials 1.8 ml	Nunc GmbH & Co. KG , Langenselbold, Germany
Culture flask CellBIND 25 cm^2/ 75 cm^2	Corning Inc., Corning, NY, USA
Culture plate CellBIND 6-well, 24-well	Corning Inc., Corning, NY, USA
Culture plate Cellstar 6-well	Greiner Bio-One GmbH, Frickenhausen, Germany
Dako pen	Dako Deutschland GmbH, Hamburg, Germany
Disposable embedding moulds Shandon Peel-A-Way	Thermo Fisher Scientific GmbH Karlsruhe, Germany
Disposable scalpels #11/#15	Aesculap/ B. Braun Melsungen AG, Melsungen, Germany
Disposable scalpels #10/#11/#15	Servoprax, Wesel, Germany

Disposable serological pipettes	Corning Inc., Corning, NY, USA
Drape sheets Foliodrape	Paul Hartmann AG, Heidenheim, Germany
Endosgel lubricant	Farco-Pharma GmbH, Köln, Germany
Freezing container Nalgene 1°C	Thermo Fisher Scientific GmbH, Karlsruhe, Germany
Gloves DermaClean	Ansell GmbH, München, Germany
Microplate 96-well ELISA	Greiner Bio-One GmbH, Frickenhausen, Germany
Microplate 96-well round bottom Cellstar TC-plate	Greiner Bio-One GmbH, Frickenhausen, Germany
Microscope cover slips 24x50 mm	R. Langenbrinck Labor- und Medizintechnik, Emmendingen, Germany
Microscope slides SuperFrost	R. Langenbrinck Labor- und Medizintechnik, Emmendingen, Germany
Pasteur pipettes small/large	Wilhelm Ulbrich GdbR, Bamberg, Germany
Petri dish plastic	Greiner Bio-One GmbH, Frickenhausen, Germany
Pipette tips	Greiner Bio-One GmbH, Frickenhausen, Germany
Safe-lock tubes 1.5 ml/2 ml	Eppendorf AG, Hamburg, Germany
Skin marker Mediware	servoprax GmbH, Wesel, Germany
S-Monovette EDTA K, 2.7 ml	SARSTEDT AG & Co, Nürnbrecht, Germany
S-Monovette Li- Heparin, 2.7 ml	SARSTEDT AG & Co, Nürnbrecht, Germany
Stand cover Mayo	Cardinal Health Care, Dublin, Ireland
Sterile surgery gowns	CareFusion, San Diego, CA, US

Suction connecting tube Argyle	Tyco Healthcare group, Tullamore, Ireland
Suction tube CH 12	Tyco Healthcare group, Tullamore, Ireland
Suprapubic catheter Cystofix CH 10	B. Braun Melsungen AG, Melsungen, Germany
Surgical gloves Biogel	Mölnlyncke Healthcare, Göteborg, Sweden
Surgical gloves Sempermed supreme	Semperit Technische Produkte, Wien, Austria
Sutures Vicryl 5.0/ 6.0/ 7.0/ 8.0	Ethicon Inc., Somerville, NJ, US
Sutures Prolene 0	Ethicon Inc., Somerville, NJ, US
Syringes 1 ml, 5 ml, 10 ml, 20 ml	B. Braun Melsungen AG, Melsungen, Germany
Ureteral catheter CH 04	Coloplast GmbH, Hamburg, Germany

6.1.2 Technical devices

Autoclave 2540EK	Tuttnauer Europe B.V, Breda, Netherlands
Centrifuge Hettich Rotanta/S	Andreas Hettich GmbH & Co KG, Tuttlingen, Germany
Centrifuge Eppendorf 5415C	Eppendorf AG, Hamburg, Germany
Colour camera AxioCam HRc	Zeiss, Oberkochen, Germany
Cryotome LEICA CM1900	Leica Microsystems Nussloch GmbH, Nussloch, Germany
Drying cabinet BE 200	Memmert GmbH und Co. KG, Schwabach, Germany
Fluorescence filter red F41-027	AHF Analysentechnik, Tübingen, Germany
Fluorescence filter green F41-020	AHF Analysentechnik, Tübingen, Germany

Fluorescence filter blue F31-000	AHF Analysentechnik, Tübingen, Germany
Freezer Öko super -20°C	Liebherr-International Deutschland GmbH, Biberach an der Riss, Germany
Freezer V.I.P.-Series MDF-U71V -86°C	SANYO North America Corporation, IL 60191 USA
Heating plate MR82	Heidolph Instruments GmbH & Co. KG, Schwabach, Germany
Incubator Heraeus	Thermo Fisher Scientific GmbH Karlsruhe, Germany
Kinetic ELISA microplate reader Vmax	Milenia Biotec GmbH, Gießen, Germany
Laminar air flow	Waldner AG, Neuhaus, Germany
Microscope SM-LUX	Ernst Leitz GmbH, Wetzlar, Germany
Microscope IM35	Zeiss, Oberkochen, Germany
Microscope Axiovert 200M	Zeiss, Oberkochen, Germany
Microwave R-4V14	Sharp Electronics (Europe) GmbH, Hamburg, Germany
Pipette controller accu-jet	Brand GmbH & Co KG, Wertheim, Germany
Refrigerator	Robert Bosch Hausgeräte GmbH, München, Germany
Software SoftMax Pro	Molecular Devices Inc., Sunnyvale, CA, USA
Vortex mixer VM-300	Gemmy industrial corporation, Taipei, Taiwan
Water bath	Köttermann GmbH & Co KG, Uetze/Hänigsen, Germany
X-ray c-arm unit BV Pulsera	Philips Deutschland GmbH, Hamburg, Germany

6.1.3 Animals and accessories

Athymic nude rats (Crl:NIH-Foxn1nu)	Charles River Laboratories, Sulzfeld, Germany
Conventional minipig fodder	SDS Diets, Essex, UK
Göttingen Minipigs	Ellegaard, Dalmose, Denmark
Individually ventilated cage (IVC) Sealsafe	TECNIPLAST S.p.A., Buguggiate, Italy
Vegetal commercial laboratory animal food	ssniff Spezialdiäten GmbH, Soest, Germany

6.1.4 Basic reagents

Chemicals were provided by the pharmacy of the university clinics of Tuebingen and diluted in Ampuwa.

Citric acid

Ethanol solution 90%

Glacial acetic acid

Isopropanol

Paraformaldehyde 3.7%

Sodium citrate

Sulphuric acid 1 M

6.1.5 Chemicals, buffers and solutions

Ampuwa	Fresenius Kabi Deutschland GmbH, Bad Homburg, Germany
Calcium chloride 5.5%	Baxter Deutschland GmbH, Unterschleißheim, Germany
Cell proliferation ELISA, BrdU kit (colorimetric)	Roche Diagnostics Deutschland GmbH, Mannheim, Germany
Cell proliferation reagent WST-1 kit	Roche Diagnostics Deutschland GmbH, Mannheim, Germany
Dispase	BD Biosciences, San Jose, CA, USA

DMSO	Sigma-Aldrich Chemie GmbH, Steinheim, Germany
DPBS	Biochrom, Berlin, Germany
EDTA 1%	Biochrom, Berlin, Germany
EnVision+System-HRP (DAB)	Dako Deutschland GmbH, Hamburg, Germany
Eosin G Certistain	Merck KGaA, Darmstadt, Germany
Glycerol gelatine	Merck KGaA, Darmstadt, Germany
HBSS w phenol red, w 0.35 g/l $NaHCO_3$, w/o Ca^{2+}, Mg^{2+}	Biochrom, Berlin, Germany
Haematoxylin	Vector Laboratories Inc., Burlingame, CA, USA
HEPES buffer	Gibco, Karlsruhe, Germany
Immunoselect antifading mounting medium DAPI	DIANOVA GmbH, Hamburg, Germany
NaCl 0.9 %	Fresenius Kabi Deutschland GmbH, Bad Homburg, Germany
Penicillin/streptomycin	Gibco, Karlsruhe, Germany
Peritrast Infusio 31%	Dr. Franz Köhler Chemie GmbH, Bensheim, Germany
PKH26 red fluorescent cell linker Kit	Sigma-Aldrich Chemie GmbH, Steinheim, Germany
PBS w/o Ca^{2+} and Mg^{2+}	Gibco, Karlsruhe, Germany
PBS powder	bioMérieux Deutschland GmbH, Nürtingen, Germany
D-saccharose	AppliChem GmbH, Darmstadt, Germany
Saponin from quillaja bark	Sigma-Aldrich Chemie GmbH, Steinheim, Germany
Tissue freezing medium	Leica microsystems Nussloch GmbH, Nussloch, Germany

Trypan blue stain	Lonza Walkersville Inc., Walkersville, MD, USA
TrypLE Express	Gibco, Karlsruhe, Germany
Trypsin 0.25%	Gibco, Karlsruhe, Germany
Vectamount	Vector Laboratories Inc., Burlingame, CA, USA
Vectashield	Vector Laboratories Inc., Burlingame, CA, USA

6.1.6 Culture basal media and additives

Aprotinin	Bayer AG, Leverkusen, Germany
Bovine pituitary extract (BPE)	Gibco, Karlsruhe, Germany
Cholera toxin	LIST Biological Laboratories Inc., Campbell, CA, USA
CnT basal medium 1	CELLnTEC Advanced Cell Systems AG, Bern, Switzerland
CnT-02 supplements (supplements A and B)	CELLnTEC Advanced Cell Systems AG, Bern, Switzerland
CnT-07 supplements (supplements A, B, and C)	CELLnTEC Advanced Cell Systems AG, Bern, Switzerland
Epidermal growth factor (EGF), human recombinant	Gibco, Karlsruhe, Germany
Fetal calf serum (FCS)	Gibco, Karlsruhe, Germany
Keratinocyte serum-free medium (KSFM)	Gibco, Karlsruhe, Germany

6.1.7 Supplemented substances

Citrate buffer 10 mM	citric acid and sodium citrate diluted in Ampuwa and adjusted to pH 6
CnT-02 medium	CnT basal medium 1 supplemented with CnT-02 supplements A and B

CnT-07 medium	CnT basal medium 1 supplemented with CnT-07 supplements A, B, and C
Dispase working solution	dispase soluted in PBS (Gibco) in a ratio of 1/2
Eosin staining solution 0.1%	0.1 g Certistain Eosin G in 100 ml of 90% ethanol solution and 1 drop of glacial acetic acid
cKSFM	KSFM supplemented with 50 µg/ml BPE, 5 ng/ml EGF, and 30 ng/ml cholera toxin
KC stratification medium	cKSFM with calcium chloride 5.5% at a final concentration of 1.09 mM/l $CaCl_2$
PBS solution	PBS powder soluted in 1l Ampuwa
Saccharose solution 18%	18 g D-saccharose soluted in 100 ml PBS solution
Saponin stock solution 10%	10 g saponin and 23.8 g HEPES ad 100 ml PBS solution
"Stripping solution"	HBSS with 10 mmol/l HEPES, 20 kIU/ml aprotinin, and 0.1% EDTA
Transport medium	HBSS with 10 mmol/l HEPES, 20 kIU/ml aprotinin, and 1% penicillin/streptomycin

6.1.8 Sera and antibody diluent

Antibody diluent	Dako Deutschland GmbH, Hamburg, Germany
Donkey IgG normal serum	Dako Deutschland GmbH, Hamburg, Germany
Goat IgG normal serum	Dako Deutschland GmbH, Hamburg, Germany
Rabbit IgG normal serum	Dako Deutschland GmbH, Hamburg, Germany

6.1.9 Primary antibodies

identification	antibody specificity	clone	host species	isotype	species reactivity	company
epithelial phenotype	pancytokeratin	AE1/AE3	Mouse	IgG1	Human, rat, mouse, monkey, rabbit, bovine, chicken	Millipore, Billerica, MA, USA
fibroblasts	fibroblast antigen	TE - 7	Mouse	IgG1	Human	Millipore, Billerica, MA, USA
smooth muscle	α- actin	1A4	Mouse	IgG2a	Human, rat, mouse, rabbit, goat, bovine, chicken, guinea pig, sheep, snake, frog, dog	Sigma-Aldrich Chemie GmbH, Steinheim, Germany
urothelial differentiation (surface marker)	cytokeratin 20 (CK-20)	KS20.8	Mouse	IgG2a, kappa	Human	Dako Deutschland GmbH, Hamburg, Germany
urothelial differentiation	p63	4A4	Mouse	IgG2a	Human, rat, mouse	Dianova GmbH, Hamburg, Germany
tight junctions (zonula occludens)	ZO-1	ZO1-1A12	Mouse	IgG1, kappa	Human, dog	Invitrogen GmbH, Darmstadt, Germany
epithelial adherence junctions	E-Cadherin	D33	Mouse	IgG1, kappa	Human	Dako Deutschland GmbH, Hamburg, Germany

6.1.10 Secondary antibodies

fluorophore	host species	isotype	species reactivity	company
FITC	Rabbit	IgG $F(ab)_2$	Mouse, human, bovine, rat	Dako Deutschland GmbH, Hamburg, Germany
Cy2	Donkey	IgG (H+L), $F(ab)_2$	Mouse, bovine, chicken, goat, guinea pig, Syrian hamster, horse, human, rabbit, rat, sheep	Dianova GmbH, Hamburg, Germany
Cy2	Goat	IgG (H+L)	Mouse, human, bovine, horse, rabbit, swine	Dianova GmbH, Hamburg, Germany

6.1.11 Medication for the nude rat model

Xylazin 2%	Albrecht GmbH, Aulendorf, Germany
Ketamin Gräub	Albrecht GmbH, Aulendorf, Germany
Narcoren 160 mg/ml	Merial GmbH, Hallbergmoos, Germany
Regepithel eye ointment	Alcon Pharma GmbH, Freiburg, Germany

6.1.12 Medication for the minipig model

	active agent	dosage	appli-cation	trade name	company
pre-medication	atropine	0.05 mg/kg	i.m.	Atropinsulfat 100 mg	Dr. Franz Köhler Chemie GmbH, Bensheim, Germany
	azaperone	4.0 mg/kg	i.m.	Stresnil 40 mg/ml	Elanco Animal Health, Lilly Deutschland GmbH, Bad Homburg, Germany
sedation	midazolam	0.5 mg/kg	i.m.	Midazolam-ratiopharm 100 mg/50 ml	Ratiopharm GmbH, Ulm, Germany
	ketamine	14 mg/kg	i.m.	Ursotamin 100 mg/ml	Serumwerke Bernburg AG, Bernburg, Germany
anaesthesia deepening	propofol	2-5 mg/kg	i.v.	Propofol 1% MTC Fresenius	Fresenius Kabi Deutschland GmbH, Bad Homburg, Germany
anaesthesia maintenance	propofol	2-5 mg/kg	i.v.	Propofol 1% MTC Fresenius	Fresenius Kabi Deutschland GmbH, Bad Homburg, Germany
	isoflurane	0.8-1.4 Vol%	inhalative	Forene	Abbott GmbH & Co. KG, Ludwigshafen, Germany
intraoperative analgesia	fentanyl	initial bolus of 20-150 µg/kg	i.v.	Fentanyl-ratiopharm 50 µg/ml	Ratiopharm GmbH, Ulm, Germany
		continuous flow of 30-100 µg/kg	i.v.		

	active agent	dosage	application	trade name	company
intraoperative infusion	NaCl 0.9%	Slow dripping	i.v.	NaCl 0.9%	Fresenius Kabi Deutschland GmbH, Bad Homburg, Germany
postoperative analgesia (at least 2 days)	meloxicam	0.4 mg/kg	i.m.	Melovem 5 mg/ml	Dopharma Deutschland GmbH, Münster, Germany
postoperative antibiotics (2 days)	dihydrostreptomycinsulphate, benzylpenicillin-procaine, benzathine-benzylpenicillin	3 ml / 50 kg	i.m.	Veracin Compositum	Albrecht GmbH, Aulendorf, Germany
euthanasia	pentobarbital	According to effect	i.v.	Narcoren 16 g/100 ml	Merial GmbH, Hallbergmoos, Germany
	KCl	According to effect	i.v.	Kaliumchlorid 7.45%	B. Braun Melsungen AG, Melsungen, Germany
skin disinfection	propan-2-ol, povidone-iodine	-	local	Braunoderm	B. Braun Melsungen AG, Melsungen, Germany
local antibiotics	oxytetracycline	-	local	OTC-Blauspray	WDT eG, Garbsen, Germany

6.2 Tables for cell adherence on collagen cell carrier

6.2.1 Human urothelial cells' adherence

Seeding density for **proliferating** HUC cultures (2.5 x 10^4 cells/cm^2)

HUC Line and passage	Non adherent HUC on standard plastic	Non-adherent HUC on CCC
10/17 P3	0.7%	17.5%
10/18 P3	0.3%	3.5%
10/19 P3	2.0%	18.2%
10/18 P4	2.3%	19.0%
10/26 P2	1.7%	12.7%
07/49 P4	6.0%	26.0%
Mean	**2.2%**	**16.2%**

Seeding density for **stratifying** HUC cultures (4 x 10^5 cells/cm^2)

HUC Line and passage	Non adherent HUC on standard plastic	Non-adherent HUC on CCC
07/14 P5	7.7%	8.8%
10/21 P3	1.5%	1.2%
10/3 P4	0.6%	0.8%
07/47 P4	0.5%	0.8%
04/005 P6	0.6%	0.8%
10/27 P6	0.9%	1.0%
Mean	**2.0%**	**2.2%**

6.2.2 Porcine urothelial cells' adherence

Seeding density for **proliferating** PUC cultures (2.5 x 10^4 cells/cm^2)

PUC Line and passage	Non adherent PUC on standard plastic	Non-adherent PUC on CCC
79930 P4	4.3%	28.0%
106597 P4	6.3%	11.7%
79939 P7	9.0%	15.3%
79930 P7	4.7%	9.0%
79939 P5	4.0%	17.0%
106597 P7	11.0%	11.0%
Mean	**6.6%**	**15.3%**

Seeding density for **stratifying** PUC cultures (4 x 10^5 cells/cm^2)

PUC Line and passage	Non adherent PUC on standard plastic	Non-adherent PUC on CCC
79930 P6	6.8%	7.5%
106597 P6	26.0%	25.9%
200201 P5	1.5%	1.2%
79930 P7	5.1%	6.2%
79939 P5	7.2%	15.4%
106597 P6	29.5%	25.3%
Mean	**12.7%**	**13.6%**

7 Literature

Al-Qudah HS, Santucci RA. Extended complications of urethroplasty. Int Braz J Urol 2005; 31: 315-23.

Atalan G, Cíhan M, Sozmen M, Ozaydin I. Repair of Urethral Defects Using Fascia Lata Autografts in Dogs. Veterinary Surgery 2005; 34: 514-8.

Bass M, Howard J, Gerber B, Messmer M. Retrospective study of indications for and outcome of perineal urethrostomy in cats. Journal of Small Animal Practice 2005; 46: 227-31.

Bennett SL, Edwards GE, Tyrrell D. Balloon dilation of a urethral stricture in a dog. Australian Veterinary Journal 2005; 83: 552-4.

Bhargava S, Chapple CR. Buccal mucosal urethroplasty: is it the new gold standard? BJU Int 2004; 93: 1191-3.

Boothe HW. Managing traumatic urethral injuries. Clinical Techniques in Small Animal Practice 2000; 15: 35-9.

Brehmer B, Rohrmann D, Becker C, Rau G, Jakse G. Different types of scaffolds for reconstruction of the urinary tract by tissue engineering. Urol Int 2007; 78: 23-9.

Cattan V, Bernard G, Rousseau A, Bouhout S, Chabaud S, Auger FA, Bolduc S. Mechanical Stimuli-induced Urothelial Differentiation in a Human Tissue-engineered Tubular Genitourinary Graft. Eur Urol 2011; 60: 1291-8.

Cavalcanti AG, Costa WS, Baskin LS, McAninch JA, Sampaio FJ. A morphometric analysis of bulbar urethral strictures. BJU Int 2007; 100: 397-402.

Chambers RM, Baitera B. The anatomy of the urethral stricture. Br J Urol 1977; 49: 545-51.

Cheng EY, Kropp BP. Urologic tissue engineering with small-intestinal submucosa: potential clinical applications. World J Urol 2000; 18: 26-30.

Corgozinho KB, de Souza HJM, Pereira AN, Belchior C, da Silva MA, Martins MCL, Damico CB. Catheter-induced urethral trauma in cats with urethral obstruction. Journal of Feline Medicine & Surgery 2007; 9: 481-6.

Cruz-Arambulo RJ, Tan L, Callan RJ, Van Metre DC, Park RD. What is your diagnosis? Communication between the urethra and the corpus spongiosum, urethral stricture, mild cystitis, and presence of a urachal diverticulum. J Am Vet Med Assoc 2003; 222: 1211-2.

Davis NF, Mooney R, Piterina AV, Callanan A, McGuire BB, Flood HD, McGloughlin TM. Construction and evaluation of urinary bladder bioreactor for urologic tissue-engineering purposes. Urology 2011; 78: 954-60.

De Filippo RE, Yoo JJ, Atala A. Urethral replacement using cell seeded tubularized collagen matrices. J Urol 2002; 168: 1789-92.

De Vocht TF, van Venrooij GE, Boon TA. Self-expanding stent insertion for urethral strictures: a 10-year follow-up. BJU Int 2003; 91: 627-30.

Dehoux JP, Gianello P. The importance of large animal models in transplantation. Front Biosci 2007; 12: 4864-80.

Desmond AD, Evans CM, Jameson RM, Woolfenden KA, Gibbon NO. Critical evaluation of direct vision urethrotomy by urine flow measurement. Br J Urol 1981; 53: 630-3.

Dorin RP, Pohl HG, De Filippo RE, Yoo JJ, Atala A. Tubularized urethral replacement with unseeded matrices: what is the maximum distance for normal tissue regeneration? World J Urol 2008; 26: 323-6.

El-Kassaby A, AbouShwareb T, Atala A. Randomized comparative study between buccal mucosal and acellular bladder matrix grafts in complex anterior urethral strictures. J Urol 2008; 179: 1432-6.
El-Kassaby AW, Retik AB, Yoo JJ, Atala A. Urethral stricture repair with an off-the-shelf collagen matrix. J Urol 2003; 169: 170-3.
Engel O, Fisch M. Urethral reconstruction after failed primary surgery. Urologe A 2010; 49: 822-6.
Feil G, Christ-Adler M, Maurer S, Corvin S, Rennekampff HO, Krug J, Hennenlotter J, Kuehs U, Stenzl A, Sievert KD. Investigations of urothelial cells seeded on commercially available small intestine submucosa. Eur Urol 2006; 50: 1330-7.
Feil G, Maurer S, Nagele U, Sievert KD, Stenzl A. Bioartificial urothelium generated from bladder washings. A future therapeutic option for reconstructive surgery. Urologe A 2008a; 47: 1091-2, 4-6.
Feil G, Maurer S, Nagele U, Krug J, Bock C, Sievert KD, Stenzl A. Immunoreactivity of p63 in monolayered and in vitro stratified human urothelial cell cultures compared with native urothelial tissue. Eur Urol 2008b; 53: 1066-72.
Feil G, Daum L, Amend B, Maurer S, Renninger M, Vaegler M, Seibold J, Stenzl A, Sievert KD. From tissue engineering to regenerative medicine in urology - The potential and the pitfalls. Adv Drug Deliv Rev 2011; 63: 375-8.
Feng C, Xu YM, Fu Q, Zhu WD, Cui L, Chen J. Evaluation of the biocompatibility and mechanical properties of naturally derived and synthetic scaffolds for urethral reconstruction. J Biomed Mater Res A 2010; 94: 317-25.
Feng C, Xu YM, Fu Q, Zhu WD, Cui L. Reconstruction of 3D neo-urethra using lingual keratinocytes & corporal smooth muscle cells seeded acellular corporal spongiosum. Tissue Eng Part A 2011; December 2011: 3011-9.
Fenton AS, Morey AF, Aviles R, Garcia CR. Anterior urethral strictures: etiology and characteristics. Urology 2005; 65: 1055-8.
Fiala R, Vidlar A, Vrtal R, Belej K, Student V. Porcine small intestinal submucosa graft for repair of anterior urethral strictures. Eur Urol 2007; 51: 1702-8.
Fichtner J, Filipas D, Fisch M, Hohenfellner R, Thuroff JW. Long-term outcome of ventral buccal mucosa onlay graft urethroplasty for urethral stricture repair. Urology 2004; 64: 648-50.
Fisch M. Urethral reconstruction in children. Curr Opin Urol 2001; 11: 253-5.
Fortier LA, Travis AJ. Stem cells in veterinary medicine. Stem Cell Res Ther 2011; 2: 9.
Fossum M, Nordenskjöld A, Kratz G. Engineering of multilayered urinary tissue in vitro. Tissue Eng 2004; 10: 175-80.
Fossum M, Svensson J, Kratz G, Nordenskjöld A. Autologous in vitro cultured urothelium in hypospadias repair. J Pediatr Urol 2007; 3: 10-8.
Fossum M, Nordenskjöld A. Long-Term Follow-Up After Hypospadias Repair With Cultured Autologous Cells. Journal of Pediatric Urology 2009; 5: S55-S6.
Fossum M, Nordenskjöld A. Tissue-engineered transplants for the treatment of severe hypospadias. Horm Res Paediatr 2010; 73: 148-52.
Francoeur A-M, Assalian A. MICROCAT: A Novel Cell Proliferation and Cytotoxicity Assay Based on WST-1. Biochemica 1996; 3: 19-25.
Fraser M, Thomas DF, Pitt E, Harnden P, Trejdosiewicz LK, Southgate J. A surgical model of composite cystoplasty with cultured urothelial cells: a controlled study of gross outcome and urothelial phenotype. BJU Int 2004; 93: 609-16.
Fu Q, Deng CL, Song XF, Xu YM. Long-term study of male rabbit urethral mucosa reconstruction using epidermal cell. Asian J Androl 2008; 10: 719-22.

Fuchs JR, Nasseri BA, Vacanti JP. Tissue engineering: a 21st century solution to surgical reconstruction. Ann Thorac Surg 2001; 72: 577-91.
Gill MS, Sod GA. Buccal mucosal graft urethroplasty for reversal of a perineal urethrostomy in a goat wether. Vet Surg 2004; 33: 382-5.
Gorham S, McCafferty I, Baraza R, Scott R. Preliminary development of a collagen membrane for use in urological surgery. Urol Res 1984; 12: 295-9.
Guan Y, Ou L, Hu G, Wang H, Xu Y, Chen J, Zhang J, Yu Y, Kong D. Tissue engineering of urethra using human vascular endothelial growth factor gene-modified bladder urothelial cells. Artif Organs 2008; 32: 91-9.
Hauser S, Bastian PJ, Fechner G, Muller SC. Small intestine submucosa in urethral stricture repair in a consecutive series. Urology 2006; 68: 263-6.
Hauser S, Fechner G, Ellinger J, Müller SC. Die plastische Rekonstruktion der Harnröhre. Der Urologe A 2010; 49: 727-30.
Hautmann R (2010) Urologie, 4., überarb. und aktualisierte Aufl. edn. Springer, Heidelberg. XV, 551 S.
Held M, Knoeller T, Wilkomm L, Just L, Schaller H-E, Rahmanian-Schwarz A (2010) A novel Collagen Cell Carrier (CCC) for the regeneration and reconstruction of skin and soft tissue: An in vivo evaluation. Biostar 2010- 4th Congress on Regenerative Biology and Medicine. Stuttgart, Germany. 130
Hodde JP, Record RD, Tullius RS, Badylak SF. Retention of endothelial cell adherence to porcine-derived extracellular matrix after disinfection and sterilization. Tissue Eng 2002; 8: 225-34.
Hussain M, Greenwell TJ, Shah J, Mundy A. Long-term results of a self-expanding wallstent in the treatment of urethral stricture. BJU Int 2004; 94: 1037-9.
Kashefi C, Messer K, Barden R, Sexton C, Parsons JK. Incidence and prevention of iatrogenic urethral injuries. J Urol 2008; 179: 2254-7.
Kleinman HK, Klebe RJ, Martin GR. Role of collagenous matrices in the adhesion and growth of cells. J Cell Biol 1981; 88: 473-85.
Klevecka V, Kroepfl D, Musch M. Harnröhrenstriktur: Ursachen, Klassifikation, Diagnostik und Behandlung. Journal für Urologie und Urogynäkologie 2010; 17: 16-24.
Knoeller T, Held M, Wilkomm L, Just L, Schaller H-E, Rahmanian-Schwarz A (2010) A novel Collagen Cell Carrier (CCC) for in vivo application. An analysis of Biocompatibility in a rat model. Biostar 2010- 4th Congress on Regenerative Biology and Medicine. Stuttgart, Germany. 100
Koch TG, Berg LC, Betts DH. Current and future regenerative medicine - principles, concepts, and therapeutic use of stem cell therapy and tissue engineering in equine medicine. Can Vet J 2009; 50: 155-65.
Kohler TS, Yadven M, Manvar A, Liu N, Monga M. The length of the male urethra. Int Braz J Urol 2008; 34: 451-4.
Kropp BP, Ludlow JK, Spicer D, Rippy MK, Badylak SF, Adams MC, Keating MA, Rink RC, Birhle R, Thor KB. Rabbit urethral regeneration using small intestinal submucosa onlay grafts. Urology 1998; 52: 138-42.
Kundu AK, Gelman J, Tyson DR. Composite thin film and electrospun biomaterials for urologic tissue reconstruction. Biotechnol Bioeng 2011; 108: 207-15.
Langer R, Vacanti JP. Tissue engineering. Science 1993; 260: 920-6.
le Roux PJ. Endoscopic urethroplasty with unseeded small intestinal submucosa collagen matrix grafts: a pilot study. J Urol 2005; 173: 140-3.
Lewis SA. Everything you wanted to know about the bladder epithelium but were afraid to ask. Am J Physiol Renal Physiol 2000; 278: F867-74.

Macura KJ, Genadry R, Borman TL, Mostwin JL, Lardo AC, Bluemke DA. Evaluation of the female urethra with intraurethral magnetic resonance imaging. J Magn Reson Imaging 2004; 20: 153-9.
Madersbacher H. Editorial. Journal für Urologie und Urogynäkologie 2001; 8: 5.
Maghni K, Nicolescu OM, Martin JG. Suitability of cell metabolic colorimetric assays for assessment of CD4+ T cell proliferation: comparison to 5-bromo-2-deoxyuridine (BrdU) ELISA. J Immunol Methods 1999; 223: 185-94.
Maurer S, Feil G, Stenzl A. In vitro stratified urothelium and its relevance in reconstructive urology. Urologe A 2005; 44: 738-42.
McMillan A, Pakianathan M, Mao JH, Macintyre CC. Urethral stricture and urethritis in men in Scotland. Genitourin Med 1994; 70: 403-5.
Montzka K, Laufer T, Becker C, Grosse J, Heidenreich A. Microstructure and cytocompatibility of collagen matrices for urological tissue engineering. BJU Int 2011; 107: 1974-81.
Mundy AR, Andrich DE. Urethral strictures. BJU Int 2011; 107: 6-26.
Murphy CM, O'Brien FJ. Understanding the effect of mean pore size on cell activity in collagen-glycosaminoglycan scaffolds. Cell Adh Migr 2010; 4: 377-81.
Nagele U, Maurer S, Feil G, Bock C, Krug J, Sievert KD, Stenzl A. In vitro investigations of tissue-engineered multilayered urothelium established from bladder washings. Eur Urol 2008; 54: 1414-22.
Naude AM, Heyns CF. What is the place of internal urethrotomy in the treatment of urethral stricture disease? Nat Clin Pract Urol 2005; 2: 538-45.
Nelson RW, Couto CG (2003) Small Animal Internal Medicine, 3 edn. Elsevier Science
Nissen E, Pauli G, Vollenbroich D. WST-1 assay--a simple colorimetric method for virus titration. In Vitro Cell Dev Biol Anim 1997; 33: 28-9.
Nuininga JE, van Moerkerk H, Hanssen A, Hulsbergen CA, Oosterwijk-Wakka J, Oosterwijk E, de Gier RP, Schalken JA, van Kuppevelt T, Feitz WF. Rabbit urethra replacement with a defined biomatrix or small intestinal submucosa. Eur Urol 2003; 44: 266-71.
Nuininga JE, Koens MJ, Tiemessen DM, Oosterwijk E, Daamen WF, Geutjes PJ, van Kuppevelt TH, Feitz WF. Urethral reconstruction of critical defects in rabbits using molecularly defined tubular type I collagen biomatrices: key issues in growth factor addition. Tissue Eng Part A 2010; 16: 3319-28.
O'Brien FJ, Harley BA, Yannas IV, Gibson LJ. The effect of pore size on cell adhesion in collagen-GAG scaffolds. Biomaterials 2005; 26: 433-41.
O'Brien FJ, Harley BA, Waller MA, Yannas IV, Gibson LJ, Prendergast PJ. The effect of pore size on permeability and cell attachment in collagen scaffolds for tissue engineering. Technol Health Care 2007; 15: 3-17.
Petersen RO (1992) Urologic pathology, 2. ed. edn. Lippincott, Philadelphia. XVI, 781
Powers MY, Campbell BG, Weisse C. Porcine small intestinal submucosa augmentation urethroplasty and balloon dilatation of a urethral stricture secondary to inadvertent prostatectomy in a dog. J Am Anim Hosp Assoc 2010; 46: 358-65.
Pradidarcheep W, Wallner C, Dabhoiwala NF, Lamers WH. Anatomy and histology of the lower urinary tract. Handb Exp Pharmacol 2011: 117-48.
Rand J (2009) Praxishandbuch Katzenkrankheiten. Elsevier, Urban & Fischer, München. 1621
Raya-Rivera A, Esquiliano DR, Yoo JJ, Lopez-Bayghen E, Soker S, Atala A. Tissue-engineered autologous urethras for patients who need reconstruction: an observational study. Lancet 2011; 377: 1175-82.

Ribitsch I, Burk J, Delling U, Geissler C, Gittel C, Julke H, Brehm W. Basic Science and Clinical Application of Stem Cells in Veterinary Medicine. Adv Biochem Eng Biotechnol 2010; 123: 219-63.
Rödder K, Olianas R, Fisch M. Urethral strictures--operative strategy. Urologe A 2006; 45: 499-511; quiz 2-3.
Rosenblum N, Nitti VW. Female urethral reconstruction. Urol Clin North Am 2011; 38: 55-64.
Sabbagh W, Masters JR, Duffy PG, Herbage D, Brown RA. In vitro assessment of a collagen sponge for engineering urothelial grafts. Br J Urol 1998; 82: 888-94.
Santucci RA, Joyce GF, Wise M. Male urethral stricture disease. J Urol 2007; 177: 1667-74.
Schmidt T, Stachon S, Mack A, Rohde M, Just L. Evaluation of a thin and mechanically stable collagen cell carrier. Tissue Eng Part C Methods 2011; 17: 1161-70.
Seibold J, Selent C, Feil G, Wiedemann J, Colleselli D, Mundhenk J, Gakis G, Sievert KD, Schwentner C, Stenzl A. Development of a porcine animal model for urethral stricture repair using autologous urothelial cells. J Pediatr Urol 2011; 8: 194-200.
Selent C, Gustaffson E, Wiedemann J, Feil G, Greiner TO, Sievert KD, Stenzl A, Seibold J. Development of a large animal model (minipig) for endoscopic therapy of urethral strictures with autologous urothelial cells. European Urology Supplements 2008; 7: 73.
Selim M, Bullock AJ, Blackwood KA, Chapple CR, MacNeil S. Developing biodegradable scaffolds for tissue engineering of the urethra. BJU Int 2011; 107: 296-302.
Sievert K-D, Selent-Stier C, Wiedemann J, Greiner TO, Amend B, Stenzl A, Feil G, Seibold J. Introducing a Large Animal Model to Create Urethral Stricture Similar to Human Stricture Disease: A Comparative Experimental Microscopic Study. The Journal of Urology 2012; 187: 1101-9.
Sievert KD, Tanagho EA. Organ-specific acellular matrix for reconstruction of the urinary tract. World J Urol 2000; 18: 19-25.
Sievert KD, Bakircioglu ME, Nunes L, Tu R, Dahiya R, Tanagho EA. Homologous acellular matrix graft for urethral reconstruction in the rabbit: histological and functional evaluation. J Urol 2000; 163: 1958-65.
Sievert KD, Wefer J, Bakircioglu ME, Nunes L, Dahiya R, Tanagho EA. Heterologous acellular matrix graft for reconstruction of the rabbit urethra: histological and functional evaluation. J Urol 2001; 165: 2096-102.
Sievert KD, Nagele U, Brinkmann O, Wuelfing C, Praetorius M, Seibold J, Stenzl A, Hertle L. Off-shelf commercially available acellular collagen matrix SIS® by cook for urethral reconstruction. European Urology Supplements 2005; 4: 242.
Sökeland J, Schulze H, Rübben H (2008) Taschenlehrbuch Urologie : 39 Tabellen, 14., vollst. überarb. Aufl. edn. Thieme, Stuttgart [u.a.]. XIV, 470 S.
Southgate J, Hutton KA, Thomas DF, Trejdosiewicz LK. Normal human urothelial cells in vitro: proliferation and induction of stratification. Lab Invest 1994; 71: 583-94.
Southgate J, Harnden P, Trejdosiewicz LK. Cytokeratin expression patterns in normal and malignant urothelium: a review of the biological and diagnostic implications. Histol Histopathol 1999; 14: 657-64.
Stack RS, Schlossberg SM. Principles of urethral stricture repair. Der Urologe A 1998; 37: 10-20.

Stone WC, Bjorling DE, Trostle SS, Hanson PD, Markel MD. Prepubic urethrostomy for relief of urethral obstruction in a sheep and a goat. J Am Vet Med Assoc 1997; 210: 939-41.
Tang SH, Hammer CC, Doumanian L, Santucci RA. Adult urethral stricture disease after childhood hypospadias repair. Adv Urol 2008: 150315.
Tritschler S, Roosen A, Bastian PJ, Stief C. Offene Harnröhrenchirurgie bei der Frau. 2011; 50
Turner A, Subramanian R, Thomas DF, Hinley J, Abbas SK, Stahlschmidt J, Southgate J. Transplantation of autologous differentiated urothelium in an experimental model of composite cystoplasty. Eur Urol 2011; 59: 447-54.
Wagner U, Burkhardt E, Failing K. Evaluation of canine lymphocyte proliferation: comparison of three different colorimetric methods with the 3H-thymidine incorporation assay. Vet Immunol Immunopathol 1999; 70: 151-9.
Wallner C, Dabhoiwala NF, DeRuiter MC, Lamers WH. The anatomical components of urinary continence. Eur Urol 2009; 55: 932-43.
Wang J, Luo C, Xu H, Ran X, Yan G, Su Y, Cheng T. Experimental study on the myogenic differentiation of marrow mesenchymal stem cells in the local muscle tissues. Zhongguo Xiu Fu Chong Jian Wai Ke Za Zhi 2005; 19: 70-3.
Wang T, Xu Z, Jiang W, Ma A. Cell-to-cell contact induces mesenchymal stem cell to differentiate into cardiomyocyte and smooth muscle cell. Int J Cardiol 2006; 109: 74-81.
Wood MW, Vaden S, Cerda-Gonzalez S, Keene B. Cystoscopic-guided balloon dilation of a urethral stricture in a female dog. Can Vet J 2007; 48: 731-3.
Wu XR, Kong XP, Pellicer A, Kreibich G, Sun TT. Uroplakins in urothelial biology, function, and disease. Kidney Int 2009; 75: 1153-65.
Wünsch L, Ehlers EM, Russlies M. Matrix testing for urothelial tissue engineering. Eur J Pediatr Surg 2005; 15: 164-9.
Xie H, Campbell CE, Shaffer BS, Gregory KW. Different outcomes in urethral reconstruction using elastin and collagen patches and conduits in rabbits. J Biomed Mater Res B Appl Biomater 2007; 81: 269-73.
Xu YM, Qiao Y, Sa YL, Zhang J, Zhang HZ, Zhang XR, Wu DL, Chen R. One-stage urethral reconstruction using colonic mucosa graft: an experimental and clinical study. World J Gastroenterol 2003; 9: 381-4.
Yiee JH, Baskin LS. Penile embryology and anatomy. ScientificWorldJournal 2010; 10: 1174-9.

Illustration register

Fig. 15: Representative WST-1 assay: Development of optical density (OD) in a WST-1 assay experiment of a proliferating HUC culture (2.5 x 10^4 cells/cm^2, human ureter cell line HL 10/18 in culture passage 3). Red curve represents control (HUC on plastic surface), blue curve represents HUC on CCC.

Fig. 16: BrdU assay: mean values of proliferating PUC cultures (n = 3) seeded on CCC, optical densities as percentage of the control which was set as 100% for each experiment. Seeding density 2.5 x 10^4 cells/cm^2

Fig. 17: WST-1 assay: mean values of proliferating PUC cultures (n = 3) seeded on CCC, optical densities as percentage of the control which was set as 100% for each experiment. Seeding density 2.5 x 10^4 cells/cm^2

Fig. 18: BrdU assay: mean values of stratifying PUC cultures (n = 3) seeded on CCC, optical densities as percentage of the control which was set as 100% for each experiment. Seeding density 4 x 10^5 cells/cm^2

Fig. 19: WST-1 assay: mean values of stratifying PUC cultures (n = 3) seeded on CCC, optical densities as percentage of the control which was set as 100% for each experiment. Seeding density 4 x 10^5 cells/cm^2

Fig. 20: Representative BrdU assay: Development of optical density (OD) in a BrdU assay experiment of a stratifying PUC culture (4 x 10^5 cells/cm^2, minipig bladder cell line MSBL 79939 in culture passage 5). Red curve represents control (PUC on plastic surface), blue curve represents PUC on CCC.

Fig. 21: Initial adherence of HUC: Mean values in percentage of total number of seeded cells. Non-adherent cells counted in the culture supernatant one day after seeding in low (Prol = 2.5 x 10^4 cells/cm^2) and high (Strat = 4 x 10^5 cells/cm^2) density on CCC and on plastic surface as a control, n = 6

Fig. 22: Initial adherence of PUC: Mean values in percentage of total number of seeded cells. Non-adherent cells counted in the culture supernatant one day after seeding in low (Prol = 2.5 x 10^4 cells/cm^2) and high (Strat = 4 x 10^5 cells/cm^2) density on CCC and on plastic surface as a control, n = 6

Fig. 23: Immunocytochemical staining of HUC in culture passage 4 for smooth muscle α-actin (left), fibroblast marker (centre), and pancytokeratin cocktail (right). Brown colour indicates positive staining. Bright field

Fig. 24: Immunocytochemical staining of PUC in culture passage 7 for smooth muscle α-actin (left), fibroblast marker (centre), and pancytokeratin cocktail (right). Brown colour indicates positive staining. Bright field

Fig. 25: Positive **pancytokeratin** staining of HUC seeded on **plastic surface**. Merged red fluorescence of PKH26, blue cell nucleus fluorescence of DAPI and bright field (left); merged green fluorescence of AE1/AE3, blue fluorescence of DAPI and bright field (centre); composite image w/o bright field (right)

Fig. 26: Positive **pancytokeratin** staining of HUC seeded on **CCC**. Merged red fluorescence of PKH26, blue cell nucleus fluorescence of DAPI and bright field (left);

merged green fluorescence of AE1/AE3, blue fluorescence of DAPI and bright field (centre); composite image w/o bright field (right)

Fig. 27: Positive **CK-20** staining of HUC seeded on plastic surface (left) and on CCC (right); red fluorescence (PKH26) of HUC, blue fluorescence (DAPI) of cell nuclei and green fluorescence of CK-20 expression as a composite

Fig. 28: Positive **p63** staining of HUC seeded on plastic surface (left) and on CCC (right); red fluorescence (PKH26) of HUC, blue fluorescence (DAPI) of cell nuclei and green fluorescence of p63 expression as a composite

Fig. 29: Positive **E-Cadherin** staining of HUC seeded on plastic surface (left) and on CCC (right); red fluorescence (PKH26) of HUC, blue fluorescence (DAPI) of cell nuclei and green fluorescence of E-Cadherin expression as a composite.

Fig. 30: Positive **ZO-1** staining of HUC seeded on plastic surface (left) and on CCC (right); red fluorescence (PKH26) of HUC, blue fluorescence (DAPI) of cell nuclei and green fluorescence of ZO-1 expression as a composite

Fig. 31: Tissue sample extracted one week after surgery was divided into two pieces. Transplant is not visible macroscopically (left). Tissue extraction two weeks after surgery with connective tissue formation (right). Arrow indicates transplant position

Fig. 32: Cryostat section **one week after transplantation**. Unstained section showing red fluorescence of PKH26-labelled transplanted HUC (left). HE-stained section (right). S = skin, M = rectus abdominis muscle. Bright field

Fig. 33: Cryostat section **two weeks after transplantation**. Unstained section showing red fluorescence of PKH26-labelled transplanted HUC (left). HE-stained section (right). S = skin, M = rectus abdominis muscle. Bright field

Fig. 34: Cryostat section **four weeks after transplantation** Unstained section showing red fluorescence of PKH26-labelled transplanted HUC (left). HE-stained section (right). Transplant almost vanished in the subcutaneous tissue. S = skin, M = rectus abdominis muscle. Arrows indicate CCC in degeneration. Bright field

Fig. 35: Positive pancytokeratin expression of cryostat section two weeks after transplantation. Merged red fluorescence of PKH26-labelled transplanted HUC, blue cell nucleus fluorescence of DAPI and bright field (left). Merged green fluorescence for pancytokeratin, blue cell nucleus fluorescence of DAPI and bright field (centre). Composite image w/o bright field (right)

Fig. 36: Positive CK-20 expression of cryostat section two weeks after transplantation. Merged red fluorescence of PKH26-labelled transplanted HUC, blue cell nucleus fluorescence of DAPI and bright field (left). Merged green fluorescence for CK-20, blue cell nucleus fluorescence of DAPI and bright field (centre). Composite image w/o bright field (right)

Fig. 37: Positive p63 expression of cryostat section two weeks after transplantation. Merged red fluorescence of PKH26-labelled transplanted HUC, blue cell nucleus fluorescence of DAPI and bright field (left). Merged green

fluorescence for p63, blue cell nucleus fluorescence of DAPI and bright field (centre). Composite image w/o bright field (right)

Fig. 38: Positive E-Cadherin expression of cryostat section two weeks after transplantation. Merged red fluorescence of PKH26-labelled transplanted HUC, blue cell nucleus fluorescence of DAPI and bright field (left). Merged green fluorescence for E-Cadherin, blue cell nucleus fluorescence of DAPI and bright field (centre). Composite image w/o bright field (right)

Fig. 39: Positive ZO-1 expression of cryostat section two weeks after transplantation. Merged red fluorescence of PKH26-labelled transplanted HUC, blue cell nucleus fluorescence of DAPI and bright field (left). Merged green fluorescence for ZO-1, blue cell nucleus fluorescence of DAPI and bright field (centre). Composite image w/o bright field (right)

Fig. 40: Negative pancytokeratin expression of cryostat section four weeks after transplantation. Merged red fluorescence of PKH26-labelled transplanted HUC, blue cell nucleus fluorescence of DAPI and bright field (left). Merged green fluorescence for pancytokeratin, blue cell nucleus fluorescence of DAPI and bright field (centre). Composite image w/o bright field (right)

Fig. 41: Preoperative status of the urethra determined by urethrography demonstrating a physiological urethral lumen. Arrow indicates the end of the urethral catheter.

Fig. 42: Urethral status three weeks after stricture induction by thermocoagulation. Arrow indicates potential stricture site with slight narrowing.

Fig. 43: Urethral status four weeks after urethroplasty. Urethral patency is established. Arrow indicates former stricture site.

Fig. 44: Cryostat section at **one week after transplantation**. CCC can be located clearly in HE-stained section (top left). Parts of the transplanted cells (red fluorescence) are lying in direct contact to the native urothelium and to the matrix (top right and enlarged section below). L = urethral lumen, N = native urothelium, T = transplant; Bright field

Fig. 45: Cryostat section at **two weeks after transplantation**. Pieces of the CCC can be located in HE-stained section (top left). Parts of the transplanted cells (red fluorescence) are lying in direct contact to the native urothelium (top right and enlarged section below). L = urethral lumen, N = native urothelium, T = transplant; Bright field

Fig. 46: Cryostat section at **four weeks after transplantation**. Pieces of the CCC can be located in HE-stained section (top left). Parts of the transplanted cells (red fluorescence) are lying in direct contact to the native urothelium (top right and enlarged section below). Strong red fluorescence of suture material (s). L = urethral lumen, N = native urothelium, T = transplant; Bright field

Fig. 47: Positive **pancytokeratin expression** proven by double fluorescence of cryostat section **one week after transplantation**. Merged red fluorescence of

PKH26-labelled transplanted HUC, blue cell nucleus fluorescence of DAPI and bright field (left). Merged green fluorescence for pancytokeratin, blue cell nucleus fluorescence of DAPI and bright field (centre). Composite image w/o bright field (right)

Fig. 48: Positive **pancytokeratin expression** proven by double fluorescence of cryostat section **two weeks after transplantation**. Merged red fluorescence of PKH26-labelled transplanted HUC, blue cell nucleus fluorescence of DAPI and bright field (left). Merged green fluorescence for pancytokeratin, blue cell nucleus fluorescence of DAPI and bright field (centre). Composite image w/o bright field (right)

Fig. 49: Weak **pancytokeratin expression** proven by double fluorescence of cryostat section **four weeks after transplantation**. Merged red fluorescence of PKH26-labelled transplanted HUC, blue cell nucleus fluorescence of DAPI and bright field (left). Merged green fluorescence for pancytokeratin, blue cell nucleus fluorescence of DAPI and bright field (centre); Composite image (right). s = suture material

Fig. 50: Positive **CK-20 expression** proven by double fluorescence of cryostat section **two weeks after transplantation**. Merged red fluorescence of PKH26-labelled transplanted HUC, blue cell nucleus fluorescence of DAPI and bright field (left). Merged green fluorescence for CK-20, blue cell nucleus fluorescence of DAPI and bright field (centre). Composite image (right)

Fig. 51: Positive **p63 expression** proven by double fluorescence of cryostat section **two weeks after transplantation**. Merged red fluorescence of PKH26-labelled transplanted HUC, blue cell nucleus fluorescence of DAPI and bright field (left). Merged green fluorescence for p63, blue cell nucleus fluorescence of DAPI and bright field (centre). Composite image (right)

Fig. 52: Positive **E-Cadherin expression** proven by double fluorescence of cryostat section **one week after transplantation**. Merged red fluorescence of PKH26-labelled transplanted HUC, blue cell nucleus fluorescence of DAPI and bright field (left). Merged green fluorescence for E-Cadherin, blue cell nucleus fluorescence of DAPI and bright field (centre). Composite image (right)

Fig. 53: Positive **ZO-1 expression** proven by double fluorescence of cryostat section **one week after transplantation**. Merged red fluorescence of PKH26-labelled transplanted HUC, blue cell nucleus fluorescence of DAPI and bright field (left). Merged green fluorescence for ZO-1, blue cell nucleus fluorescence of DAPI and bright field (centre). Composite image (right)

Table register

Danksagungen

Zunächst möchte ich Herrn Prof. A. Stenzl für die Bereitstellung des Arbeitsplatzes an der Klinik für Urologie danken.

Herrn Prof. K.-D. Sievert danke ich für die Betreuung der Doktorarbeit. Meine Arbeit profitierte sehr von seiner langjährigen klinischen Erfahrung, seinen Tips bezüglich der Dissertationsschrift und seinem Engagement unter anderem bei der Umsetzung der experimentellen Arbeit.

Herrn Prof. F. Sinowatz danke ich für seine Bereitschaft, die extern durchgeführte Arbeit vor dem Fachbereich Veterinärmedizin der LMU zu vertreten und für seine Hilfsbereitschaft.

Außerdem danke ich Viscofan Bioengineering, insbesondere Herrn Dr. Falkenburg für die Bereitstellung der finanziellen Mittel und die freundliche und konstruktive Kooperation.

Martin Vaegler danke ich für die kritische Durchsicht meiner Arbeit, die fruchtbaren Diskussionen und die Unterstützung. Nicht nur bei fachlichen und formellen Fragen sondern auch was über die wissenschaftliche Arbeit hinausgeht konnte ich auf deinen Rat zählen!

Mein herzlichster Dank geht auch an Sabine Maurer, die mir den Start im Labor so angenehm wie nur möglich gestaltete und sehr schnell meine Freude an der Zellkultur weckte. Ihre praktische Unterstützung aber auch das Feedback bezüglich der Dissertationsschrift waren eine große Bereicherung. Vielen Dank für die fachliche Beratung aber auch für das ehrliche Verständnis und die aufmunternden Worte mit denen du mir so manchen Tag gerettet hast.

Nicht zuletzt danke ich allen aktuellen und ehemaligen Kollegen des Labors für Tissue Engineering für die nette Einarbeitung in die Labortechniken und die aktive Unterstützung und Hilfsbereitschaft. Vielen Dank an Conny Bock, Margret Geiger, Elli und Leon Gustafsson, Gitte Schumacher und Erika Senger für die gute Zusammenarbeit und die schöne Atmosphäre im Labor!

Herrn Dr. med. J. Seibold danke ich für die kompetente und tatkräftige Unterstützung bei den chirurgischen Eingriffen. Nicht zuletzt seine Erfahrung und sein Geschick haben zum guten Gelingen der Versuche beigetragen.

Auch Tim-Oliver Greiner und dem Team der experimentellen Medizin danke ich für die praktische Hilfe bei den Tier-OPs und die unkomplizierte freundliche Zusammenarbeit.

Meiner Familie, insbesondere meinen Eltern danke ich von ganzem Herzen für die bedingungslose Unterstützung und den Rückhalt auf den ich mich immer verlassen kann.

Zuletzt danke ich meinen Freunden und Vetmed-Kollegen für das Verständnis und die netten Gespräche, die auch mal für die nötige Ablenkung sorgten.